UNIVERSITÀ DEGLI STUDI DI TRIESTE

XXIX CICLO DEL DOTTORATO DI RICERCA IN CHIMICA

DEVELOPMENT AND CHARACTERIZATION OF NEW METHODS FOR PALYTOXIN DETECTION

Settore scientifico-disciplinare: **BIO/15**

DOTTORANDO / A

VALENTINA BROVEDANI

COORDINATORE

PROF. MAURO STENER

SUPERVISORE DI TESI

DOTT. SILVIO SOSA

ANNO ACCADEMICO 2015/2016

RIASSUNTO

La palitossina (PLTX) ed i suoi analoghi sono composti marini non proteici ad elevata tossicità individuati in coralli del genere *Palythoa*, in dinoflagellati del genere *Ostreopsis* ed in cianobatteri del genere *Trichodesmium*. Attraverso la catena trofica, tali tossine possono accumularsi in organismi marini eduli e causare intossicazioni alimentari nell'uomo. In aree tropicali, intossicazioni anche fatali sono state associate al consumo di pesci e crostacei contaminati da palitossine. Nel Mar Mediterraneo, invece, effetti avversi attribuiti alle palitossine erano associati ad esposizione inalatoria e/o cutanea all'aerosol o all'acqua marina durante proliferazioni di *Ostreopsis* cf. *ovata*. Tuttavia, non sono stati documentati casi di intossicazioni alimentari attribuibili a tali composti. Sebbene non esista una legislazione che regoli il tenore massimo ammissibile delle palitossine nei prodotti ittici, l'Autorità Europea per la Sicurezza Alimentare (EFSA) ha proposto un limite massimo provvisorio di 30 μg/kg di polpa di molluschi, evidenziando la necessità di sviluppare nuovi metodi rapidi, sensibili e specifici per il rilevamento e la quantificazione delle palitossine in prodotti ittici. Inoltre, dato il numero crescente di effetti avversi registrati durante le proliferazioni di *Ostreopsis* nel Mar Mediterraneo, risulta necessario lo sviluppo di metodi in grado di quantificare le PLTXs anche in campioni di microalghe, al fine di permettere un'allerta precoce della presenza di tossine, prima del loro accumulo nei prodotti ittici.

In questo studio, sono stati sviluppati e caratterizzati due metodi per la quantificazione delle palitossine: il saggio emolitico, basato sulla capacità della PLTX di trasformare il suo *target*, la Na^+/K^+ ATPasi, in un canale ionico aspecifico, causando la lisi dell'eritrocita, ed il *cell-based* ELISA, in cui la frazione di tossina legata alla Na^+/K^+ ATPasi espressa da cheratinociti immortalizzati umani (linea cellulare HaCaT) viene rilevata da un anticorpo murino anti-PLTX, riconosciuto a sua volta da un anticorpo secondario anti-*mouse* coniugato con la perossidasi di rafano. Il limite di rilevabilità

(LOD) e di quantificazione (LOQ) della PLTX mediante il saggio emolitico sono $1.4x10^{-10}$ e $3.4x10^{-10}$ M, rispettivamente. Il LOD e LOQ del *cell-based* ELISA sono invece pari a $1.2x10^{-11}$ e $2.8x10^{-11}$ M, rispettivamente.

E' stata inoltre valutata la capacità dei saggi di quantificare le palitossine nei mitili (*Mytilus galloprovincialis*) e nelle microalghe, verificando l'interferenza della matrice (mitili e microalghe) sulla quantificazione della PLTX. Il LOQ della PLTX nei mitili ottenuto tramite il saggio emolitico è di 650 μg/kg, valore circa 20 volte maggiore rispetto al limite massimo suggerito dall'EFSA (30 μg/kg di polpa di molluschi). Al contrario, il LOQ della PLTX nei mitili mediante il *cell-based* ELISA (LOQ = 9.3 μg/kg) è risultato essere inferiore rispetto al limite massimo suggerito dall'EFSA, rendendo il *cell-based* ELISA un possibile metodo di *screening* utilizzabile nel monitoraggio delle PLTXs nei molluschi.

Nelle microalghe, il LOQ del saggio emolitico è 0.03 pg/cellula, mentre quello del *cell-based* ELISA è 0.007 pg/cellula.

La seconda parte della tesi è focalizzata sulla valutazione della sensibilità di diversi modelli cellulari alla PLTX, allo scopo di caratterizzarne ulteriormente il meccanismo d'azione e di sviluppare nuovi metodi funzionali per il rilevamento delle PLTXs. La sensibilità dei diversi modelli cellulari è stata valutata sia in termini di citotossicità indotta da PLTX, sia in termini di *binding* della tossina al suo *target*. La linea cellulare Caco-2 è risultata essere la linea cellulare più sensibile agli effetti citotossici indotti da PLTX (EC_{50} = $3.1x10^{-11}$ M; 95% C.I. = $5.9x10^{-12}$ – $3.4x10^{-11}$ M), mentre la linea cellulare HaCaT il modello cellulare più sensibile in termini di *binding* della tossina al suo *target* (Bmax = 0.043, Kd = $1.4x10^{-10}$ M). L'elevata sensibilità di entrambi i modelli cellulari non è tuttavia correlata all'espressione della Na^+/K^+ ATPasi, suggerendo il coinvolgimento di altri fattori, quali l'espressione

di specifiche isoforme dell'enzima, nel determinare la diversa sensibilità alla PLTX dei modelli cellulari studiati.

ABSTRACT

Palytoxin (PLTX) and its analogs are toxic marine polyethers detected in *Palythoa* corals, *Ostreopsis* dinoflagellates and *Thricodesmium* cyanobacteria. The main concern for human health related to these toxins is their accumulation in marine edible organisms and the possible entrance in the food chain up to humans. In tropical areas, human cases of even fatal foodborne poisonings had been ascribed to consumption of PLTXs contaminated seafood. On the other hand, in the Mediterranean Sea, human poisonings ascribed to PLTXs were associated to inhalation of marine aerosol and/or cutaneous exposure to seawater during *Ostreopsis* blooms and no foodborne poisoning associated with these toxins were documented in this area, so far. Although PLTXs are not regulated, the European Food Safety Authority (EFSA) suggested a maximum limit of 30 µg PLTXs/kg of shellfish meat, recommending the development of suitable, specific and rapid detection methods in seafood. Moreover, given the growing cases of adverse effects during *Ostreopsis* blooms in the Mediterranean Sea, the development of methods for PLTXs detection also in microalgae is suggested. Thus, two methods for PLTXs quantitation were developed and characterized: a hemolytic assay, based on PLTXs ability to convert the Na^+/K^+ ATPase into an unspecific cationic channel leading to erythrocytes lysis, and a cell-based immunoenzymatic assay (ELISA), measuring the binding of PLTXs to Na^+/K^+ ATPase of HaCaT cells by a mouse monoclonal anti-PLTX antibody targeted by an enzyme-conjugated anti-mouse detection antibody. The limits of PLTX detection (LOD) and quantitation (LOQ) by hemolytic assay were $1.4x10^{-10}$ M and $3.4x10^{-10}$ M, respectively, while those by the cell-based ELISA were $1.2x10^{-11}$ M and $2.8x10^{-11}$ M, respectively. The two methods were assessed for their suitability to quantify PLTXs in mussels (*Mytilus galloprovincialis*) and microalgae. The LOQ for PLTX in mussels by the hemolytic assay was 650 µg/kg meat, a value about 20 times higher than the limit suggested by EFSA (30 µg PLTXs/kg meat). On the other hand, the LOQ for PLTX in mussels by the cell-based ELISA was 9.3 µg/kg meat, a value below the safety

limit suggested by EFSA. The high sensitivity of the cell-based ELISA, make this method suitable for PLTX detection in monitoring program. The LOQ by the hemolytic assay and the cell-based ELISA in microalgae were 0.03 pg/cell and 0.007 pg/cell, respectively.

The second part of this thesis was focalized on the investigation of the sensitivity of different cell models to PLTX on which subsequent studies could be carried out to further characterize PLTX mechanism of action and to develop a new functional detection method for PLTXs. The sensitivity was evaluated by means of cytotoxicity and binding assay. The MTT assay showed Caco-2 cells as the most sensitive to PLTX cytotoxic effect with an EC_{50} = $3.1x10^{-11}$ M (95% C.I. = $5.9x10^{-12}$ - $3.4x10^{-11}$), while HaCaT cell line was assumed as the most sensitive cell line for PLTX binding, as confirmed by the Bmax and Kd values, equal to 0.043 and $1.4x10^{-10}$ M, respectively. The high sensitivity to PLTX demonstrated for Caco-2 cell line by the MTT assay and for HaCaT cell line by the binding assay, was not related to the expression of the Na^+/K^+ ATPase, suggesting that other factors, such as the expression of specific Na^+/K^+ ATPase isoforms may play an important role in cells sensitivity to PLTX.

1. Introduction

1.1 Palytoxin

Palytoxin (PLTX) is one of the most potent non-proteinaceous toxins known to date and was firstly isolated from soft corals belonging to the Zoanthidae family in Hawai'i. The history of PLTX started in 1961, when a University of Hawai'i researcher, interested on local natural products, had discovered the Hawaiian legend "*limu-make-o-Hana*", literally "the toxic seaweed of Hana". This legend tells of a man, carrying a mouth of a shark on his back, who used it to kill all the fishermen entering in its fishing area. This man was then killed by a fisherman and his body burned. His ashes were spread across the tide pool in Hana bay, and in that location, a "toxic algae" started to grow. The legend tells that the warriors used to go to the bay and dip the tips of their spears to make them venomous.

Over the centuries, the legend has become a taboo: anyone who went to this place would fall in disgrace. In the 60s, Prof. Helfrich discovered the exact location of this place and the "toxic algae" was found to be a soft coral belonging to the genus *Palythoa* (*P. toxica*). Thus, ten years later, the toxin identified in this soft coral by Prof. Scheuer was called palytoxin. Over the years, chemical, biological, and toxicological studies on PLTX have elucidated the properties of this marine toxin (Moore and Scheuer, 1971).

1.1.1 Producing organisms

PLTX has been identified in different marine organisms from diverse positions in the ecosystem. It is of global dimension, as it is found in tropical, subtropical, and temperate regions. PLTX was firstly isolated in 70s from the Hawai'i soft coral *Palythoa toxica* (Figure 1), belonging to the Zoanthidae family (Moore and Scheuer, 1971). Subsequently, PLTX and a series of its analogues were identified also in other *Palythoa* species from different geographical areas, such as *P. tuberculosa* (Ishida et al., 1983), *P.* aff. *margaritae* (Oku et al., 2004), *P. caribaeorum* (Attaway and Ciereszko, 1974; Béress et al., 1983), and *P. mammillosa* (Attaway and Ciereszko, 1974), the latter two collected from Caribbean coral reefs. PLTX and its analogue 42-hydroxy-PLTX (42-OH-PLTX) have been isolated from *P. heliodiscus* and *P. mutuki* (Deeds et al., 2011).

PLTX has been found also in Zoanthids species belonging to the genus *Zoanthus*, such as *Z. solanderi* and *Z. sociatus*, living in coral reefs colonies close to aggregations of *Palythoa* species and competing with them for the reef ecological niche (Gleibs et al., 1995). The toxin content of corals varies from species to species. A study showed that the most toxic one was *P. toxica* that contained significant PLTX levels during all the year (Moore et al., 1982), whereas other species, such as *P. tuberculosa* (Hashimoto et al., 1969) and *P. mammilosa* (Attawy and Ciereszko, 1974), were shown to be contaminated by PLTX only in a period of the year, specifically June-August.

In 1995, a PLTX-like compound was discovered in benthic dinoflagellates of the genus *Ostreopsis*: the compound was isolated from *Ostreopsis siamensis* and named ostreocin-D (Ost-D) (Ukena et al., 2001). Other species of *Ostreopsis*, such as *O. mascareniensis* (Lenoir et al., 2004) and *O.* cf. *ovata* (Figure 2) (Ciminiello et al., 2006, 2008, 2011), were later found to contain PLTX-like molecules as well. *Ostreopsis* is a genus of epiphytic dinoflagellates thriving in tropical areas (i.e. Pacific, Atlantic and Indian Oceans), but in the last years *Ostreopsis* species have been observed with increasing

intensity and frequency also in the temperate areas, such as the Mediterranean Sea (Brissard et al., 2015; Carnicer et al., 2015). In Italy, *Ostreopsis* cf. *ovata* was recorded for the first time in 1994, along the Tirrhenian coasts. Later, *Ostreopsis* spp., mainly *O.* cf. *ovata*, has been frequently recorded along the Italian coasts, including the Northern areas, such as the Gulfs of Genoa and Trieste (Ciminiello et al., 2006; Guerrini et al., 2010; Honsell et al., 2011; Tognetto et al., 1995).

Figure 1: *Palythoa toxica corals.*

Figure 2: *Ostreopsis cf. ovata cells.*

Since PLTX-like compounds had been detected in phylogenetically different organisms (*Palythoa* corals and *Ostreopsis* dinoflagellates), it had been hypothesized that the real toxin-producing organism could be a bacterial species living in symbiosis with those organisms (Frolova et al., 2000). With this respect, first studies focused on Gram negative bacteria of genus *Vibrio* and *Aeromonas*, isolated from *P. caribaeorum* which was shown to exert PLTX-like hemolytic activity (Seemann et al., 2009). Later, Kerbrat et al. (2011) demonstrated the presence of PLTXs also in cyanobacteria of the genus *Trichodesmium*.

1.1.2 Chemical structure and properties

PLTX was isolated for the first time in 1971 from soft corals of the genus *Palythoa*. Ten years later its chemical structure was independently elucidated by two different research groups, professor Hirata's group in Japan (Uemura et al., 1981) and professor Moore's group at Honolulu, O'ahu, Hawai'i (Moore & Bartolini, 1981). They defined the chemical structure of PLTX which empirical formula is $C_{129}H_{223}N_3O_{54}$ and molecular weight 2680.13 Da (Figure 3).

PLTX is one of the most complex natural non-polymeric molecules. Its skeleton contains 129 carbon atoms with 8 double bonds, cyclic ethers, 64 chiral centers, 42 hydroxyl groups and 2 amino groups (Uemura et al., 1985).

PLTX is an amorphous, hygroscopic, white solid. It is not soluble in non-polar solvent such as chloroform, diethyl ether and acetone. It is scarcely soluble in methanol and ethanol while it is well soluble in dimethyl sulfoxide, pyridine and water. In aqueous solution, after agitation, it develops a foam, probably due to its amphipathic nature. The melting point is not defined and the toxin is heat-resistant. PLTX is optically active with a specific rotation of +26° ± 2 ° in water (Katikou, 2008).

The conformation of the toxin in aqueous solution was investigated by X-ray crystallography (SAXS, Small-angle X-ray Scattering) and nuclear magnetic resonance (NMR). In addition, the structure of PLTX has been compared to that of N-acetyl-PLTX, which is characterized by an acetyl group on the primary amino group in C115. In particular, in aqueous solution N-acetyl-PLTX shows a monomeric form, assuming the shape of a horseshoe, which measures 30.6 x 23.4 x 13.0 Å. On the other hand, PLTX assumes a dimeric form in aqueous solution, with a ∞ shape measuring 52.3 x 22.0 x 15.1 Å. The molecular portions of PLTX involved in the dimer formation have not been identified, although it is supposed that the hydrophobic region (C21-C40) and the region around the conjugated double bonds (C60-C84) are probably implicated. Moreover, also the terminal amino group is probably

involved in the interaction between two PLTX molecules since N-acetyl-PLTX is unable to dimerize, but also its biological activity is about 100 times lower than that of the reference compound PLTX (Inuzuka et al., 2008).

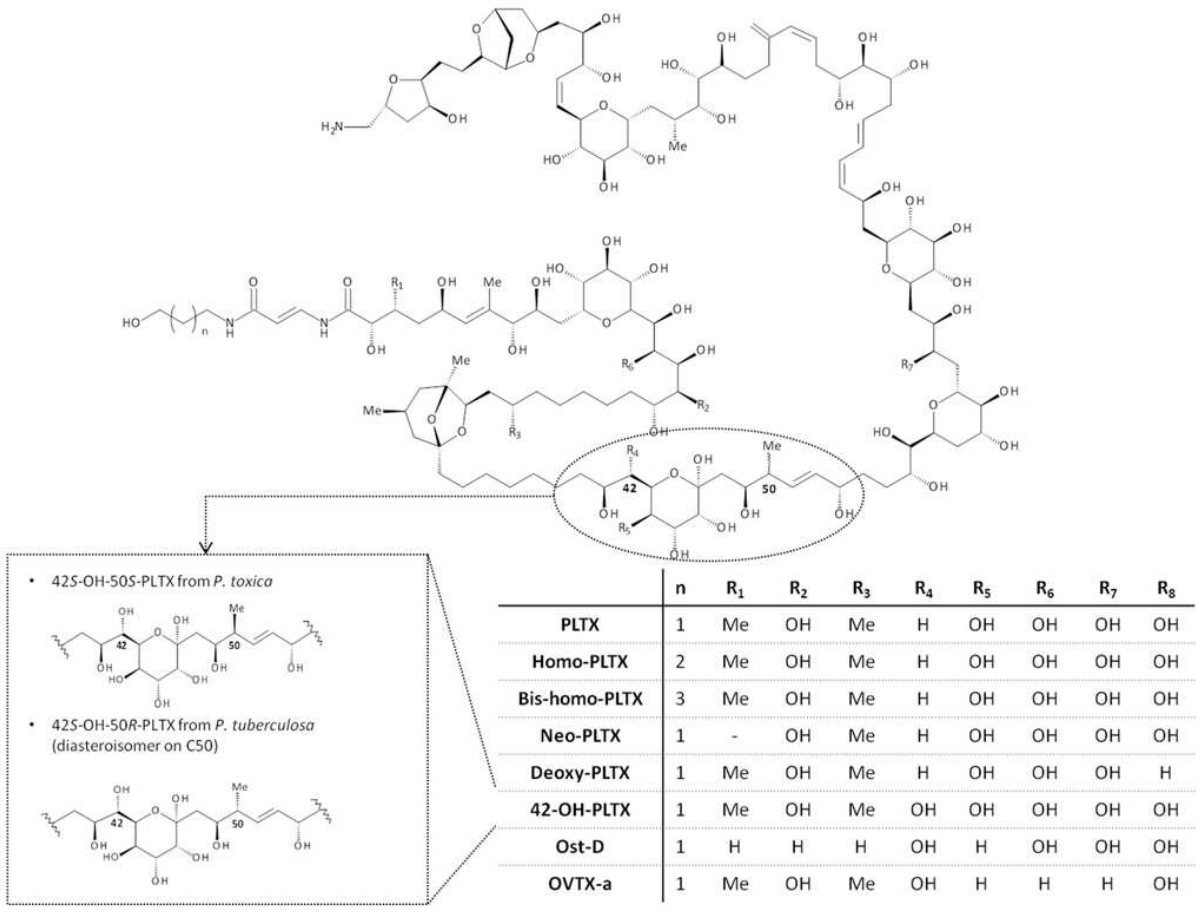

	n	R_1	R_2	R_3	R_4	R_5	R_6	R_7	R_8
PLTX	1	Me	OH	Me	H	OH	OH	OH	OH
Homo-PLTX	2	Me	OH	Me	H	OH	OH	OH	OH
Bis-homo-PLTX	3	Me	OH	Me	H	OH	OH	OH	OH
Neo-PLTX	1	-	OH	Me	H	OH	OH	OH	OH
Deoxy-PLTX	1	Me	OH	Me	H	OH	OH	OH	H
42-OH-PLTX	1	Me	OH	Me	OH	OH	OH	OH	OH
Ost-D	1	H	H	H	OH	H	OH	OH	OH
OVTX-a	1	Me	OH	Me	OH	H	H	H	OH

Figure 3: *Chemical structure of PLTX and PLTX-analogues (Pelin et al., 2016a).*

A series of PLTX analogues have been isolated over the years from different marine organisms (Figure 3). They differ from PLTX for the presence of additional hydroxyl and/or methyl groups and/or the lack of part of these groups, or for chiralities. Among these compounds, the most studied analogs under chemical and/or biological point of view are: (i) Ostreocin-D (Ost-D) from *Ostreopsis*

siamensis (Usami et al.,1995). Its empirical formula is $C_{127}H_{219}N_3O_{53}$ and the molecular weight is 2636.47 Da. Ost-D seems to be less toxic than PLTX in mice (Ito and Yasumoto, 2009);

(ii) two stereoisomers of 42-hydroxy-PLTX (42-OH-PLTX), differing only for the configurational inversion at C50, identified in *Palythoa toxica* and *Palythoa tuberculosa,* respectively. It was demonstrated that this small structural change can significantly influence the potency of their cytotoxic effect (Ciminiello et al., 2014a);

(iii) ovatoxin-a (OVTX-a), the major toxin produced by *Ostreopsis* cf. *ovata* in the Mediterranean Sea (Ciminiello et al., 2012a). Its empirical formula is $C_{129}H_{224}N_3O_{52}$ with a molecular weight of 2647.5 Da. Toxicological *in vitro* studies showed that OVTX-a is less toxic than PLTX, even though its effect after short exposure to nanomolar concentrations rises some concern for human health (Pelin et al., 2016b). In addition to OVTX-a, a series of OVTX-a analogues, such as OVTX-b to -k and isobaric palytoxin, have been identified in *Ostreopsis* cells (Brissard et al., 2015; García-Altares et al., 2015; Tartaglione et al., 2016a).

1.1.3 Mechanism of action

Studies on the mechanism of action of PLTX and its analogues have represented one of the most active research fields on this family of toxins. They showed that the main molecular target of PLTX is the Na^+/K^+ ATPase, a plasma membrane-embedded protein complex of eukaryotic cells (Habermann, 1989).

Na^+/K^+ ATPase is a transmembrane pump belonging to the P-type ATPases family, essential for the cell functions and ions homeostasis. It transports three Na^+ ions out of the cell in trade for two K^+ ions in the cytoplasm against the concentration gradient. This is an active transport requiring the hydrolysis of ATP as energy source (Figure 4).

Na^+/K^+ ATPase is a hetero-oligomer composed of a catalytic α subunit, β subunit and a FXYD protein (γ subunit). The catalytic α subunit, characterized by 10 transmembrane segments, is involved in the transmembrane transport of the cations. The catalytic α subunit can be expressed as four isoforms (α1-4), having different kinetic properties and specific tissue distribution. The β subunit, represented by three isoforms (β1-3), is a type II glycoprotein involved in the correct folding and targeting of the enzyme to the plasma membrane. The γ subunit forms part of the ATPase, it influences the pump function and distribution and can increase its affinity for ATP (Geering, 2008).

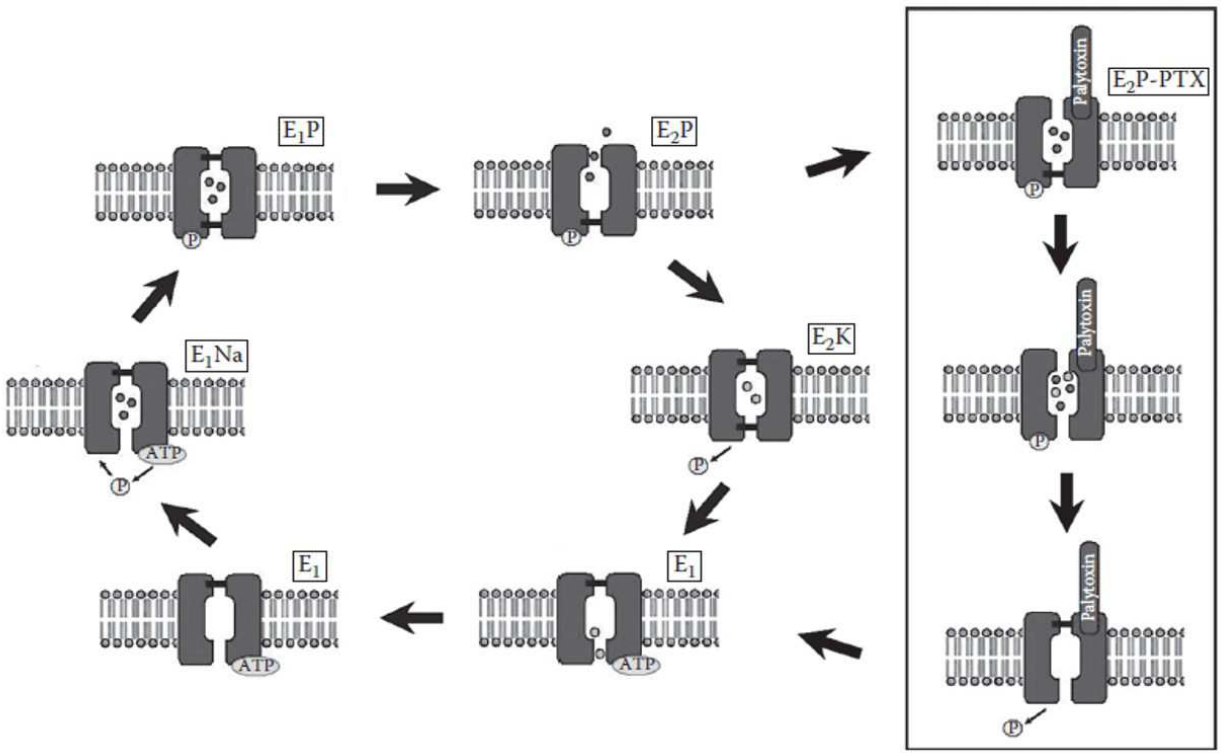

Figure 4: *Albert-Post model for Na^+/K^+ ATPase pump function and PLTX effect. The pump alternates cyclically in two main conformational states: E_1 and E_2, differing in conformation and Na^+ and K^+ affinity. The transition between these two states depends on voltage and concentrations of Na^+, K^+ and ATP, and is coupled to the consecutive Na^+ export and K^+ import. In the phosphorylated E_2 state (E_2P), the pump conformation allows the binding of PLTX which, in turn, induces changes in the α -helices leading to the intracellular gate opening. The toxin binding impairs also the dephosphorylation of the pump, prolonging the opening of the so constituted unspecific cationic channel. Finally, the pump is dephosphorylated and returns into its physiological state (Tubaro et al., 2014).*

The interaction between PLTX and the α-β heterodimer of the Na^+/K^+ ATPase changes the pump conformation from a transmembrane pump to a nonselective cationic channel, allowing Na^+ and K^+ diffusion across the membrane according to their gradient and inducing a strong ionic imbalance at the cellular level (Artigas and Gadsby, 2004; Hilgemann, 2003). The highest affinity of PLTX for the pump occurs when the ATPase is in E_2P conformational state (Artigas and Gadsby, 2004; Rodrigues

et al., 2008). Moreover, when the extracellular gate is physiologically opened in the E_2P conformational state, the contemporary opening of the intracellular gate induces the formation of an open channel as long as the pump is phosphorylated. On the contrary, pump dephosphorylation leads to a conformational change into the E1 state. PLTX binding also reduces the rate of pump dephosphorylation, protracting the channel opening (Artigas and Gadsby, 2004; Harmel and Apell, 2006; Rodrigues et al., 2008). Once dephosphorylated, the pump returns to its normal cycle.

The cardiac glycoside ouabain (OUA) is well known for its ability to bind to Na^+/K^+ ATPase and inhibit *in vitro* PLTX effects (Pelin et al., 2012; Vale-González et al., 2007). However, incomplete abolishment of PLTX biological activity by OUA suggests that the latter does not completely compete with PLTX on the binding sites. Moreover, competitive binding experiments suggested that OUA acts as a negative allosteric modulator against high PLTX concentrations ($0.3 - 1.0\times10^{-7}$ M) and possibly as a non-competitive antagonist against low PLTX concentrations ($0.1 - 3.0\times10^{-9}$ M) (Pelin et al., 2013a).

Other potential molecular targets of PLTX have been investigated in the last years: the sarcoplasmic-endoplasmic reticulum Ca^{2+} pump (SERCA) (Coca et al., 2008; Kockskämper et al., 2004) and the nongastric H^+/K^+ ATPase pump (Guennoun-Lehmann et al., 2007; Qiu et al., 2006). PLTX does not induce channel formation from nongastric H^+/K^+ ATPase (Guennoun-Lehmann et al., 2007; Qiu et al., 2006) or SERCA but it was shown that it inhibits SERCA ATPase activity (Coca et al., 2008).

1.1.4 *In vitro* and *in vivo* toxic effects

The interaction of PLTX with Na^+/K^+ ATPase and the pump transformation into a nonselective cationic channel, lead to an altered cellular ions homeostasis. Firstly, the increased intracellular concentration of Na^+ ions causes a depolarization of the cellular membrane which is also enhanced by the leakage of K^+ and entrance of Ca^{2+} ions (Wu, 2009). The massive influx of sodium ions activates the reverse functioning of the Na^+/Ca^{2+} exchanger (NCE), leading Ca^{2+} ions entering in the cell. This event leads to an increased intracellular Ca^{2+} concentration, which seems to be sustained also by voltage-dependent L-type Ca^{2+} channels, depending on the cell type. The massive entrance of Ca^{2+} ions seems to induce the opening of K^+ and Cl^- channels, whereas the increased intracellular concentration of Na^+ can lead to a reverse functioning of the Na^+/H^+ exchanger (NHE), which causes an acidification of the cytoplasm (Rossini and Bigiani, 2011). In turn, this ions imbalance induces a series of cytotoxic effects, including actin cytoskeleton disorganization, loss of membrane integrity and cell death (Ares, 2005; Schilling et al., 2006; Sheridan et al., 2005).

These events have different consequences on cell viability, depending on the cell model. A series of *in vitro* studies were performed to characterize the toxic effects of PLTX in different cell models. In excitable cells, such as neuronal and muscular cells, the Ca^{2+}-dependent PLTX effects are neurotransmitters release and uncontrolled muscle contraction (Rossini and Bigiani, 2011). In cerebellar granule cells, the influx of Ca^{2+} ions mediated by the activation of voltage dependent Na^+ and Ca^{2+} channels induced by PLTX, leads to the activation of excitatory amino acid (EAA) receptors through glutamate release (Vale et al., 2006). In cardiac cells, Kockskämper et al. (2004) demonstrated that PLTX induces disruption of the cardiac excitation-contraction coupling, impairing heart functions.

As for the excitable cells, the toxin effects on non-excitable cells are dependent on the ions imbalance. In particular, the intracellular overload of Na^+ is the first step involved in PLTX-induced cell damage. Studies on skin keratinocytes demonstrated that PLTX impairs mitochondrial activity by a mechanism dependent on Na^+ ions, but only partially dependent on Ca^{2+} ions, indicating that the increased intracellular Na^+ concentration is an important step of cytotoxicity. Moreover, it was shown that this event triggers a sequence of cell dysfunctions involving mitochondria and oxidative stress which lead to an irreversible cell death (Pelin et al., 2011). In addition, the H^+ intracellular overload that follows PLTX-induced intracellular Na^+ increase, seems to be the driving force for superoxide anions production by reversing mitochondrial electron transport (Pelin et al., 2013b).

The toxic effects of PLTX on erythrocytes were also investigated, in particular its hemolytic activity. PLTX is a potent but slow hemolysin, as observed in erythrocytes from different species (i.e. human, mouse, rat, pig, sheep) (Habermann et al., 1981). The toxin interaction with its molecular target causes an ionic imbalance that leads to erythrocytes swelling followed by lysis (Habermann, 1989).

Other studies on different cell models demonstrated that PLTX acts as a tumor promoter. PLTX, like other tumor promoters, stimulates also the metabolism of arachidonic acid and prostaglandins production (Wattenberg, 2007).

The toxic effects observed *in vitro* can be related to those observed *in vivo.* A series of *in vivo* studies were performed on a series of animal species by different exposure routes. However, some of these studies were performed before the chemical and structural elucidation of PLTX, using a PLTX of unknown purity obtained from different matrices, making dose–effect comparisons problematic. Recent studies after single oral PLTX administration in mice estimated a median lethal dose (LD_{50}) lower than 1 mg/kg: 510 µg/kg (Munday, 2011) and 756 µg/kg (Sosa et al., 2009). Sosa et al. (2009) observed also that mice treated with PLTX doses higher than 600 µg/kg showed scratching, jumping,

dyspnea and limb paralysis. Furthermore, hematochemical analyses demonstrated a dose-dependent increase of LDH (lactate dehydrogenase), CPK (creatine phosphokinase), AST (alanine aminotransferase) and ALT (alanine transaminase) serum levels. Moreover, histological analysis showed inflammation at the forestomach, as recorded also by Ito and Yasumoto, (2009), who described also gastric erosions after oral PLTX administration in mice (500 μg/kg PLTX).

Recently, the toxic effects after repeated oral administration of PLTX were studied in mice by Del Favero et al. (2013). A provisional NOAEL (No Observed Adverse Effect Level) was estimated at 3 μg/kg/day. Macroscopic alterations were observed at gastrointestinal level in mice dead during the treatment. Other lesions were observed in the lungs (inflammation and necrosis) and myocardium (hyper-eosinophilic and separated fibers).

Toxicity studies showed also that PLTX is more toxic after parenteral administration than after oral route. In particular, the LD_{50} after intravenous administration in mice was 0.74 μg/kg (Mahnir et al., 1992), about three orders of magnitude lower than that recorded by oral administration (Munday, 2011; Sosa et al., 2009).

In vivo studies on PLTX analogs are limited to Ost-D and 42-OH-PLTX. Ost-D administration to mice induces toxic effects similar to those of PLTX, but less severe at similar doses (Ito and Yasumoto, 2009). After acute oral administration of 42-OH-PLTX in mice, a LD_{50} close to that of PLTX (650 μg/kg) was recorded by Tubaro et al. (2011a).

1.1.5 Human poisonings

PLTXs can cause human poisonings after oral, cutaneous and inhalational exposure. The main concern for human health associated to these toxins is their accumulation in marine edible organisms and the possible entrance in the food chain up to humans. PLTX was detected in crustaceans (*Platypodiella* spp.), porifera and starfishes (*Acanthaster* spp.) as well as mollusks (mussels, oysters, gastropods, cephalopods), echinoderms (sea urchins, sponges) and polychaete worms (Biré et al., 2013; Gleibs and Mebs, 1999; Gleibs et al., 1995). Studies carried out on tropical fishes like *Herklotsichthys quadrimaculatus* (goldspot herrings), *Scarus ovifrons* (parrot fish) and *Decapterus macrosoma* (mackerel) revealed the presence of the toxin in the skin, muscles, gills, gut and egg cells. Most of these marine organisms tolerated the toxin, showing no signs of toxicity, even at concentrations causing poisonings in humans (Gleibs and Mebs, 1999). Cases of poisonings after the ingestion of contaminated seafood have been recorded mainly in tropical and subtropical areas, sometimes with fatal outcomes (see section 1.1.5.1).

Although the oral exposure can be considered as the most dangerous for the human health, in the Mediterranean Sea adverse effects ascribed to PLTXs were associated to inhalational and/or cutaneous exposure to marine aerosol and/or seawater during *Ostreopsis* blooms. Originally found in tropical areas, since the beginning of the 1970s, *Ostreopsis* bloomed with increasing frequency also in temperate areas, such as Mediterranean basin and along the Atlantic coasts (Figure 5) (Rhodes, 2011). Specifically, *Ostreopsis* has been mainly recorded along the Italian, French and Spanish coastlines (Accoroni et al., 2011; Brissard et al., 2014; Guerrini et al., 2010; Mangialajo et al., 2011; Monti et al., 2007; Tichadou et al., 2010; Totti et al., 2010; Vila et al., 2012). *Ostreopsis* presence in Mediterranean Sea seems not to be related to a recent introduction, whereas its invasive behavior seems to be an effect of the interaction between chemical, physical and biological factors. Peculiar climatic and marine conditions, the high availability of nutrients and low hydrographic conditions

coupled with the construction of new touristic harbors could have played an important role in the development and amplification of this phenomenon (Barone and Prisinzano, 2006). *Ostreopsis* blooms can cause adverse effects in humans due to inhalational exposure to sea-spray aerosol containing fragments of algal cells and/or PLTXs during recreational or occupational activities, as well as after direct contact to seawater. PLTXs had been also detected in edible marine organisms, even though no foodborne poisonings were attributed to these toxins in this area, so far (Aligizaki et al., 2011; Ciminiello et al., 2014b; Del Favero et al., 2012).

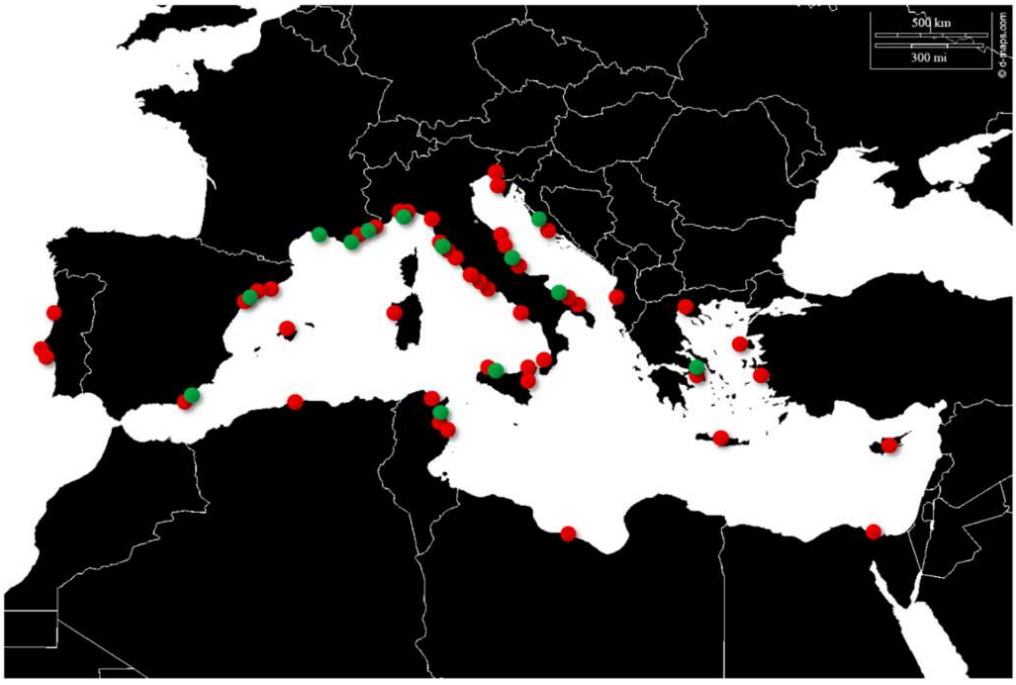

Figure 5: *Occurrence of Ostreopsis cf. ovata blooms (red dots) and adverse effects in concurrency with O. cf. ovata blooms (green dots) along Mediterranean and Atlantic coasts.*

Anyway, despite the possible adverse effects associated to PLTXs as seafood contaminants, there is no regulation for these toxins in seafood. Only the European Food Safety Authority (EFSA) suggested a maximum limit of 30 μg PLTXs/Kg of shellfish meat (EFSA, 2009).

Surveillance activities of *Ostreopsis* are performed along the Italian coasts in summer, in concurrency with the touristic season, with the aim to avoid sanitary issues related to inhalation or direct contact with PLTXs through marine aerosol or seawater. The emergency step is associated to *Ostreopsis* cells concentration in seawater ≥ 10.000 cells/L (D.M. 119/2010). Recently, new guidelines for the management of *Ostreopsis* cf. *ovata* blooms in relation to bathing and other recreational activities in Italian marine coastal waters have been proposed even though they have not been yet adopted. These guidelines indicate different monitoring activities in relation to the risk profile of the involved area. It is possible to distinguish a routine step, which is performed from June to September, while, in case of blooms, the samplings are carried out with increased frequency. In the routine step, the cellular density in the water column is around ≤10.000 cells/L or 10.000-30.000 cells/L if in concurrency with adverse weather conditions for long periods of time (7-10 days). Health risks are negligible and no actions are needed. The alert step requires a cell density equal to 10.000-30.000 cells/L in the water column and favorable weather and sea conditions linked with long-lasting blooms (7-10 days), or 30.000-100.000 cells/L with adverse conditions. In these conditions, cases of poisoning can occur, such as mild cutaneous symptoms and irritation of the eyes and mucous membranes. During this step, people should be aware and well informed about the health risks, especially swimmers, tourists and fishermen, regarding also the possibility of contaminated seafood. Finally, the emergency step requires a cellular density >30.000 cells/L with favorable weather and sea conditions or >100.000 cells/L, independently from the weather. *Ostreopsis* cells could be found also above the water surface. In this case, recreational activities in near-shore areas should be prohibited (Rapporti ISTISAN 14/19).

Recently, growing cases of human poisonings after cutaneous and/or inhalational exposure to PLTXs after handling PLTX-contaminated soft corals during maintenance of home marine aquaria have been reported. The toxic potential of PLTXs and the uncontrolled trade of these zoanthids lead to a serious concern for human health and, due to the growing number of documented cases, these kind of exposure to PLTXs can be considered as an emerging sanitary problem (Pelin et al., 2016a). Despite the increasing number of poisonings by exposure to PLTX-containing soft corals, only human poisonings ascribed to ingestion of contaminated seafood and those ascribed to inhalational and/or cutaneous exposure to marine aerosol and/or seawater during *Ostreopsis* blooms will be described.

1.1.5.1 Oral exposure

As reported above, cases of poisonings ascribed to PLTXs and associated to ingestion of contaminated seafood, with some fatal outcomes, have been recorded in tropical and subtropical areas. Only in some of the documented cases, a direct PLTX detection in the seafood leftovers was made. On the other hand, most cases of poisoning have been ascribed to PLTX without a direct toxin detection and only on the basis on screening tests carried out on seafood samples collected before the poisonings, or on the basis of symptoms and background information from the patients (Tubaro et al., 2011b).

The first case occurred in 1984 in Philippines, where a 49-years old man reported a metallic taste after eating a crab (*Demania reynaudii).* Soon after, he developed general weakness with nausea, vomiting and diarrhea, muscular weakness and respiratory problems. Some hours post ingestion, the man was hospitalized and experienced severe bradycardia, rapid and shallow breathing and cyanosis around the hands. He died 15 hours after the crab ingestion. This case was ascribed to PLTX on the basis of chromatographic analysis and mouse bioassay on leftovers (Alcala et al., 1988).

Another case of fatal poisoning occurred in 1987 in Japan. A man (54 years old) and a woman (79 years old) felt sick after the consumption of parrot fish (*Scarus ovifrons*). Within 49 hours, the patient experienced dyspnea, myalgia and convulsion. After hospitalization, high serum levels of CPK, AST and LDH were recorded in the patients. The man was dismissed from the hospital, while the woman death for respiratory failure 4 days later. Also in this case the mouse bioassay was performed, confirming the presence of "parrotfish toxin", with chemical and pharmacological properties close to those of PLTX (Kodama et al., 1989).

Some years later, Onuma et al. (1999) described a case occurred in Madagascar in 1994. Two hours after the ingestion of tropical herrings (*Herklotsichthys quadrimaculatus*), a woman experienced a

metallic taste, general weakness vomiting and diarrhea. The woman died the day after the consumption of the contaminated seafood, whereas her son, who ate the same fishes, did not show signs of poisonings. This case was ascribed to PLTXs based on the hemolytic activity of the seafood sample that was inhibited by an anti-PLTX antibody as well as chromatography and mass spectrometry data.

More recently, a case of poisoning involving many people (33 people, ages between 27 and 57) occurred in Japan after the ingestion of serranid fish (*Epinephelus bruneus*). The patients experienced muscle pain, weakness, dark coloring of the urine and high serum level of CPK (24,000 IU/l). In this case, all the patients recovered within one month. Mouse bioassay and hemolytic assay for the presence of PLTX were performed on the leftovers (Taniyama et al., 2002).

The last case occurred in Taiwan in 2014 (Wu et al., 2014). Seven family members consumed fish soup prepared with *Herklotsichthys quadrimaculatus* and *Pempheris nyctereutes* whole fishes and only four of them became ill while the other three family member were asymptomatic. All the family members reported a bitter or sour taste during the consumption of the soup. The most serious patient was a 67 years old man, who experienced dizziness, nausea, tingling and numbness of face and limbs and weakness, and recurred to the emergency department. After intravenous fluid and oxygen therapy, the man was dismissed. However, he developed myalgia, arthralgia, abdominal cramps, respiratory distress and anuria which required re-hospitalization. Hematological analyses revealed high serum levels of ALT and CPK. Moreover, an irregular electrocardiogram (ECG) was observed. The man died 21 hours post ingestion. The other three family members reported similar but milder gastrointestinal and neurologic symptoms. The presence of PLTX in leftovers was confirmed by the hemolytic assay, high-performance liquid chromatography (HPLC) and liquid chromatography coupled with mass spectrometry (LC-MS) (Wu et al., 2014).

1.1.5.2 Inhalational exposure

As described above, humans can be exposed to sea-spray aerosol containing fragments of algal cells and/or PLTXs during *Ostreopsis* blooms (Casabianca et al., 2013; Ciminiello et al., 2014b). The frequency of *Ostreopsis* blooms in the Mediterranean Sea increased in the last years, and reports of PLTXs presence make a huge concern for public health (Ramos and Vasconcelos, 2010). The first documented cases of adverse effects in humans after inhalational exposure to marine aerosol during *Ostreopsis* blooms occurred along the Tuscany coast and Bari coast in 1998, 2000 and 2001 (Di Turi et al., 2003; Sansoni et al., 2003). In 2003, 28 persons were exposed to marine aerosol along the Italian coast (Southern Adriatic Sea) and experienced rhinorrhea, cough, dyspnea, fever, lacrimation and dermatitis (Tubaro et al., 2011b).

One of the most important episode of human poisonings associated to *Ostreopsis* cf. *ovata* blooms occurred during the summer of 2005 along the Ligurian coasts close to Genoa and La Spezia. In that period, there was an unusual and abundant bloom of *O.* cf. *ovata*, and the presence of PLTXs was confirmed by chemical analyses (Ciminiello et al., 2008). The consequences were quite important on the ecosystem. Moreover, a huge number of people (209) required hospitalization after exposure to marine aerosol during recreational activities at the beach. The patients experienced cough, dyspnea, sore throat, rhinorrhea, fever ≥ 38 °C, bronchoconstriction, headache and nausea. Conjunctivitis and skin irritation were occasionally noted. All the symptoms appeared around 4 hours after exposure (Durando et al., 2007). Durando and coworkers (2007) described also another episode of poisoning occurred in 2006, in same geographical area: 19 persons presented adverse effects concomitantly to *O.* cf. *ovata* bloom. The signs and symptoms of these patients was similar to those described during the episode occurring the previous year. After this episode, *Ostreopsis* was monitored along all the Italian coasts and further blooms were observed in Sicily in 2005-2006 and close to Ancona in 2006.

Other cases of human illness concomitantly to *O.* cf. *ovata* blooms, without analytical data on PLTXs detection in microalgae, occurred in Spain in 2004. Three hours after seawater aerosol exposure, 200 persons experienced rhinorrhea, rhinitis, throat irritation, cough, eye irritation and headache (Kermarec et al., 2008). Two years later, in Spain, people from a small village located on the coast, experienced mainly sneezing, mucous hypersecretion, cough, rhinitis, dry throat, eye irritation. The concentration of *Ostreopsis* cf. *ovata* cells in seawater was 1200 cells/L (Barroso García et al., 2008).

Along the French coastline, a total of 47 suspected cases of *Ostreopsis* poisoning together with five documented microalgae blooms were identified by the French Mediterranean Coast *Ostreopsis* Surveillance Network along the French Mediterranean and Monaco coasts from 2006 to 2009. Well-documented cases of human illness in concomitance to an *Ostreopsis* bloom (25.000-900.000 cells/L) were reported during the summer 2006. Four divers referred lips and tongue irritation, headache, throat irritation, fever and diarrhea (Tichadou et al., 2010).

1.1.5.3 Cutaneous exposure

Cutaneous exposure is the most underrated route, but epidemiological data show an increasing number of cases, mainly after contact with soft corals that are sold to aquarium hobbyist as decorative element. These soft corals are commercialized without any regulation and there is a huge lack of education and information regard the dangerousness of these organisms (Pelin et al., 2016a).

Moreover, cutaneous exposure to PLTXs can occur after contact to seawater during *Ostreopsis* blooms. Documented cases of adverse effects after exposure to marine seawater during *Ostreopsis* blooms were also characterized by dermatitis (Durando et al., 2007; Gallitelli et al., 2005). However, dermatitis incidence is probably underestimated because of the non-required hospitalization due to the low hazard of this damage.

In France, from 2006 to 2009, different cases of adverse effects in humans after skin exposure to seawater during *Ostreopsis* blooms were documented. The first one occurred in Frioul Island, where patients reported skin irritation, pruritus ad mucosal irritation. The patients were treated with nonsteroidal anti-inflammatory drugs (NSAIDs) with success within 6-12 hours after exposure. In the same years, other three outbreaks were reported, in Nice, Villefranche Sur Mer and Larvotto beach. Also in these cases all patients were treated with NSAIDs and have a full recovery within 12 hours post exposure (Tichadou et al., 2010; Tubaro et al., 2011b).

At the end of September 2009, in the Gulf of Trieste, some people referred itching of the arms and dermatitis after swimming along the beach. Simultaneously, an *Ostreopsis* bloom ($6x10^6$ cells/L) was recorded (Honsell et al., 2011).

1.2 Methods for palytoxin detection

Several methods for PLTXs detection have been developed over the years on the basis of the toxicity in animals, cytotoxicity, antibodies and/or receptor binding. Among them, the biological assays are based on the functional properties of these toxins and have the advantage of their ability to detect all the PLTX analogues on the basis of their effects (Riobó and Franco, 2011). In last years, chemical detection methods that exploit the structural peculiarities of the PLTX and its analogues have been developed. Nowadays, the biological methods and the immunoassays play an important role as preliminary screening methods before to apply definitive instrumental techniques or when chemical analytical methods are not available. Despite different methods for PLTXs detection have been developed in the last years, none of them has been completely validated for PLTX detection in different natural matrices such as fish, shellfish or microalgae samples. For this reason, the investigation to develop new analytical methods to quantify PLTX and its analogues in different matrices represented one of the most active fields of research on these toxins. Over the years, many studies have been focused on the development of PLTXs detection to overcome the limits characterizing the available methods (i.e. low specificity, sensitivity and/or matrix effect).

Moreover, given the huge concerns for public health due to the expanding distribution of the toxic *Ostreopsis* species also in the temperate areas such as the Mediterranean Sea, suitable detection methods to monitor PLTXs also in microalgae are needed.

1.2.1 Biological methods

Mouse bioassay

The mouse bioassay (MBA) is a standard simple method for toxins detection in different matrices. It is based on the lethality in mice after intraperitoneal (i.p.) injection of a sample extract. One of the main advantages of the MBA is that this biological method is able to detect all the toxins in the extract by its toxic effect (lethality) without the need of expensive equipment and complicated sample extraction procedures (Riobò and Franco, 2011).

The methods used to prepare the extracts can vary in efficiency and is determinant for the MBA outcome. Over the years, different extraction methods have been reported. An extraction protocol for lipophilic toxins requires the use of acetone as solvent, drying of the extract and its re-suspension in aqueous 1% Tween 60 solution (Yasumoto et al., 1978). However, this method is not efficient to extract relatively polar compounds, such as PLTX and its analogues. Moreover, also other toxins, such as domoic acid, saxitoxin, yessotoxin and cyclic imines, can be extracted and can interfere with the assay (Riobó and Franco, 2011). Therefore, other extraction procedures were applied to reduce the interference by other toxins. An initial extraction with 75% aqueous ethanol followed by partitioning between water and n-butanol to obtain aqueous and butanol phases was also used, but interference from water-soluble toxins still remained (Aligizaki et al., 2008; Taniyama et al., 2002). Other extraction procedures were set up on *Ostreopsis* cf. *ovata* samples using 50% aqueous methanol and on fish tissue using ethanol (Onuma et al., 1999; Rhodes et al., 2002).

The characteristic symptoms in mice after i.p. injection of PLTXs-containing extracts are stretching of hind limbs, lower backs and concave curvature of the spinal column within 15 minutes of the administration. However, a high variability in results due to specific animal sensitivity related to strain, sex, age, weight, diet and stress conditions was observed (Riobò and Franco, 2011). Riobó et

al. (2008a) proposed a standardized protocol for MBA with 24 h observation period following the i.p. injection in order to minimize the variability of the assay results. However, in addition to the low specificity and high variability, the MBA is characterized by other disadvantages which justified the development of new methods and the adoption of LC-MS as a standard method by the European Commission (EC, 2011). These disadvantages are mainly related to ethical problems due to the use of animals and the low specificity of MBA.

Cytotoxicity assays

Cytotoxicity-based assays are considered biological assays and are based on PLTXs ability to bind to its molecular target in the cell, leading to a measurable cytotoxic effect. A clear advantage of such functional assays is their ability to detect all the functionally active compounds in a sample (Rossini, 2005). Specifically, when PLTX binds to the Na^+/K^+ ATPase of excitable or non-excitable cells, transforming the pump in a non-selective cationic channel, early cellular response to the toxin is the ionic imbalance followed by a series of cellular events (i.e. membrane depolarization) and cell death (Wu, 2009). These cellular responses were used to develop cytotoxicity assays to detect and quantify PLTXs. These methods represent a good alternative to the use of animals, with the possibility to quantify PLTXs at low (picomolar) concentrations and analyze a series of samples in the same time using multiwell microplates (Riobò and Franco, 2011). However, these methods need the facilities for maintenance and handling cell culture and they are not able to provide any information on the toxin profile in the tested sample: many toxins induce cytotoxic effects. Moreover, a chemical confirmatory analysis is necessary because of possible interferences due to the presence of other toxins or cytotoxic constituents that can co-occur with PLTXs in the analyzed extract (Riobò and Franco, 2011).

Over the years, different cell models were used to try to specifically quantify PLTXs. In particular, different research groups used neuroblastoma cell lines evaluating the cell damage or the cell death measuring mitochondrial dehydrogenase or oxidoreductase activity after a cells pre-treatment with ouabain (OUA). Manger et al. (1993) developed an assay using murine neuroblastoma Neuro-2a cells for the detection of marine toxins acting on sodium channels (brevetoxins, ciguatoxins and saxitoxins) by measuring mitochondrial dehydrogenase activity (MTT assay) in presence of OUA or veratridine, an activator of the sodium channel. This method provides concentration-dependent results and can discriminate the toxin activating the channel from those inhibiting it. Some years later, Cañete and Diogène (2008) applied the method developed by Manger and coworkers on Neuro-2a and NG108-15 cells to detect also PLTX. The same end-point (cell viability) was evaluated to detect PLTX in mussel samples and *O. ovata* extracts. Using this method, Neuro2-a cells were exposed to PLTX for 19 hours, which induced a concentration-dependent reduction of cell viability (the concentration inhibiting cell viability by 50 %, IC_{50}, was 42.9 pM). PLTXs specific effect was confirmed by cells pre-exposure to 500 µM OUA which inhibited PLTX cytotoxic effect (Ledreux et al., 2009). Recently, the suitability of gene expression measured as fluorescence in Neuro 2-a cells was defined as functional endpoint alternative to cytotoxicity in an assay for marine toxins detection. In particular, seven biomarkers based on mRNA expression were defined as potential biomarkers of PLTX induced effects (Nicolas et al., 2015).

Espiña et al. (2009) developed a PLTX detection assay based on the measurement of mitochondrial oxidoreductase activity in BE (2)-M17 human neuroblastoma cells, using Alamar blue as fluorescent or colorimetric probe. The assay was characterized by a detection limit of 75 pM after cells exposure to the toxin for 72 h and of 150 pM after 4 h exposure. This method was also used to quantify PLTX in *O. ovata* samples: it was able to discriminate PLTXs from other toxins (i.e. okadaic acid) through the inhibition of cytotoxicity by a cell pre-exposure to OUA.

Bellocci et al. (2008) used another cell model (human breast adenocarcinoma cell line, MCF-7) to develop a cytolytic assay for the detection of PLTX, based on the release of cytosolic LDH. Cells exposure to PLTX or its analog Ost-D induces a concentration-dependent release of LDH (IC_{50} = 50 pM and 3 nM, respectively). Cytolysis was not detected after MCF-7 cells exposure to unrelated marine toxins, such as tetrodotoxin, okadaic acid and yessotoxin. Anyway, the assay specificity was confirmed by the inhibition of PLTX and Ost-D effect using OUA.

Hemolytic assay

The delayed hemolytic assay is one of the most used screening methods for PLTX quantitation, due to its simplicity, cheapness, rapidity and sensitivity. It is based on the toxin ability to convert the Na^+/K^+ ATPase of mammal erythrocytes to a nonspecific cationic channel, leading to an ions imbalance and a delayed lysis of erythrocytes, measurable spectrophotometrically as hemoglobin release. The amount of released hemoglobin depends on the toxin concentration and time of erythrocytes exposure to the toxin (Habermann et al., 1981).

The hemolytic assay is usually carried out following Bignami's protocol (Bignami, 1993), with or without modifications, but a standardized and universally accepted procedure has not yet been defined. Most literature studies report the original assay with a series of modifications mainly concerning the origin of erythrocytes, the time and temperature of their incubation with PLTX, and/ or the working buffer composition (Aligizaki et al., 2008; Biré et al., 2013; Brissard et al., 2014; Brovedani et al., 2016; Gleibs et al., 1995; Kim et al., 2002; Lenoir et al., 2004; Malagoli D., 2007; Onuma et al., 1999; Pezzolesi et al., 2012; Riobó et al., 2006, 2008b, Taniyama et al., 2001, 2003; Volpe et al., 2014; Wachi and Hokama, 2001). In the original method developed by Bignami (1993), mouse erythrocytes were diluted in phosphate buffered saline (PBS) containing 1 mM calcium

chloride and 1 mM sodium tetraborate, that increases the hemolysis induced by PLTX promoting the toxin interaction with Na^+/K^+ ATPase (Ahnert-Hilger et al., 1982; Habermann, 1983). Blood cells suspension was incubated with PLTX for up to 24 hours at 37 °C. After centrifugation, the supernatants were used to measure the absorption at 540-595 nm.

To improve the specificity of the hemolytic assay, PLTX-specific neutralizing antibodies (monoclonal anti-PLTX antibody 73D3 and anti-PLTX rabbit polyclonal antibodies) and/or OUA (PLTX antagonist) were used. Riobò et al. (2008) carried out an exhaustive study on PLTX-induced hemolysis and its inhibition by OUA using sheep erythrocytes to define a sensitive and reliable method: it is necessary to operate at a moderate temperature and partial inhibition of PLTX by OUA.

Due to its simplicity, cheapness and rapidity, the hemolytic assay is widely used to detect PLTXs in different natural samples such as zoanthids, fish, sea urchins, *Ostreopsis* and mussels extracts. However, the hemolytic assay presents some disadvantages due to the high variable results related to the origin of erythrocytes (sheep, rabbit, pig, mouse, rat, human) and other parameters (i.e. age, sex) (Riobò and Franco, 2011). Indeed, it has been demonstrated that erythrocytes containing K^+ as the main intracellular cation with respect to Na^+ are the most sensitive ones to PLTX (Habermann et al., 1981). Moreover, marine organisms could contain hemolytic compounds different from PLTXs, which could interfere with the assay giving false positive results. For instance, a recently developed biosensor to quantify PLTX in mussels, based on lactate dehydrogenase release from sheep erythrocytes, appeared to be influenced by a significant matrix effect, besides low PLTX recovery (Volpe et al., 2014).

1.2.2 Immunoassays

Radioimmunoassay

Radioimmunoassay (RIA) is a sensitive and specific antibody-based method. In 1988, a RIA for PLTX detection able to quantify picomolar concentrations of the toxin was developed by Levine et al. (1988). It was a competitive radioimmunoassay based on the use of anti-PLTX polyclonal antibodies obtained for the first time by Levine and coworkers (Levine et al., 1987) and PLTX labeled with ^{125}I-Bolton-Hunter reagent on its terminal amino group. However, the use of radioiodine-labeled PLTX as competitive antigen makes this method unfavorable in term of costs and stability of the reagent as well of precautions needed due to the use of a radioactive substance.

Enzyme-linked immunosorbent assay

Enzyme-linked immunosorbent assays (ELISAs) are based on highly specific and sensitive interaction between an antigen and a specific antibody. Due to their specificity, rapidity, and simplicity, these easily automated methods are widely used for routine analysis in biochemistry and clinical laboratories. Different enzyme immunoassays have been reported for PLTX quantitation: some of them are competitive assays, based on competitive binding between the toxin present in the sample and the toxin add-in, or non-competitive assays, characterized by a "sandwich" architecture in which PLTX binding to a primary antibody is detected by a secondary anti-PLTX antibody. In this case, PLTX is bound between two layers of antibodies recognizing different toxin epitopes (Bignami et al., 1992; Boscolo et al., 2013; Frolova et al., 2000; Garet et al., 2010).

In 1992, Prof. Bignami's group focused the research on enzyme immunoassays (Bignami et al., 1992) where selected antibodies were used to develop five PLTX-specific enzyme-linked immunosorbent assays (ELISA) formats for PLTX quantitation in biological matrices, including crude extracts of *P.*

tuberculosa. These ELISA formats included an indirect competitive inhibition enzyme-linked immunoassay (CIEIA), two types of direct CIEIA as well as an indirect and a direct sandwich ELISA. The sandwich ELISAs can detect as low as 10 pg PLTX per test, while the direct competitive inhibition enzyme-linked immunoassays detect as low as 30 pg of toxin per test within 4 hours. The immunoassay developed by Bignami and coworkers was subsequently improved by Frolova and coworkers, who developed a competitive ELISA using the unmodified toxin as coating antigen, able to detect PLTX in the range of 6 – 250 ng/mL (Frolova et al., 2000).

Garet et al. (2010) described the development of a recombinant human single chain anti-PLTX antibody (scFv) by phage display techniques and its use in the development of a competitive ELISA. The assay allowed to quantify PLTX in mussel samples with a mean recovery rate of 90%. The method was accurate and very sensitive as shown by the instrumental detection limit of 0.5 pg/mL and the working range between 0.0005 and 500 ng/mL, but impaired by a high variability.

Another ELISA (indirect sandwich) was developed later by Boscolo et al. (2013). This ELISA employed the mouse monoclonal anti-PLTX antibody 73D3 as capturing antibody and rabbit polyclonal anti-PLTX antibodies as detection antibody, the latter is in turn recognized by a horseradish peroxidase (HRP)-conjugated polyclonal anti-rabbit antibody. This method detects PLTX at concentrations ranging from 1.25 – 40 ng/mL and it can quantify also some PLTX congeners, such as biotinylated PLTX and 42-OH-PLTX. An intra-laboratory study demonstrated its sensitivity (instrumental limit of detection, LOD = 1.1 ng/mL; limit of quantitation, LOQ = 2.2 ng/mL), accuracy, repeatability and specificity. Indeed, other marine toxins, such as okadaic acid, domoic acid, saxitoxins, brevetoxins and yessotoxins, does not cross-react in this assay. The ability of this ELISA to quantify PLTX in different matrices was also assessed, demonstrating its performance to quantify the toxin in mussels (LOQ = 11 µg/kg), microalgae (LOQ = 9.6 ng/mL) and seawater (LOQ = 2.4 ng/mL).

Biosensors

In the last years, the investigation of analytical methods to detect and quantify PLTXs has been focused on the development of biosensors as innovative techniques. A surface plasmon resonance (SPR) biosensor incorporating the murine monoclonal anti-PLTX antibody 73D3 was developed by Yakes et al. (2011). This method can quantify PLTX at really low concentrations in buffer as well as in two seafood matrices: groupers and clams. The PLTX detection limits were 0.52 ng/mL, 2.8 ng/mL and 1.4 ng/mL, respectively. Although this method is sensitive and rapid, it requires expensive equipment not available in all laboratories.

Zamolo et al. (2012) developed a very sensitive electrochemiluminescence (ECL) based sensor for the detection of PLTX. This innovative method takes advantage of the specificity provided by the anti-PLTX antibodies, the good conductive properties of carbon nanotubes and the high sensitivity obtained by a luminescence based transducer. The instrumental LOD and LOQ for PLTX were 0.07 and 0.24 ng/mL respectively. Moreover, this biosensor allows PLTX quantitation also in mussels (*M. galloprovincialis*) with a limit of quantitation of 2.2 µg/kg mussel meat.

In the last year, two new biosensors for PLTX detection were developed. The first is a flow cytometry-based immunoassay developed by Fraga et al. (2016). It is a competitive assay where PLTX immobilized on the surface of microspheres competes with PLTX-like molecules in solution for binding to a specific mouse monoclonal anti-PLTX antibody. The anti-PLTX antibody bounded to the microspheres is in turn detected by a phycoerythrin labeled goat anti-mouse immunoglobulin G. The instrumental LOD for PLTX was 0.47 ± 0.15 nM. The matrix effect was also evaluated using mussel extracts, showing a detection range between 374 and 4430 µg/kg mussel meat after a 30-fold extract dilution. Moreover, this method does not seem to detect efficiently the analog 42-OH-PLTX.

Another biosensor recently developed is an immune-enzymatic assay in which biolayer interferometry (BLI) was coupled with a competitive binding assay through an enzyme-linked aptamer. Horseradish peroxidase-labeled aptamers were used as biorecognition receptors to competitively bind with PLTX, that was immobilized on the biosensor surface. Then, the PLTX-HRP-aptamer complex was submerged in a 3,3'-diaminobenzidine solution, resulting in formation of a precipitated product directly on the biosensor surface and a change in the optical thickness of the biosensor layer. This change could then shift the interference pattern and generate a response profile on the BLI biosensor. This method allowed a real-time, sensitive (LOD = 0.04 pg/mL) and rapid (10 min) detection of PLTX (Gao et al., 2017).

1.2.3 Chemical methods

Thin Layer Chromatography (TLC)

Thin layer chromatography (TLC) is based on the separation of the constituents of a mixture by their repartition between a mobile and a stationary phase, due to the different affinity of each molecule for the two phases. The stationary phase is a 1 mm thick sorbent layer lodged on a glass, plastic or aluminum plate. The sorbent material can be silica, aluminum oxide or powdered cellulose. The mobile phase is an appropriately chosen solvent able to separate the sample components that needs to be little compatible regarding polarity to the stationary phase. Nowadays, TLC is not widely used, its use was restricted to isolation and purification processes and can't be considered as quantitative detection method.

TLC was used by Yasumoto et al. (1986) to isolate and identify the toxins extracted from two crabs species, comparing them with reference PLTX. By TLC, the crab toxins were indistinguishable from the reference compound, as shown by the same retention factor (Rf). Tan et al. (2000) reported a variation of this analytical method in which bi-dimensional TLC was used to identify PLTX analogues using red iodinated vapor after the application of ninhydrine.

High Performance Capillary Electrophoresis (HPCE) and High Performance Liquid Chromatography (HPLC) coupled with UV detection

The characteristic ultraviolet (UV) absorption profile of PLTX is considered a good parameter used to verify the toxin presence in a sample. Using diode array detection (DAD), the PLTX UV spectrum is characterized by two absorption peaks at 233 and 263 nm (Riobò and Franco, 2011). Mereish et al. (1991) applied both HPCE-UV and HPLC-UV for PLTX detection. The LOD obtained were 0.5 pg/injection and 125 ng/injection, respectively. As shown by the LOD values, the sensitivity of the

HPCE was higher than that of HPLC. In addition, HPCE allowed to identify small concentrations of toxin in small volumes of sample.

HPLC-UV has been used to detected the presence of PLTX-like substances in cultured or natural *Ostreopsis* ssp. samples collected in Indian Ocean, Brazil and the western Mediterranean Sea (Lenoir et al., 2004; Riobó et al., 2006). In particular, Lenoir et al. (2004) demonstrated the presence of mascarenotoxin A and B in a n-butanol extract from *O. mascarenensis* cells, comparing the retention time and the UV spectra with those of the reference PLTX. Riobò and coworkers applied HPLC-UV on cultured *O. ovata* and *O. siamensis,* recording a LOD for PLTX of about 1-2 µg/injection. However, there are no studies in which HPLC-UV analyses were used for PLTXs detection in other matrices, such as mussels, probably due to the strong matrix effect that may cause false positive results and decrease the method sensitivity (Riobò and Franco, 2011).

High Performance Liquid Chromatography coupled with fluorescent detection (HPLC-FLD)

A pre-column PLTX derivatization method that make the toxin a fluorescent compound has been reported by Riobò et al. (2006). The molecule was derivatized by 6-aminoquinolyl-N-hyroxysuccinimidylcarbamate (AccQ) that can react with the amino terminal group of PLTX. Subsequently, sample was analyzed by reverse-phase HPLC coupled with FLD detection, which allowed to detect and quantify PLTXs in *Ostreopsis* extracts. The instrumental LOD and LOQ for derivatized PLTX were 0.75 ng and 2 ng, respectively, making this analytical method really sensitive for the quantitation of PLTX, even if results regarding its sensitivity for PLTX detection in mussels are not still available.

Liquid Chromatography coupled with Mass Spectrometry (LC-MS)

The European Commission has adopted liquid chromatography–mass spectrometry (LC–MS) as a standard method to detect lipophilic toxins in bivalve mollusks (EC, 2011). In the last years, the LC-MS methods has been also used to quantify PLTX and its analogues in different matrices, such as shellfish, microalgae and seawater (Ciminiello et al., 2006, 2011a, 2011b, 2015; Lenoir et al., 2004; Pezzolesi et al., 2012; Riobó et al., 2006; Selwood et al., 2012; Suzuki et al., 2013; Uchida et al., 2013). LC-MS is an analytical chemistry technique that combines the physical separation ability of liquid chromatography (LC) with the mass analysis ability of mass spectrometry (MS).The latter is a technique that ionizes chemical species and sort the ions based on their mass-to-charge ratio. Thus, it allows the measurement of the molecular mass of PLTX and the elucidation of its chemical structure, distinguishing it from other congeners, thanks to its characteristic and unique MS spectrum. MS spectrum of PLTX-group toxins is characterized by the presence of *m/z* 327 fragment ion, the bicharged ion *m/z* 1340 and/or the tricharged ion *m/z* 912. Moreover, the cluster generated by multiple losses of water molecules is another characteristic of the spectrum of PLTXs (Riobò and Franco, 2011).

Over the years, this analytical method has been further optimized evaluating new chromatography and mass spectrometry conditions, with the aim to further improve the sensitivity and the specificity for PLTX. The introduction of tandem mass spectrometry (MS/MS), in which two analyzers are used in series, has proven to be useful to identify and quantify PLTX and its analogues in complex matrices. This analytical method was used to confirm the presence of isobaric PLTX and OVTX-a in a *Ostreopsis* cf. *ovata* sample obtained during the bloom in Genoa in 2005, as well as, to determine the toxin profile of *Palythoa toxica* and *P. tuberculosa* (Ciminiello et al., 2006, 2008, 2009).

Recently, the research group of Prof. Ciminiello, has developed a liquid chromatography–high-resolution mass spectrometry analysis (LC-HRMS) which included one-step extraction procedure and clean-up of the samples through solid phase extraction (SPE) before the chemical analysis. This method was proven to be very sensitive with a LOD and LOQ equal to 14 and 44 ng/mL, respectively. Moreover, it was applied in the quantitation of PLTXs in mussel samples with a LOD for PLTX of 70 µg/kg and 15 µg/kg after SPE clean-up (Ciminiello et al., 2015). LC-HRMS was then used by Ciminiello and coworkers to quantify PLTXs also in other matrices, such as *Ostreopsis* cells, soft-corals and seawater samples (Tartaglione et al., 2016a, 2016b).

In conclusion, the main advantages of the LC-MS methods are the rapid execution, sensitivity, the possibility to be automated, screening and quantitation of PLTXs individually to give information on the toxic profile of the sample. However, it requires very expensive equipment as well as specialized personnel to perform the analyses. Moreover, the LC-MS is a disruptive method that does not allow a reuse of the sample (Riobò and Franco, 2011).

2. Aim of the study

Palytoxin (PLTX), initially identified in corals of the genus *Palythoa*, and later in *Ostreopsis* dinoflagellates and *Trichodesmium* cyanobacteria, is considered the most toxic non-proteinaceous marine compounds. The molecular target of PLTX is the Na^+/K^+ ATPase: its binding to the α-β heterodimer of the ATPase changes the transmembrane pump into a nonspecific cationic channel. Consequently, a consistent ionic imbalance at the cellular level is induced by the toxin. Over the years, a series of PLTX analogues have been detected in different marine organisms, among which two stereoisomers 42-OH-PLTX identified in *P. tuberculosa* and *P. toxica*, respectively, ostreocin-D (Ost-D) identified in *Ostreopsis siamensis* and ovatoxin-a (OVTX-a) as the major toxin produced by *Ostreopsis* cf. *ovata* in the Mediterranean Sea.

The main concern for human health associated to these toxins is their accumulation in marine edible organisms and their possible entrance in the food chain up to humans. Indeed, a series of human poisonings characterized by gastrointestinal symptoms, respiratory distress, myalgia, cardiac problems, and sometimes death, were ascribed to these compounds in tropical and subtropical areas after ingestion of contaminated seafood. In the last decades, *Ostreopsis* dinoflagellates frequently bloomed in the temperate areas, including the Mediterranean Sea, and the relevant toxins (mainly OVTX-a) have been detected in marine edible organisms, even though no foodborne poisonings were associated to these toxins in this area, so far. In temperate areas, adverse effects ascribed to PLTX were associated with the inhalational and cutaneous exposure to marine aerosol and/or seawater during *Ostreopsis* blooms. In addition to health impact, *Ostreopsis* blooms have a negative economic impact on the tourism industry due to hotel cancellations in presence of *Ostreopsis* species.

Although there is no regulation for PLTXs in seafood, the European Food Safety Authority (EFSA) suggested a maximum limit of 30 μg PLTXs/Kg of shellfish meat, recommending the development of suitable, specific and rapid detection methods in seafood, due to their high toxic potential. Moreover, given the growing cases of adverse effects ascribed to inhalational exposure to marine

aerosol and skin contact with seawater during *Ostreopsis* blooms, as well as PLTXs detection both in *Ostreopsis* and marine aerosols in the Mediterranean Sea, the development of methods for PLTXs detection also in microalgae is suggested. PLTXs detection in microalgae would also give an early alert of the presence of PLTXs before their accumulation in seafood.

Thus, the purpose of the research presented by this thesis was to develop and characterize new methods for PLTXs detection in mussels and microalgae that can be used within monitoring programs. These methods had to be rapid, sensitive, specific and easy to use in the attempt of overcoming the lacks and the limitations of previous developed methods (i.e. low specificity and sensitivity, matrix effect, expensive equipment).

With this aim, two methods for PLTXs detection have been developed and characterized: the hemolytic assay and the cell-based ELISA. The hemolytic assay is a functional method widely used to detect PLTX due to its simplicity, cheapness and rapidity, without characterization of matrix effect. This method is based on PLTX ability to convert the Na^+/K^+ ATPase into a nonspecific cation channel leading to a late lysis of red blood cell. A standardized and accepted protocol for this assay to quantify PLTXs has not yet been defined. Given the lack of a standardized protocol for the hemolytic assay as a reference procedure for PLTXs quantitation, a novel standardized protocol was firstly set up. Then, its suitability to detect PLTXs in mussels (*Mytilus galloprovincialis*) and microalgae was evaluated.

Starting from recently published data by our research group, concerning the characterization of PLTX binding to intact HaCaT skin keratinocytes using a monoclonal anti-PLTX antibody, a second method has been developed and characterized. It is a cell-based immunoenzymatic assay (cell-based ELISA), which measures the binding of PLTXs to Na^+/K^+ ATPase of HaCaT cells by a mouse monoclonal anti-PLTX antibody targeted by a HRP-conjugated anti-mouse detection antibody. Also this method was evaluated for its suitability to quantify PLTXs in mussels and microalgae.

Finally, with the aim to improve the sensitivity of the cell-based ELISA and to develop other cell-based assays for PLTXs detection, experiments to identify the most sensitive cell models to PLTX had been carried out. The sensitivity of different cell lines to PLTX were evaluated by means of cytotoxicity (MTT assay) and toxin binding measured by a monoclonal anti-PLTX mouse antibody and a HRP-conjugated secondary anti-mouse IgG antibody.

3. Materials and methods

3.1 Chemicals

PLTX, isolated from *P. tuberculosa*, was purchased from Wako Pure Chemicals Industries Ltd. (Osaka, Japan; purity > 90%). 42*S*-hydroxy-50*S*-palytoxin and 42*S*-hydroxy-50*R*-palytoxin were isolated from *Palythoa toxica* and *P. tuberculosa*, respectively, as previously reported (Ciminiello et al., 2009, 2014b). Ovatoxin-a and the mixture of ovatoxin-a, -d, -e were kindly provided by Prof. P. Ciminiello (Università di Napoli "Federico II", Naples, Italy). The mouse monoclonal anti-PLTX antibody 73D3 (mAb-PLTX) was produced by a hybridoma cell culture as previously described by Bignami et al. (1992). Ostreocin-D was cordially supplied by Prof. T. Yasumoto (Japan Food Research Laboratories, Tokyo, Japan). The peroxidase-conjugated anti-mouse IgG was purchased from Jackson ImmunoResearch (Newmarket, England). HaCaT cell line and Caco-2 cell line were purchased from Cell Line Service (DKFZ, Eppelheim, Germany) and from the Istituto Zooprofilattico della Lombardia e dell'Emilia Romagna (Brescia, Italy), respectively. All the other cell lines (LoVo, IHH, HepG2, HCT-116, MDA- MB-231, MCF-7, PANC-1) were bought from American Type Culture Collection (ATCC, Manassas, Virginia). All cell culture reagents were bought from Euroclone (Milan, Italy). All other reagents were of analytical grade and purchased from Sigma-Aldrich (Milan, Italy), if not otherwise specified.

3.2 Hemolytic assay for palytoxin detection

3.2.1 Erythrocytes purification

Blood samples from healthy human volunteers were obtained from the Transfusion Center, Azienda Ospedaliera Universitaria, Trieste, Italy. All donors signed an approved consent form giving permission for the collection and use of blood for research purposes (WMA Declaration of Helsinki). Blood was drawn by venipuncture between 08.00 a.m. and 10.00 a.m. to minimize variability due to circadian rhythms, and immediately processed. Blood, collected into standard triple bag systems, was fractionated following standard procedures to obtain buffy-coats. Buffy coats (50 mL) were diluted 1:1 (v/v) in the erythrocytes preservation solution (specified in Section 3.2.2) and then centrifuged at 2400 rpm for 10 min at 4 °C. The erythrocyte pellet (2 mL), suspended in the red blood cell preservation solution (10 mL), was washed three times by centrifugation at 1500 rpm for 5 min at 15 °C. Then, the final pellet was re-suspended 1:10 (v/v) in the preservation solution.

3.2.2 Red blood cells storage

Three storage solutions were used to evaluate erythrocyte preservation at 4 °C: Saline-Adenine-Glucose-Mannitol solution (SAGM, containing $5x10^{-2}$ M dextrose, 0.15 M NaCl, $2.4x10^{-3}$ M adenine and $2.9x10^{-2}$ M d-mannitol) (Zehnder et al., 2008), Adenine-Dextrose Solution (ADSOL, containing 0.12 M dextrose, 0.15 M NaCl, $3.9x10^{-3}$ M adenine and $4.1x10^{-2}$ M d-mannitol) (Moore, 1991) and Dulbecco's Phosphate Buffered Saline (D-PBS) containing 1 mM ethylenediaminetetracetic acid (EDTA) and 5 mM glucose (Lowe et al., 1973). Erythrocyte preservation was evaluated by means of resistance to spontaneous lysis and erythrocyte concentration. For the first parameter, 0.4 mL of red blood cells suspension was centrifuged at 1500 rpm for 5 min and the optical density of the supernatant was then measured at 405/540 nm (Microplate autoreader; Bio-Tek Instruments; Vinooski, VT). Erythrocyte concentration was evaluated by visual cell counting at microscope, following the Trypan Blue Exclusion Test. Acceptable thresholds were constant cell concentration and optical densities lower than 0.5, a value close to the average optical densities of the negative controls (125 µL of an erythrocyte suspension incubated with K^+-free D-PBS without toxin). Both parameters were assessed daily for 36 days.

3.2.3 Experimental design for assay optimization

The hemolytic assay was standardized considering the following parameters: the use of purified human erythrocytes *vs* whole blood, the influence of selected ions (borates, calcium, sodium, and potassium ions) on PLTX-induced hemolysis, and the incubation temperature of erythrocytes exposed to PLTX. The standardized assay was subsequently characterized according to the international principles, as described by the Eurachem Guide (Magnusson and Ornemark, 2014).

3.2.4 Hemolytic assay protocol

After washing, erythrocytes were pelleted by centrifugation (1500 rpm for 5 min) and re-suspended in K^+-free D-PBS at $1x10^8$ cells/mL. In 96-well plates, 125 µL of PLTX solution and 125 µL of the erythrocyte suspension were added to each well and incubated for 5 h at 41 °C (PLTX final concentrations: $1.22x10^{-11}$ - $4.00x10^{-7}$ M). As negative controls, 125 µL of erythrocyte suspensions were incubated with 125 µL K^+-free D-PBS without toxin. As a positive control, 100% hemolysis was achieved by incubating the erythrocytes suspension with 125 µL of 0.1% Tween 20 (v/v) for 5 h at 41 °C. After incubation, the plate was centrifuged at 1500 rpm for 5 min at 15 °C and, using a multichannel pipette, the supernatant was carefully transferred into a clear flat bottom 96-well plate, avoiding pellet break-up. Optical density (O.D.) of the supernatant was then measured by an Automated Microplate Reader EL 311s (Bio-Tek Instruments, Winooski, VT) at 405/540 nm and the percentage of hemolysis calculated with respect to the positive control by the following formula:

$$\% \text{ of hemolysis: } \frac{100 \times (\text{O.D. PLTX exposed sample} - \text{O.D. Negative control})}{(\text{O.D. Positive control} - \text{O.D. Negative control})}$$

3.3 Cell-based ELISA for palytoxin detection

3.3.1 Experimental design for assay optimization

The cell-based ELISA was developed considering the following parameters: i) different fixative solutions and incubation temperature of HaCaT cells with the primary and secondary antibodies; ii) interchange of the fixation phase and the treatment of cells with PLTX; iii) different blocking agents; iv) primary antibody dilutions. The developed assay was then characterized according to the international principles as defined by the Eurochem Guide (Magnusson and Ornemark, 2014).

3.3.2 Cell-based ELISA protocol

HaCaT cells ($1.5x10^4$ cells/well) were seeded in 96-well plates and maintained in culture for 3 days. After 10 min exposure to PLTX ($5.1x10^{-13}$ – $1.0x10^{-8}$ M), cells were washed twice with PBS and fixed for 30 min with 4% paraformaldehyde (PFA, 50 µL/well). Subsequently, cells were blocked for 30 min in 200 µL/well TBB buffer [50 mM Tris-HCl, 0.15 M NaCl, 2% bovine serum albumin (BSA) and 0.2% Tween 20, pH 7.5] added with 10% horse serum and washed twice with PBS. The cell-bound toxin was detected by 0.5 µg/mL anti-PLTX mouse monoclonal antibody (mAb, 73D3) for 1 h at 50 °C under gentle agitation. HaCaT cells were then washed three times with PBS containing 0.1% Tween 20 followed by three washes with PBS. The cell bound anti-PLTX mouse antibody (mAb) was then detected by exposing the cells to 1:6000 HRP-conjugated secondary anti-mouse IgG antibody for 1 h at 50 °C under gentle agitation. After three washes with PBS containing 0.1% Tween 20 and three washes with PBS, 60 µL 3′,5,5′-Tetramethylbenzidine (TMB) substrate were added to start a colorimetric reaction, which was stopped after 1 h adding 30 µL/well of 1 M H_2SO_4. The

absorbance was measured by a Spectra® photometer (Tecan Italia; Milan, Italy) at 450 nm. The nonspecific binding was determined in presence of 1 mM OUA (20 µL/well).

3.4 Evaluation of mussels matrix effect and toxin recovery

Evaluation of mussels matrix effect

To assess the suitability of the hemolytic assay and cell-based ELISA to quantify PLTX in mussels at levels below the suggested EFSA limit (30 µg PLTXs/kg edible parts, corresponding to about $11.2x10^{-9}$ mol/kg; EFSA, 2009), different extracts of *Mytilus galloprovincialis* edible parts were prepared. Each extract was previously analyzed by liquid chromatography high resolution mass spectrometry (LC-HRMS) to verify the absence of PLTX. Mussels were collected in the Gulf of Trieste (Italy) and shucked meat (200 g) was homogenized (14000 rpm, 3 min) using an Ultra-Turrax (Ika-Werk; Staufen, Germany). The homogenate (1 g) was extracted three times with 3 mL of different solvents (80%, 50% or 20% aqueous ethanol or aqueous methanol). Each extractive solution was then centrifuged at 5500 rpm for 30 min, the corresponding supernatants were pooled and the volumes adjusted to 10 mL with the relevant extraction solvents to obtain six extracts at a final concentration of 0.1 g mussels meat equivalents/mL. The hemolytic activity of each extract was then evaluated at five dilutions (1:1, 1:10, 1:50, 1:100 and 1:1000, v/v) to assess background hemolysis. At dilutions devoid of background hemolysis, extracts were spiked with different PLTX concentrations to prepare matrix matched-samples at PLTX levels ranging from $3.9x10^{-10}$ to $2.5x10^{-8}$ M. The matched samples were then analyzed using the hemolytic assay. The relevant hemolytic activity was compared to that induced by the same PLTX concentrations without matrix.

To evaluate the mussels matrix effect at the cell-based ELISA, different dilutions (1:1, 1:5, 1:10 and 1:50, v/v) of the PLTX-free extract of *Mytilus galloprovincialis* were spiked with known PLTX

concentrations to prepare a series of matrix matched-samples at PLTX levels ranging from $1.4x10^{-11}$-$1.1x10^{-9}$ M. Each sample was then analyzed by the cell-based ELISA, as previously described, comparing the results with those obtained analyzing the same PLTX concentrations without matrix.

The effect of different dilutions of each solvent (80%, 50% or 20% aqueous ethanol or aqueous methanol) at the hemolytic assay and the cell-based ELISA was also evaluated.

Evaluation of PLTX recovery from mussels

Portions of the PLTX-free mussel sample were spiked with PLTX, and then extracted as described above, to obtain extracts containing different concentrations of PLTX ($1.4x10^{-11}$ – $1.1x10^{-9}$ M). Each extract was then analyzed by the cell-based ELISA, as previously described.

3.5 Evaluation of microalgae matrix effect and toxin recovery

Evaluation of microalgae matrix effect

To assess the suitability of the hemolytic assay and of the cell-based ELISA to quantify PLTX in microalgae, different extracts of *Coolia monotis*, a benthic dinoflagellate species bred in artificial seawater by Prof. Honsell (University of Udine, Italy), were prepared. Each extract was previously analyzed by LC-HRMS to confirm the absence of PLTXs. Cell pellet of *Coolia monotis* was extracted with 50 % aqueous methanol (v/v) by sonication for 5 minutes, in a pulse mode for three times while cooling in an ice bath. Each mixture was then centrifuged at 4500 rpm for 30 minutes, the corresponding supernatants were pooled and the volume adjusted with 50% aqueous methanol to obtain an extract at a final concentration of $2x10^6$ cells equivalents/mL (Rapporti ISTISAN 14/19). Different dilutions (undiluted, 1:1, 1:5, 1:10 and 1:100) of the aqueous methanol microalgae extract were spiked with different PLTX concentrations to prepare matrix matched-samples at PLTX levels ranging from $3.9x10^{-10}$ to $2.5x10^{-8}$ M for the hemolytic assay, and from $1.4x10^{-11}$ to $1.1x10^{-9}$ M for the cell-based ELISA. The extracts dilutions spiked with different concentrations of PLTX were then analyzed by the hemolytic assay and cell-based ELISA in comparison to the same PLTX concentration without matrix.

Evaluation of PLTX recovery from microalgae

Portions of the PLTX-free microalgae sample were spiked with PLTX and then extracted as described above to obtain extracts containing different concentrations of PLTX ($1x10^{-8}$, $2x10^{-9}$, $4x10^{-10}$ M for the hemolytic assay and $1x10^{-9}$, $2x10^{-10}$, $4x10^{-11}$ M for the cell-based ELISA). Each sample was then analyzed by the hemolytic assay and the cell-based ELISA, as previously described.

3.6 Sampling and analysis of natural algal populations

Different samples of microalgae were collected once a week or every two weeks between August and September 2015 and 2016 along the Adriatic (Trieste, Italy and Split, Croatia), Ligurian and Tuscany (La Spezia and Massa Carrara, Italy) coasts, depending on the occurrence of *Ostreopsis*, in collaboration with Prof. Ninčević Gladan, from the Institute of Oceanography and Fisheries (Split, Croatia) and Dr. Varello from Istituto Zooprofilattico Sperimentale del Piemonte, Liguria e Valle d'Aosta (Torino, Italy). Each seawater sample was collected in shallow waters (30 to 100 cm) by bottles and divided into subsamples for the taxonomic microalgae identification, cells counting and Scanning Electron Microscopy (SEM) analysis that were performed in collaboration with Prof. Honsell of the Department of Agriculture and Environmental Sciences, University of Udine (Udine, Italy). Part of each sample was filtered by gravity on 0.45 μm filter (Durapore HV membrane filters, Millipore) to separate algal cells from seawater and pellets were frozen at -20 °C until extraction. Cell pellets were extracted as described above (Rapporti ISTISAN 14/19). Microalgae extracts were then analysed by the haemolytic assay and by the cell-based ELISA in comparison with LC-HRMS. LC-HRMS were performed in collaboration with Prof. Dell'Aversano of the Department of Pharmacy, University of Napoli "Federico II" (Naples, Italy).

3.6.1 Taxonomic identification and cells counting

Analyses were performed on unfixed and fixed (1% formalin) algal samples using a Leitz Diavert inverted microscope (Ernst Leitz Wetzlar; Wetzlar, Germany) using bright field and phase contrast illumination. Unfixed seawater samples were first analyzed to detect the presence of benthic dinoflagellates, then fixed seawater samples were used for cell counting carried out by the Utermohl (1958) method at 500x magnification. Cells were also observed by epifluorescence microscopy using a Zeiss Axio Observer Z1 inverted microscope and an AxiocamMRm/3 camera together with ZEN Software (Carl Zeiss AG, Germany). Observations were carried out using Zeiss filter set 34 (exciter filter 379-401 nm, barrier filter 435-485 nm) after staining with two different fluorescent stains to show DNA (Hoechst 33342) and thecal plates (Calcofluor White M2R) (Honsell et al., 2011).

3.6.2 Scanning Electron Microscopy analysis

Cultured subsamples were left to settle on poly-L-lysine coated coverslips (BD Biosciences; San Jose, USA), fixed with 2% electron microscopy grade glutaraldehyde dissolved in filtered seawater for 30 min, washed in 1:1 seawater/distilled water and then in distilled water, dehydrated in a gradual series of ethanol, critical point dried with liquid carbon dioxide, sputter coated with gold and observed with a Leica Stereoscan 430i scanning electron microscope (Leica Microsystems; Wetzlar, Germany).

3.7 Cell Cultures

HaCaT cells (immortalized human skin keratinocytes)

HaCaT cells were cultured in Dulbecco's Modified Eagle's medium (DMEM) high glucose, supplemented with 10% fetal bovine serum (FBS), L-glutamine ($1.0x10^{-2}$ M), penicillin ($1.0x10^{-4}$ g/mL) and streptomycin ($1.0x10^{-4}$ g/mL) at 37 °C in a humidified 95% air/5% CO_2 atmosphere. Cell passage were performed two days post-confluence, once for week, and all the experiments were performed between passage 48 and 70.

IHH cells (immortalized human hepatocytes)

IHH cells were maintained in DMEM medium high glucose with the addition of 10% FBS, 1.25% L-glutamine 200 mM, penicillin ($1.0x10^{-4}$ g/mL) and streptomycin ($1.0x10^{-4}$ g/mL), 1% Hepes buffer 1M, 0.01% human insulin 10^{-4} M and 0.04% dexamethasone 1 mg/mL. Cell culture was maintained according to standard procedures in a humidified incubator at 37 °C and with 5% CO_2, and cell passage was performed at confluence, once a week.

HepG2 cells (human liver cancer cells)

HepG2 cells were maintained in Eagle's minimal essential medium (EMEM) with the addition of 10% FBS, L-glutamine ($1.0x10^{-2}$ M), penicillin ($1.0x10^{-4}$ g/mL) and streptomycin ($1.0x10^{-4}$ g/mL) and 1% sodium pyruvate 100 mM at 37 °C in a humidified 95% air/5% CO_2 atmosphere. Cell passage was performed at confluence, once a week.

PANC-1 cells (human pancreatic carcinoma cells)

PANC-1 cells were maintained in DMEM high glucose added with 10% of FBS, L-glutamine ($1.0x10^{-2}$ M), penicillin ($1.0x10^{-4}$ g/mL) and streptomycin ($1.0x10^{-4}$ g/mL) at 37 °C in a humidified 95% air/5% CO_2 atmosphere. Cell passage was performed at confluence, once a week.

LoVo cells (human colon cancer cells)

LoVo cells were maintained in RPMI 1640 containing 10% of FBS, L-glutamine ($1.0x10^{-2}$ M), penicillin ($1.0x10^{-4}$ g/mL) and streptomycin ($1.0x10^{-4}$ g/mL). Cell culture was maintained according to standard procedures in a humidified incubator at 37 °C and with 5% CO_2, and cell passage was performed at confluence, once a week.

HCT-116 cells (human colon cancer cells)

HCT-116 cells were cultured in DMEM high glucose, supplemented with 10% FBS, L-glutamine ($1.0x10^{-2}$ M), penicillin ($1.0x10^{-4}$ g/mL) and streptomycin ($1.0x10^{-4}$ g/mL) at 37 °C in a humidified 95% air/5% CO_2 atmosphere. Cell passages were performed at confluence, once for week.

Caco-2 cells (human colon cancer cells)

Caco-2 cells were cultured in EMEM supplemented with 15% fetal bovine serum, L-glutamine ($1.0x10^{-2}$ M), sodium pyruvate ($1.0x10^{-3}$ M), penicillin ($1.0x10^{-4}$ g/mL) and streptomycin ($1.0x10^{-4}$ g/mL) at 37 °C in a humidified 95% air/5% CO_2 atmosphere. Cell passages were performed at 80% confluence, once for week.

MDA- MB-231 cells (human breast cancer cells)

MDA-MB-231 cells were cultured in RPMI 1640 with the addition of 10% FBS, L-glutamine ($1.0x10^{-2}$ M), penicillin ($1.0x10^{-4}$ g/mL) and streptomycin ($1.0x10^{-4}$ g/mL) at 37 °C in a humidified 95% air/5% CO_2 atmosphere. Cell passages were performed at confluence, once for week.

MCF-7 cells (human breast cancer cells)

MCF-7 cells were maintained in RPMI 1640 containing 10% of FBS, L-glutamine ($1.0x10^{-2}$ M), penicillin ($1.0x10^{-4}$ g/mL) and streptomycin ($1.0x10^{-4}$ g/mL). Cell culture was maintained according to standard procedures in a humidified incubator at 37 °C and with 5% CO_2, and cell passage was performed at confluence, once a week.

3.8 MTT assay

Cells ($5x10^3$ cells/well) were seeded in 96 wells plates and, after 72 h, exposed to PLTX ($1x10^{-16}$ – $1x10^{-7}$ M) for 4 h. Cells were then washed, and fresh culture medium containing 3-(4,5Dimethylthiazol-2-yl)-2,5-diphenyltetrazolium bromide (MTT, 0.5 mg/mL) was added to each well. After 4 h, the supernatant was removed and wells refilled with 200 µL/well of DMSO to measure the absorbance at 540/630 nm by an Automated Microplate Reader EL 311s (BioTek Instruments, Winooski, VT, USA). Data are presented as % of control and are the mean ± standard error (SE) of three independent experiments performed in triplicate.

3.9 Palytoxin binding assay

Cells ($1.5x10^4$ cells/well) were seeded in 96-well plates and maintained in culture for 3 days. Cells were exposed for 10 min to increasing concentrations of PLTX ($5.1x10^{-13}$ – $1.0x10^{-8}$ M). Nonspecific binding was measured in presence of 1 mM OUA (20 µL/well), added 10 min before the treatment with the toxin. The specific PLTX binding was obtained subtracting the nonspecific binding from the total one. Cells were then washed, fixed with 4% PFA (50 µL/well) for 30 min and blocked for 30 min in 200 µL/well TBB buffer containing 10% horse serum. After washes, the cell-bound toxin was detected incubating the cells with the anti-PLTX mouse monoclonal antibody (mAb, 73D3) for 1 h at 50 °C under gentle agitation. The cell bound mAb was in turn detected exposing the cells to HRP-conjugated secondary anti-mouse antibody (diluted 1:6000) for 1 h at 50 °C under gentle agitation. After several washes, the colorimetric reaction was started adding 60 µL 3′,5,5′-Tetramethylbenzidine (TMB) substrate and blocked after 1 h by 30 µL/well of 1 M H_2SO_4. The absorbance was measured by a Spectra® photometer (Tecan Italia; Milan, Italy) at 450 nm. The obtained results (O.D. values)

obtained using each cell model were normalized based on the protein content and are the mean of three independent experiments.

3.10 Flow cytofluorimetry analysis

After 6 days from seeding in cell culture flask, $1x10^6$ cells were detached with a PBS solution containing 0.05% EDTA and 0.02% trypsin, and collected in cytofluorimetric tubes. Cells were washed with 10 mL of PBS and fixed with 500 µL of 3% PFA for 15 min at room temperature. After fixation, cells were washed with 5 mL of PBS, resuspended with 100 µL of saponin A solution (6 mg/mL in PBS) containing the anti-Na^+/K^+ ATPase alpha antibody diluted 1:50 (Thermo Fisher Scientific; Waltham, MA, USA) and incubated at 4 °C. After 1 h, cells were washed thrice with saponin B (12.5% saponin A solution in PBS, v/v) and resuspended with 200 µL of saponin A solution containing the Alexa Fluor® 488-conjugated secondary anti-mouse antibody diluted 1:400 for 30 min in an ice bath. Cells were then washed three times with saponin B, resuspended in 1 mL of 1% PFA and stored at 4°C until flow cytofluorimetry analysis. Flow cytometry was performed with a FACScalibur (Becton Dickinson), equipped with an air-cooled 15-mW Argon-ion laser, operating at 488 nm: 5(6)-FAM-SE green fluorescence (FL1) was collected using a 530 ± 30 bandpass filter. The data were collected using linear amplification for FSC and SSC, and logarithmic amplification for FL1. The data were then analyzed by using CellQuest software (Becton Dickinson).

Markers were used to identify positive cells. Results are represented as the geometric mean calculated on 20000 events and are the mean of three independent experiments.

3.11 Statistical analysis

Results of the hemolytic assay and of the cell-based ELISA are presented as mean ± SE of at least three independent experiments performed in triplicate. Linearity (r^2) of the calibration curve was estimated by linear regression analysis, using the GraphPad Prism software version 6.0 (GraphPad Prism; GraphPad Software, Inc.; San Diego, CA). Concentration-effect curves were compared by two-way ANOVA statistical analysis and Bonferroni post-test, and significant differences were considered at $p < 0.05$. EC_{50} (effective concentration giving 50% of maximal response) was calculated by non-linear regression using a four parameters curve-fitting algorithm while binding parameters (Kd and Bmax) by a one-site binding hyperbola nonlinear regression analysis using the GraphPad software, version 6.0 (Prism GraphPad, Inc.; San Diego, CA, USA). Correlation between Kd and Bmax values and correlation between the expression of the Na^+/K^+ ATPase with the Kd, Bmax and EC_{50} values were performed by non-parametric Spearman correlation using GraphPad software, version 6.0 (Prism GraphPad, Inc.; San Diego, CA, USA).

Hemolytic assay and cell-based ELISA were characterized according to the international principles described by the Eurachem Guide (Magnusson and Ornemark, 2014). Briefly, limit of detection (LOD) and quantitation (LOQ) were expressed as PLTX concentration corresponding to the average of 10 blank values plus 3 or 10 times the standard deviations, respectively. Accuracy was measured as % Bias (n=10), calculated as % difference between PLTX concentration measured by the assay and the theoretical concentration in the sample divided by PLTX theoretical concentration. Repeatability was expressed as relative standard deviation of repeatability (RSDr), measured as % ratio between the standard deviation of independent results and their mean value. Both independent results obtained by the same operator in one day (intra-assay RSDr; n=10) and within a 6-month period by different operators (inter-assay RSDr; n=10) were considered.

4. Results and discussion

4.1 Hemolytic assay

4.1.1 Storage of purified human erythrocytes

The human erythrocytes model was chosen due to the easy availability of human blood, rapid isolation of significant cell numbers, and low cost. The use of purified human erythrocytes poses the need for a medium suitable to preserve the cells. To this aim, three cell storage solutions were evaluated: Saline-Adenine Glucose-Mannitol Solution (SAGM), Adenine-Dextrose Solution (ADSOL) and D-PBS containing 1mM EDTA and 5mM glucose (PBS EDTA-glucose), as described in Section 3.2.2 (Lowe et al., 1973; Moore, 1991; Zehnder et al., 2008). Erythrocyte preservation in these solutions was evaluated daily for up to 36 days, monitoring the spontaneous hemolysis (measured spectrophotometrically as hemoglobin release) and the erythrocyte concentration determined by visual cell counting. Acceptable thresholds were constant cell concentration in the storage solution and optical densities lower than 0.5.

As shown in Figure 6A, the erythrocytes fragility increased over time, getting the maximum hemolysis after 10, 20, and 30 days for erythrocytes preserved in ADSOL, SAGM and PBS-EDTA-glucose, respectively. Hence, the resistance to lysis of red blood cells preserved in SAGM and ADSOL was lower than that of erythrocytes preserved in PBS-EDTA-glucose.

Only PBS-EDTA-glucose solution allowed maintenance of viable red blood cells suitable for the assay for up to 3 weeks (Figure 6B), instead of the other two storage solutions in which a decreased number of erythrocytes was observed only after 10 days post-purification. This result is probably due to the presence of crucial constituents providing the proper energy source to erythrocytes (glucose) and preventing coagulation (EDTA). Hence, these conditions allow to prepare a batch of human

erythrocytes suitable for the hemolytic assay for up to 3 weeks, reducing the working time and avoiding the necessity to purify the erythrocyte before each experiment.

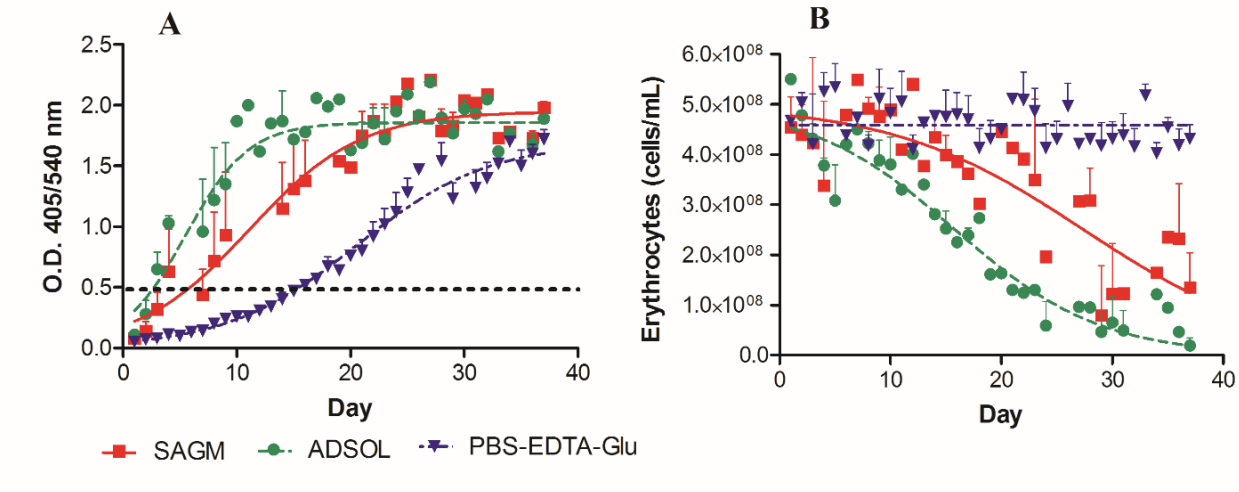

Figure 6*: Erythrocytes preservation. **A**: Spontaneous erythrocytes lysis monitored as hemoglobin release up to 36 days (optical density measured at 405/540 nm). The line at O.D. (optical density) equal to 0.5 defines the threshold indicating acceptable values. **B**: Erythrocytes preservation monitored as cells concentration up to 36 days. Each point represents the mean ± SE of 3 different measurements.*

4.1.2 Optimization of the hemolytic assay

The hemolytic assay was standardized considering different experimental parameters reported in previous published studies. In the first series of experiments, the hemolytic assay was carried out following the most recent published protocol, using human erythrocytes (Malagoli, 2007). Following Malagoli's protocol, the sensitivity of purified human erythrocytes to PLTX-induced hemolysis was compared to that of the whole human blood. The hemolytic activity of PLTX ($7.8x10^{-10}$-$5.0x10^{-8}$ M) towards purified human erythrocytes was significantly higher than that displayed by the whole human blood: 65% and 7% hemolysis were recorded at $5.0x10^{-8}$ M PLTX, respectively (Figure 7A).

The presence of borates (boric acid or sodium tetraborate: > $5.0x10^{-6}$ M) and calcium ions (> 2.0 x 10^{-5} M) in the buffer solution was reported to increase the hemolysis induced by PLTX, due to their ability to promote the interaction between the toxin and Na^+/K^+ ATPase (Ahnert-Hilger et al., 1982; Habermann, 1983). Thus, the hemolysis was evaluated using two buffers: (i) D-PBS + 1mM $CaCl_2$ + 1mM H_3BO_3 and (ii) D-PBS + 1mM $CaCl_2$ + 1mM $Na_2B_4O_7$. As shown in Figure 7B, no significant differences in PLTX-induced hemolysis were observed between buffer solution containing 1 mM H_3BO_3 and that containing 1 mM $Na_2B_4O_7$, in agreement with literature data, where H_3BO_3 or $Na_2B_4O_7$ are interchangeably used. Regarding Ca^{2+} ions, no significant differences were recorded between PLTX-induced hemolysis in D-PBS with or without $CaCl_2$ (Figure 7C). Indeed, the Ca^{2+} concentration in D-PBS solution (137 mM) is higher than that (>20 mM) reported to promote the interaction between the toxin and its target (Ahnert-Hilger et al., 1982). Thus, additional Ca^{2+} ions at millimolar concentrations in the D-PBS buffer solution containing 1 mM H_3BO_3 were not necessary to increase PLTX hemolytic activity. Based on the mechanism of action of the toxin (i.e. interaction with the Na^+/K^+ ATPase), the influence of Na^+ and K^+ ions on PLTX induced hemolysis was also evaluated. The presence of Na^+ ions ($1.8x10^{-4}$ M or $3.6x10^{-4}$ M NaCl) in the buffer solution was associated with a significant reduction of PLTX-induced hemolysis, probably due to the medium

hypertonicity causing erythrocytes shrinking and volume reduction (Kregenow, 1971) (Figure 7D). In contrast, while the K^+-free buffer containing H_3BO_3 did not significantly influence the hemolytic activity of PLTX, the latter was significantly increased using K^+-free buffer without H_3BO_3 (Figure 7E).

To further improve the assay sensitivity, the influence of incubation temperature was evaluated. After erythrocyte incubation with PLTX for 5 h at 41 °C, hemolysis was significantly higher than that recorded at 37°C, with EC_{50} values of $6.2x10^{-9}$ M (95% confidence intervals, CI = 5.3 - $7.2x10^{-9}$ M) and $4.9x10^{-8}$ M (95% CI = 4.1 - $5.9x10^{-8}$ M), respectively (Figure 7F). This result was in agreement with that reported by Habermann et al. (1981), suggesting that PLTX-induced hemolysis is temperature-dependent.

Overall, these results allowed a protocol optimization for the hemolytic assay, using purified human erythrocytes exposed to PLTX in a K^+-free D-PBS buffer at 41 °C for 5 h.

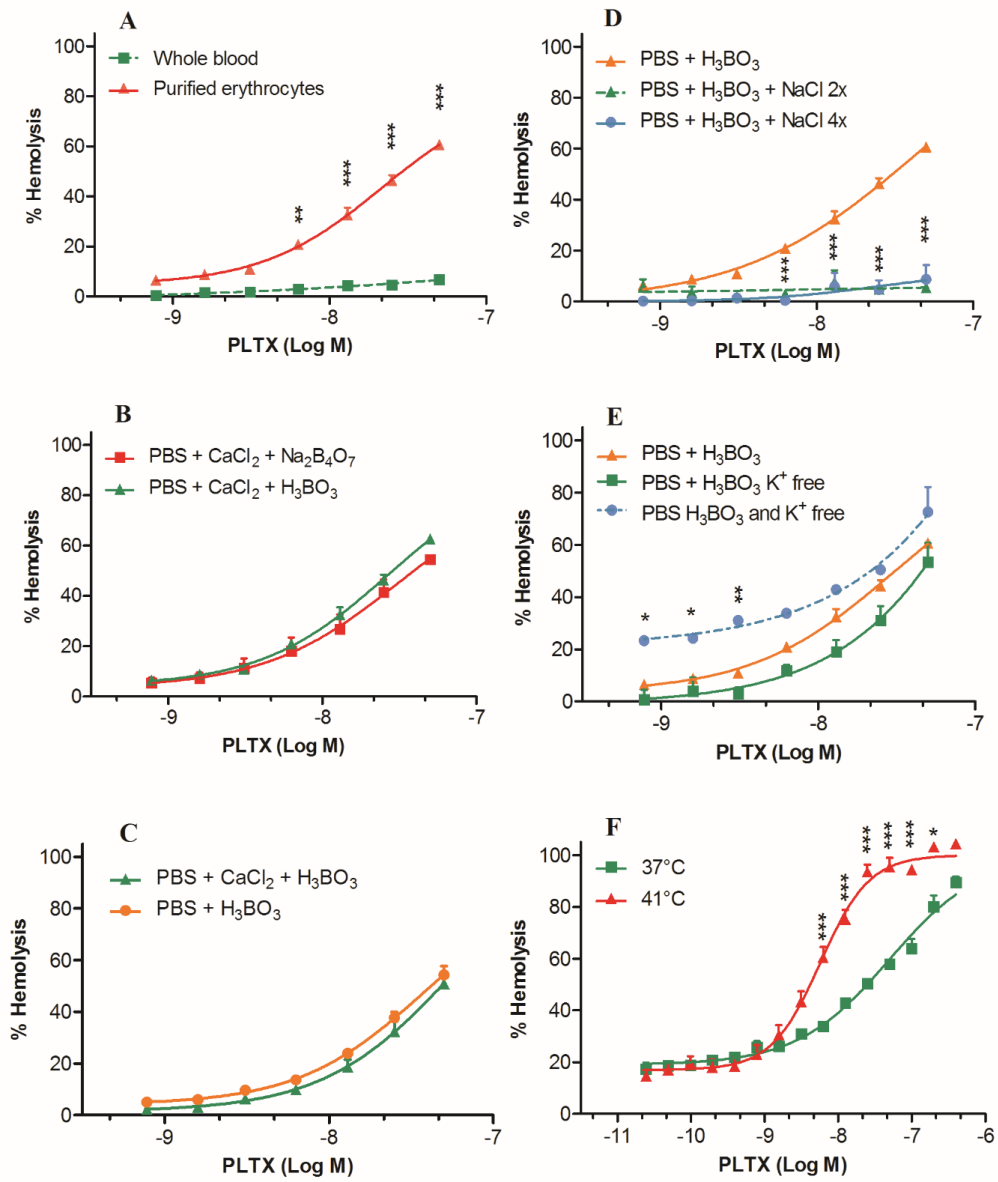

Figure 7*: Optimization of the hemolytic assay.* ***A****: PLTX-induced hemolysis using whole human blood or purified human erythrocytes.* ***B****: PLTX-induced hemolysis of human erythrocytes in presence of 1 mM boric acid or1 mM sodium tetraborate.* ***C****: PLTX-induced hemolysis of human erythrocytes with and without1 mM $CaCl_2$. D: PLTX-induced hemolysis of human erythrocytes with and without $1.8x10^{-4}$ M or $3.6x10^{-4}$ M NaCl, 2x or 4x.* ***E****: PLTX-induced hemolysis of human erythrocytes with and without K^+ ions (2.7 mM KCl, 8.1 mM KH_2PO_4).* ***F****: PLTX-induced hemolysis of human erythrocytes at 37 °C and 41 °C. Each point represents the mean ± SE of 3 different experiments. *p < 0.05; **p < 0.01; ***p < 0.001 (for D and E as compared to PBS + H_3BO_3; two-way ANOVA and Bonferroni post test).*

4.1.3 Characterization of the hemolytic assay

4.1.3.1 Calibration curve for PLTX

The optimized assay was subsequently characterized evaluating the limit of PLTX detection (LOD) and quantitation (LOQ), the accuracy, the repeatability and the specificity. Using the standardized hemolytic assay, the calibration curve for PLTX represented in Figure 8A was obtained. The working range for PLTX detection was $3.9x10^{-10}$ - $2.5x10^{-8}$ M, with an EC_{50} of 6.2 x 10^{-9} M, (95% CI = 5.3 - $7.2x10^{-9}$ M), while the limit of detection (LOD) and quantitation (LOQ) were $1.4x10^{-10}$ M (0.38 ng/mL) and $3.4x10^{-10}$ M (0.90 ng/mL), respectively.

Analyzing the working range by linear regression, plotting the theoretical toxin concentrations against the PLTX concentrations measured by the hemolytic assay, a good correlation coefficient was found (r^2 = 0.9979; n = 10) (Figure 8B). A mean Bias value (%) of -0.8% (range: -2.0% - 2.4%) highlights the accuracy of the measures (Table 1). Intra-assay and inter-assay repeatability were then evaluated. A good correlation was observed, with r^2 values of 0.9736 for intra assay (Figure 9A) and 0.9977 for inter-assay repeatability (Figure 9B). These data were confirmed by the intra-day and inter-day repeatability coefficients (relative standard deviation of repeatability, RSDr) of 15% (n = 10) and 6% (six months period, n = 10), respectively (Table 1).

The hemolytic effect of PLTX under these conditions was much higher than that reported by Malagoli (2007) and Taniyama et al. (2001): they recorded a maximum hemolysis lower than 50% at the highest tested PLTX concentrations (i.e. 103 and 102 ng PLTX/mL, corresponding to $3.7x10^{-6}$ M and $3.7x10^{-7}$ M PLTX, respectively). These concentrations were 1-2 orders of magnitude higher than the highest concentration of the assay working range determined by this study (i.e. $2.5x10^{-8}$ M, giving 94% of hemolysis). Thus, an increased PLTX-induced hemolysis was achieved lowering the

osmolarity of the working buffer (K^+ ions withdrawal) and increasing the incubation temperature (41 °C) in the optimized hemolytic assay protocol.

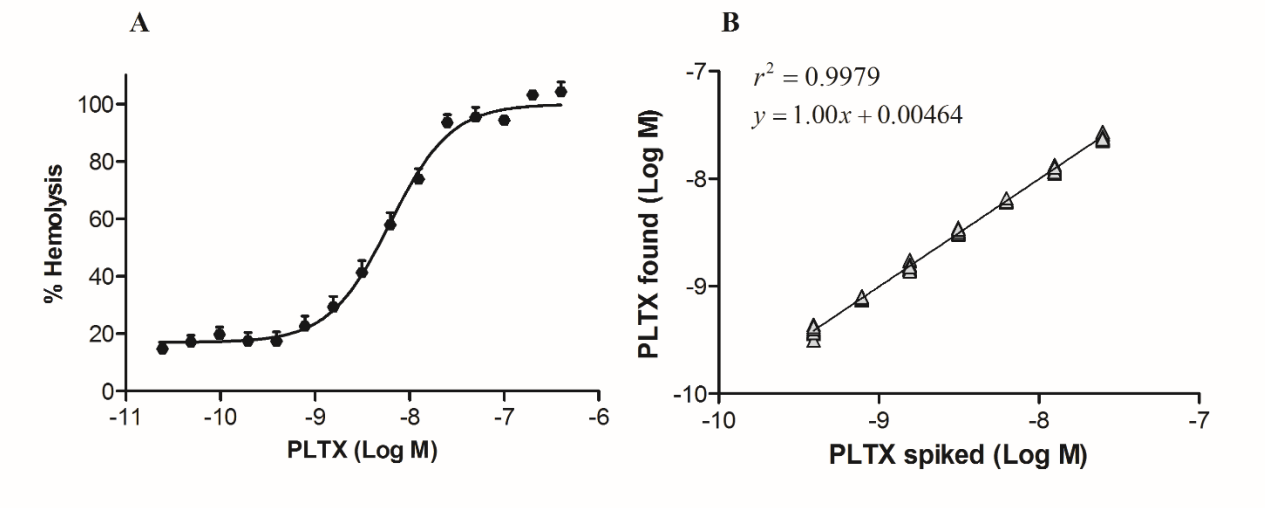

Figure 8: ***A***: *Calibration curve of the hemolytic assay for PLTX. Each point represents the mean ± SE of ten different experiments.* ***B****: Linear regression analysis performed within the working range of the hemolytic assay ($3.9x10^{-10}$ M - $2.5x10^{-8}$ M) by plotting the theoretical PLTX concentrations against the toxin concentrations measured by the hemolytic assay (n = 10).*

Table 1: *Bias values (%) for PLTX analysis, intra-day (n=10, 1 day) and inter-day (n=10, 6 months) repeatability (relative standard deviation of repeatability, RSDr %) and mean of PLTX concentrations measured by the assay.*

PLTX concentration (M)	*Bias* (%)	Intra-day repeatability		Inter-day repeatability	
		Mean (M)	RSDr %	Mean (M)	RSDr %
$3.91x10^{-10}$	-1.2	$4.55x10^{-10}$	17	$3.86x10^{-10}$	10
$7.81x10^{-10}$	-1.7	$7.60x10^{-10}$	12	$7.68x10^{-10}$	3
$1.56x10^{-9}$	-2.0	$1.63x10^{-9}$	20	$1.53x10^{-9}$	8
$3.13x10^{-9}$	2.4	$2.47x10^{-9}$	24	$3.24x10^{-9}$	7
$6.25x10^{-9}$	0.3	$6.51x10^{-9}$	12	$6.27x10^{-9}$	3
$1.25x10^{-8}$	-1.4	$1.28x10^{-8}$	8	$1.24x10^{-8}$	7
$2.50x10^{-8}$	-1.7	$3.18x10^{-8}$	14	$2.50x10^{-8}$	7
Mean	-0.8		15		6

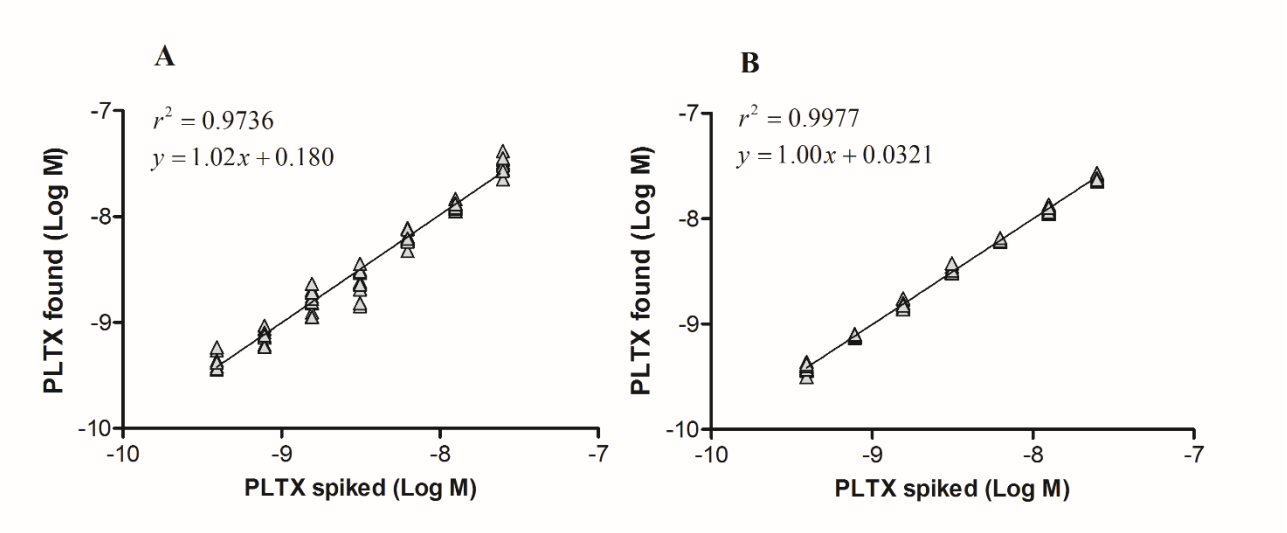

Figure 9: *Repeatability of the hemolytic assay. Linear regression analysis performed within the working range of the hemolytic assay ($3.9x10^{-10}$ M - $2.5x10^{-8}$ M) by plotting the theoretical PLTX concentrations against toxin concentrations measured by the hemolytic assay.* ***A:*** *Intra-day repeatability (n = 10).* ***B****: Inter-day repeatability (six months period, n = 10).*

4.1.3.2 Cross-reactivity with PLTX analogues

The hemolytic assay was then evaluated for its ability to detect some PLTX analogues and N-biotinyl PLTX within the working range set up for PLTX ($3.9x10^{-10}$ - $2.5x10^{-8}$ M). Although the hemolytic activity at nanomolar concentrations of 42*S*-OH-50*S*- PLTX (from *P. toxica*) was slightly lower than that of the same PLTX concentrations, its hemolytic potency (EC_{50} = $5.8x10^{-9}$ M, 95% CI = 4.1 - 8.2 $x10^{-9}$ M) was comparable to that of PLTX (EC_{50} = $6.2x10^{-9}$ M, 95% CI = 5.3 - $7.2x10^{-9}$ M) (Figure 10). The latter result was in agreement with a previous study demonstrating a similar hemolytic activity of the two compounds, using mouse erythrocytes (Tubaro et al., 2011a).

On the contrary, hemolysis induced by 42*S*-OH-50*R*-PLTX (a 42-OH-PLTX stereoisomer from *P. tuberculosa*) was significantly lower than that of PLTX (Figure 10), in agreement with its lower cytotoxic effects, previously observed on HaCaT cells (Ciminiello et al., 2014a). Also the hemolytic activity of OVTX-a and of a mixture of OVTXs (OVTX-a, -d and -e) was significantly lower than that of PLTX, similarly to their cytotoxicity toward skin keratinocytes, as recently demonstrated by Pelin et al. (2016). In contrast, the latter result was not in agreement with other studies hypothesizing that PLTX and OVTXs possess similar hemolytic activity (Brissard et al., 2014; Pezzolesi et al., 2012). However, these studies were carried out using sea urchins and *Ostreopsis ovata* extracts containing OVTX analogues different from OVTX-a, -d and -e as well as isobaric PLTX (Brissard et al., 2014; Pezzolesi et al., 2012). Thus, it can be speculated that those mixtures of toxins could display a hemolytic potency different from that of OVTX-a or of the other single OVTXs. Moreover, since complete studies on the matrices containing OVTXs were not carried out, a significant interference of the extract's matrix cannot be excluded.

In addition, the hemolytic potency of a semisynthetic PLTX derivative, biotinylated PLTX, was significantly lower than that of PLTX, inducing only 5% hemolysis at the highest concentration (2.5 $x10^{-8}$ M), while Ost-D did not induce hemolysis. Intriguingly, a biotin linked to the terminal PLTX

amino group reduces PLTX-induced hemolysis, indicating the importance of the primary amine for the hemolytic effect via Na^+/K^+-ATPase interaction. This finding agreed with previous evidences for N-acetyl-PLTX which biological activity via Na^+/K^+-ATPase was over 100 times weaker than that of the parent compound PLTX, tentatively due to a change in the global toxin conformation that prevents its dimerization (Kudo and Shibata, 1980; Ohizumi and Shibata, 1980; Inuzuka et al., 2008). Moreover, this result suggests that the functional hemolytic assay detects only biologically active PLTX analogues. In contrast, other nonfunctional analytical methods could detect also biologically inactive PLTX-like compounds (Boscolo et al., 2013), which might not contribute the whole toxic potential of PLTXs-contaminated seafood samples.

These results demonstrate that the hemolytic assay has a good sensitivity for PLTX and 42*S*-OH-50*S*-PLTX from *P. toxica*. On the contrary, the stereoisomer 42*S*-OH-50*R*-PLTX from *P. tuberculosa*, as well as OVTX-a and OVTXs mixture have lower hemolytic activity. Anyway, all the tested natural PLTX analogues exert hemolytic effects, which suggest a common mechanism of action.

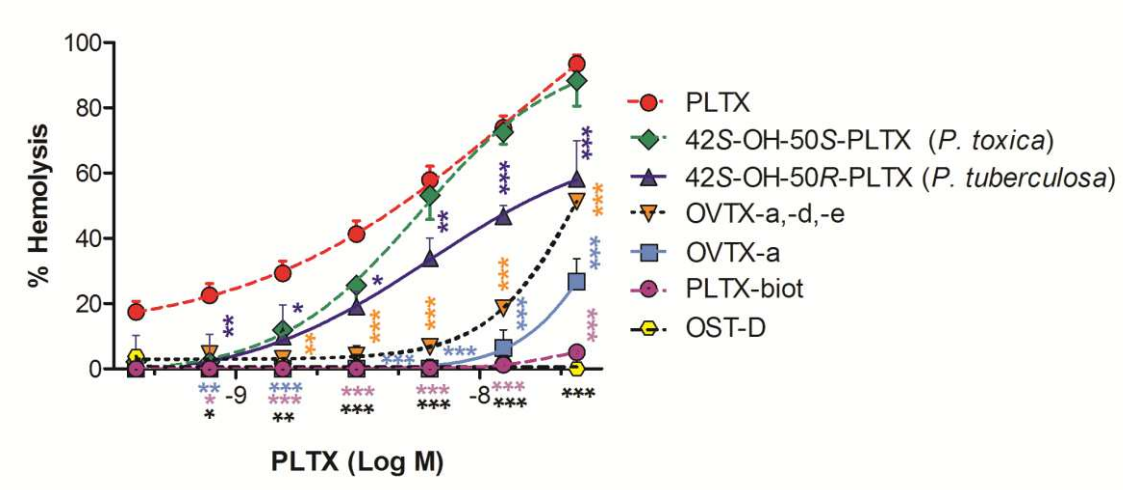

Figure 10: *Hemolytic activity of PLTX, its natural analogues and N-biotinyl-PLTX within the working range for PLTX ($3.9x10^{-10}$ M - $2.5x10^{-8}$ M). Each point represents the mean ± SE of 3 different experiments. *p < 0.05; **p < 0.01; ***p < 0.001 as compared to PLTX (two-way ANOVA and Bonferroni post test).*

4.1.3.3 Hemolysis neutralization

It is known that the cardiac glycoside ouabain (OUA), which binds to the same molecular target of PLTX, inhibits the *in vitro* effects of PLTX (Habermann and Chhatwal, 1982; Pelin et al., 2013a). Thus, to confirm the specific delayed hemolysis by PLTXs and exclude a possible hemolysis by other constituents of the samples under analysis, the standardized assay was carried out pre-incubating the red blood cells with 100 mM ouabain for 30 min at 37 °C (Aligizaki et al., 2008; Biré et al., 2013; Brissard et al., 2014; Gleibs et al., 1995; Malagoli D., 2007; Onuma et al., 1999; Pezzolesi et al., 2012; Riobó et al., 2006, 2008b, Taniyama et al., 2001, 2003; Volpe et al., 2014). Similarly, the mouse monoclonal anti-PLTX antibody (mAb-PLTX, 50 mg/mL) was used to neutralize the hemolysis induced by PLTX. The PLTX induced hemolysis was completely inhibited by OUA and only partially by the mAb-PLTX (Figure 11), in agreement with previous findings reported by Bignami, (1993).

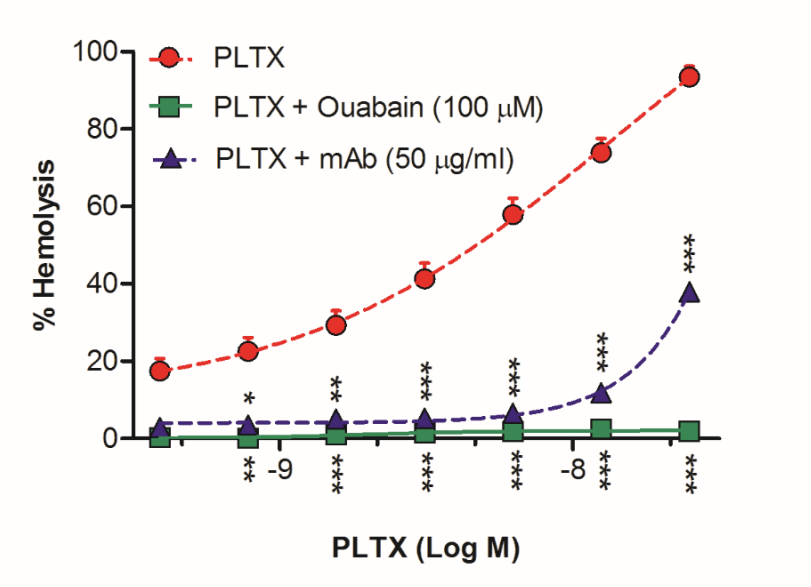

Figure 11: *Neutralization of PLTX-induced hemolysis within the working range of the hemolytic assay ($3.9x10^{-10}$ M - $2.5x10^{-8}$ M) by OUA and anti-PLTX monoclonal antibody, mAb. Each point represents the mean ± SE of 3 different experiments. *p < 0.05; **p < 0.01; ***p < 0.001 as compared to PLTX (two-way ANOVA and Bonferroni post test).*

4.1.3.4 Mussels matrix effect

To assess the interference of mussel matrix on PLTX-induced hemolysis, different extracts of *Mytilus galloprovincialis* were prepared. Firstly, 80%, 50% and 20% aqueous methanol and ethanol extracts of toxin-free mussels were tested after 1:1, 1:10, 1:50, 1:100 and 1:1000 (v/v) dilutions, to verify whether the matrix (mussel extracts) could produce false positive results. All the aqueous ethanol extracts required dilutions higher than 1:100 to avoid matrix effects in the hemolytic assay (Figure 12). On the other hand, no significant interferences were recorded for the 80% aqueous methanol extract at 1:50 dilution or 50% and 20% aqueous methanol extracts at 1:10 dilution (Figure 13). At these dilutions, also the solvents did not induce hemolysis (data not shown). Thus, the subsequent studies were carried out using the aqueous methanol extracts at these dilutions. Specifically, 80% aqueous methanol extract (1:50), as well as 50% and 20% aqueous methanol extracts (1:10) were spiked with known amounts of PLTX (final concentrations ranging from 3.9×10^{-10} M to 2.5×10^{-8} M). Then, the spiked extracts were analyzed by the hemolytic assay in comparison to the same PLTX concentrations without matrices.

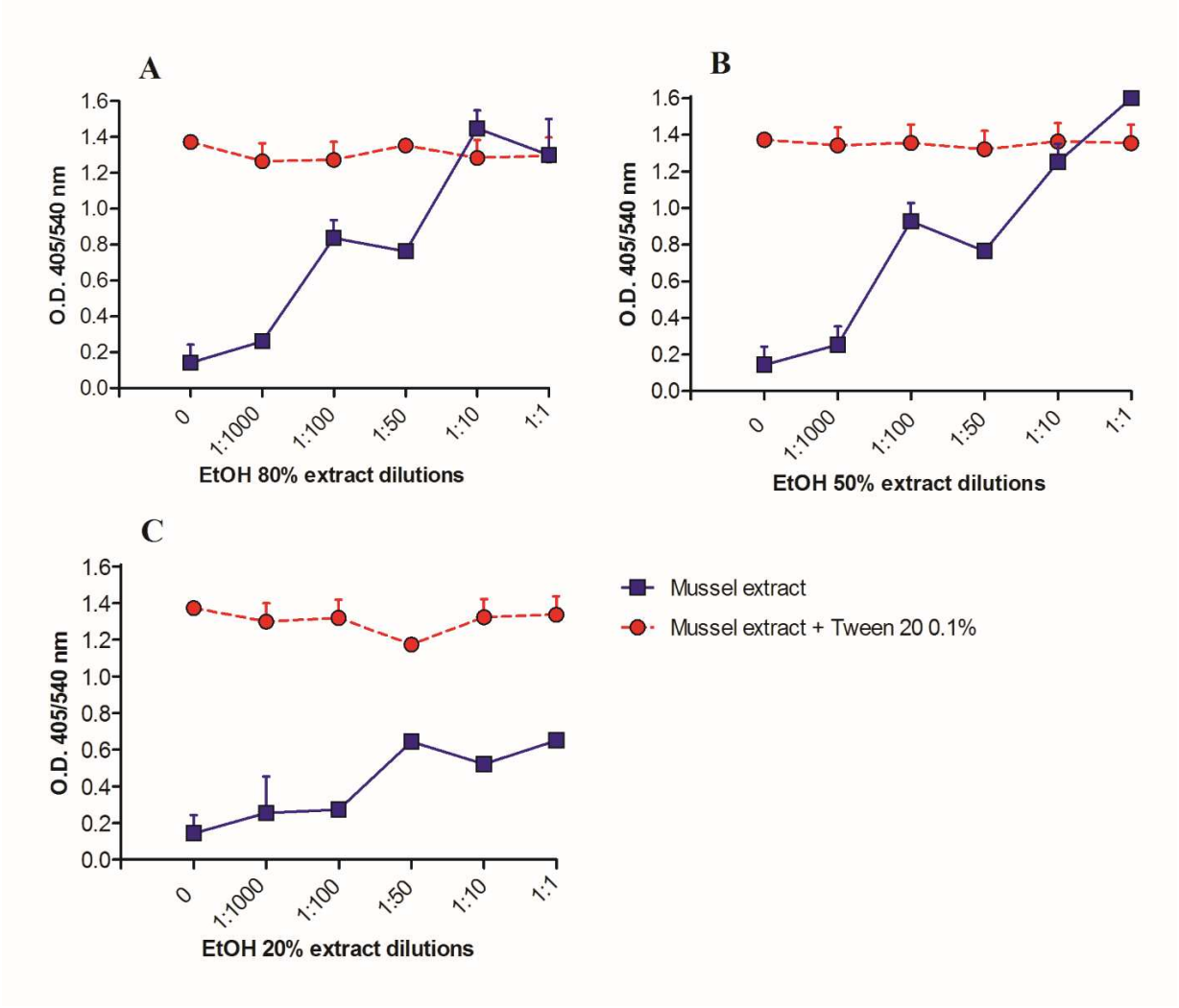

Figure 12: *Optical density values at 405/540 nm of supernatants from human erythrocytes suspensions exposed to different dilutions of aqueous ethanol mussel extracts (0.1 g mussel meat equivalents/mL) or aqueous ethanol mussel extracts containing 0.1% Tween 20.* ***A****: 80% aqueous ethanol extract;* ***B****: 50% aqueous ethanol extract;* ***C****: 20% aqueous ethanol extract. Each point represents the mean ± SE of 3 different experiments.*

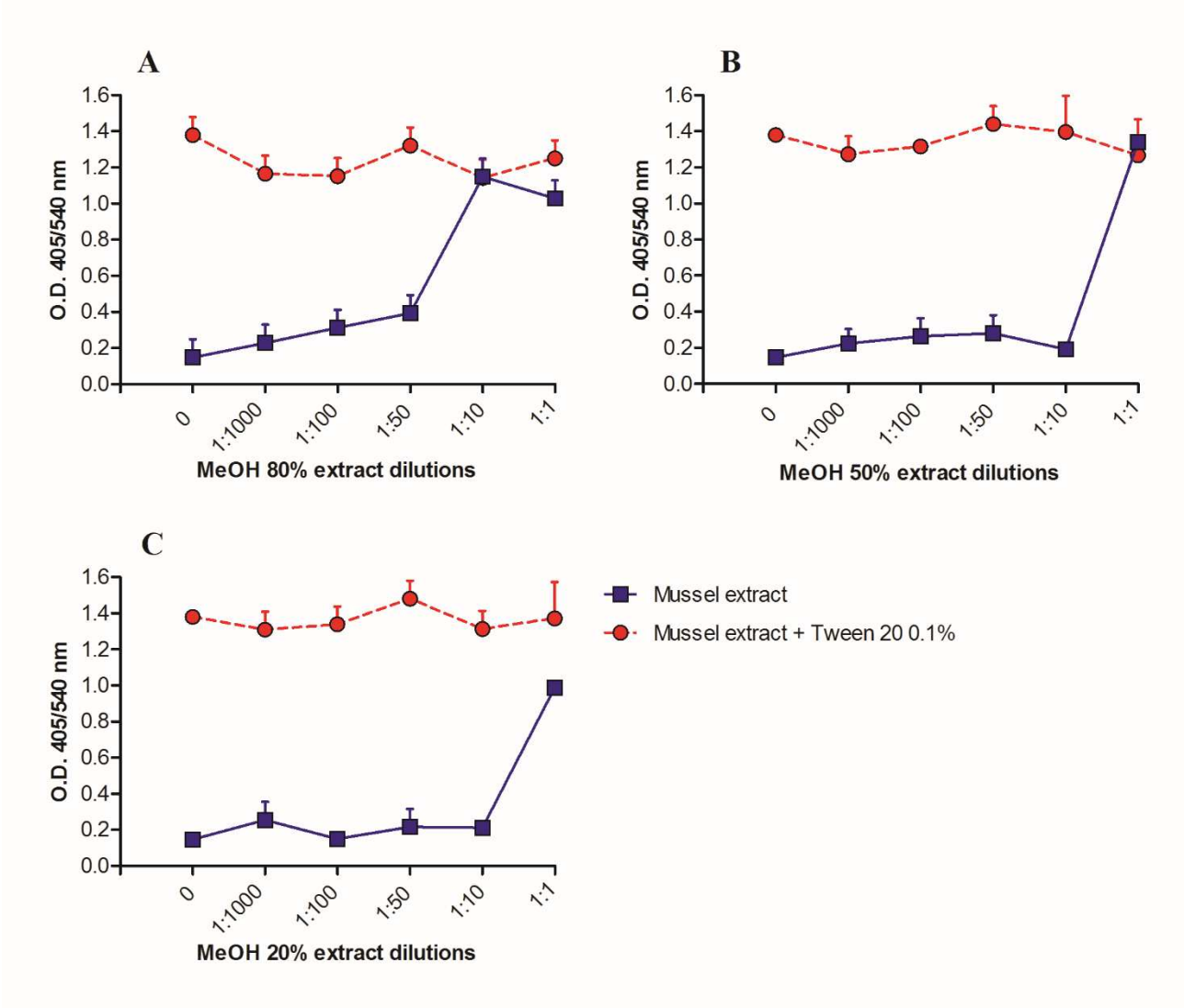

Figure 13: *Optical density values at 405/540 nm of supernatants from human erythrocytes suspensions exposed to different dilutions of aqueous methanol mussel extracts (0.1 g mussel meat equivalents/mL) and aqueous methanol mussel extracts containing 0.1 % Tween 20.* ***A****: 80 % aqueous methanol extract;* ***B****: 50 % aqueous methanol extract;* ***C****: 20 % aqueous methanol extract. Each point represents the mean ± SE of 3 different experiments.*

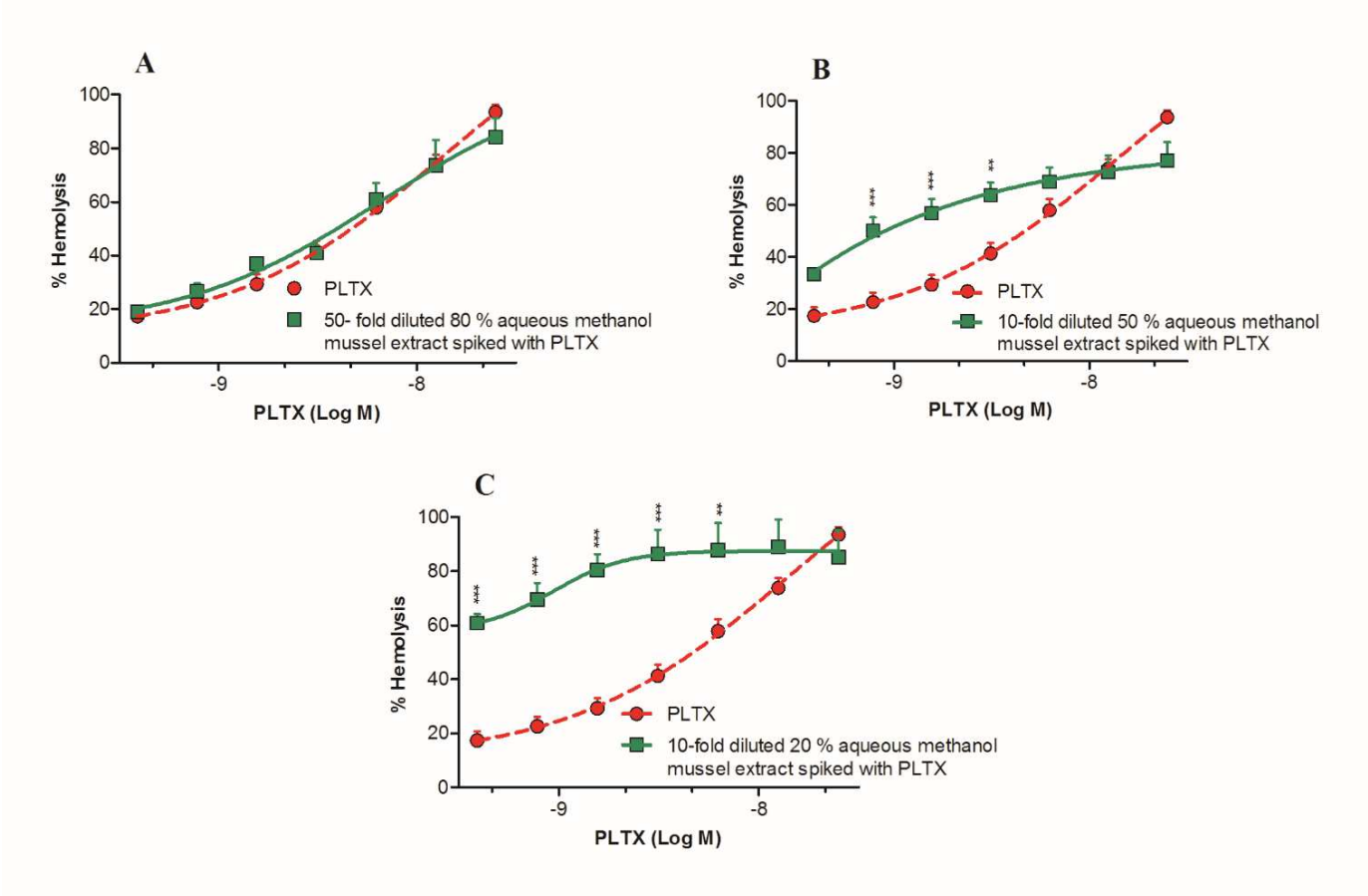

Figure 14: *Evaluation of mussels matrix effect.* ***A****: Comparison between PLTX calibration curve without matrix and 50-fold diluted 80 % aqueous methanol mussel extract spiked with PLTX;* ***B****: Comparison between PLTX calibration curve without matrix and 10-fold diluted 50 % aqueous methanol mussel extract spiked with PLTX;* ***C****: Comparison between PLTX calibration curve without matrix and 10-fold diluted 20 % aqueous methanol mussel extract. Each point represents the mean ± SE of 3 different experiments. **p < 0.01; ***p < 0.001 as compared to PLTX (two-way ANOVA and Bonferroni post test).*

The extract which did not interfere with the hemolytic assay was the 80% aqueous methanol extract diluted 1:50 (Figure 14). The most suitable solvent for PLTX extraction from mussels is 80 % aqueous methanol, giving 90-100% toxin recovery as recorded by LC-HRMS and a sandwich ELISA (Ciminiello et al., 2011; Boscolo et al., 2013). Thus, 80% aqueous methanol at 1:50 dilution was subsequently used for the matrix effect study.

Figure 15 shows the results of the linear regression analysis carried out comparing the theoretical PLTX concentrations in the spiked extract to those measured by the hemolytic assay. The LOQ for PLTX in the mussels extract was 1.3 ng/mL, corresponding to 13 µg/kg meat. Considering the 1:50 dilution, the LOQ for PLTX in mussels corresponds to 650 µg/kg meat, a value about 20 times higher than the maximum limit suggested by EFSA (30 µg PLTXs/kg meat) (EFSA, 2009). Moreover, the linear regression analysis yielded a correlation coefficient ($r^2 = 0.9259$) and a Bias range from -27.0 to 33.6% (mean Bias = 3.7%, Table 2), suggesting high dispersion of the data, low accuracy and precision of the measurement. Thus, the standardized and characterized hemolytic assay suffers from a significant mussel matrix effect, which does not allow PLTX quantitation in *Mytilus galloprovincialis* at concentrations lower than that proposed by EFSA. Interestingly, a significant interference by mussels matrix was recently observed also for a biosensor exploiting LDH release from sheep erythrocytes as hemolysis parameter to quantify PLTX (Volpe et al., 2014): similarly to our study, due to the significant matrix effect, a 1:50 dilution of the mussels extract was required to quantify PLTX in mussels, not meeting the EFSA requirements (Volpe et al., 2014). Intriguingly, the observed interference of the mussels extract is not due to the solvent used for extraction (i.e. 80% aqueous methanol) since the relevant mussels-free and PLTX-free solvents did not induce hemolysis (data not shown). On the contrary, low dilutions of mussels methanol extract (i.e. 1:1 or 1:10) displayed a hemolytic activity higher than that of higher extract dilutions, sometimes comparable to that of the positive control (0.1% Tween 20). Hence, the significant matrix effect could be due to hemolytic compounds different from PLTX, that could be extracted from mussels by 80 % aqueous methanol. Indeed, a series of potentially hemolytic compounds, such as glycoglycerolipids, lysophospholipids and unsaturated fatty acids, are known constituents of mussels edible parts. The concentration of these compounds in mussel meat could be also influenced by season, living site of mussels, mussels species, dietary composition of phytoplankton as well as temperature and enzymes

action during transportation and storage of seafood (Colles and Chisolm, 2000; Facchini et al., 2016; Ginsburg et al., 1989; Parrish et al., 1998; Pleissner and Eriksen, 2012).

All together, these results suggest that PLTX-induced erythrocytes lysis is not a suitable endpoint for the toxin quantitation in mussels at levels below the maximum limit suggested by EFSA (EFSA, 2009). In addition, since the hemolytic assay has been used worldwide to detect PLTXs in different field marine samples (also concomitantly to potential human poisonings ascribable to PLTXs), those data should be carefully considered because of possible matrices effect that could have affected the analytical outcomes.

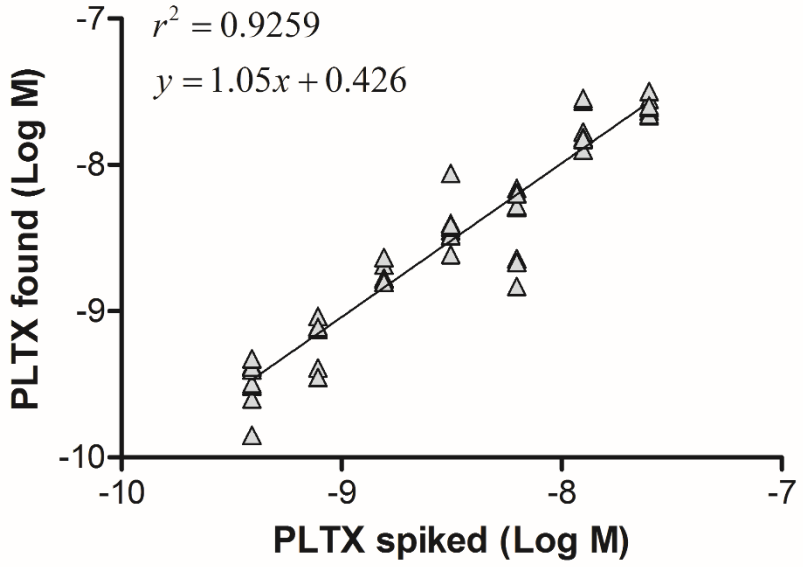

Figure 15: *Mussels (Mytilus galloprovincialis) matrix effect. Linear regression analysis within the working range of the hemolytic assay ($3.9x10^{-10}$ M - $2.5x10^{-8}$ M) performed on 80% aqueous methanol mussels extracts diluted 1:50. Linear regression analysis was performed by plotting the theoretical PLTX concentrations against toxin concentrations measured by the hemolytic assay.*

Table 2: *Bias values (%) for PLTX detected in 80% aqueous methanol mussels extracts spiked with the toxin after 1:50 dilution in comparison to the theoretical PLTX concentrations (n=10).*

PLTX concentration (M)	*Bias* (%)
$3.91x10^{-10}$	-13.8
$7.81x10^{-10}$	-12.8
$1.56x10^{-9}$	12.9
$3.13x10^{-9}$	31.7
$6.25x10^{-9}$	-27.0
$1.25x10^{-8}$	33.6
$2.50x10^{-8}$	0.9
Mean	3.7

4.1.3.5 Microalgae matrix effect and toxin recovery

To assess the suitability of the hemolytic assay to quantify PLTX in microalgae samples, the interference of microalgae matrix on PLTX-induced hemolysis and PLTX recovery from microalgae were evaluated. Different dilutions (undiluted, 1:1, 1:5, 1:10 and 1:100) of a 50% aqueous methanol *Coolia monotis* extract (obtained as described in section 3.5) were spiked with known concentrations of PLTX (from $3.9x10^{-10}$ M to $2.5x10^{-8}$ M) and analyzed by the hemolytic assay. The relevant hemolytic activity was then compared to that obtained by the same PLTX concentrations without matrices. *Coolia monotis* often co-occur with *O. ovata* in the Mediterranean Sea (Monti et al., 2007; Pagliara and Caroppo, 2012; Penna et al., 2005; Vila et al., 2001), and for this reason it has been chosen as matrix to evaluate the interference of microalgae extract on PLTX-induced hemolysis.

As shown in Figure 16**,** the minimum extract dilution that did not interfere with the hemolytic assay was 1:10. The linear regression analysis, performed by plotting the theoretical PLTX concentrations in the spiked extract after 10-fold dilution against those measured by the hemolytic assay (Figure 17), revealed a good correlation coefficient (r^2=0.9830) and a *Bias* ranged from -3.7 to 14.4% (mean *Bias*=1.6%; Table 3).

The LOQ for PLTX in microalgae extract was 0.83 ng/mL. Considering the extraction procedure and the minimum extract dilution that did not interfere with the assay, this value corresponds to 0.03 pg of PLTX equivalents/cell. The sensitivity of the hemolytic assay to quantify PLTX in microalgae sample was more than 10 times higher than that of the sandwich ELISA (LOQ = 9.6 ng/mL) developed by Boscolo et al. (2013).

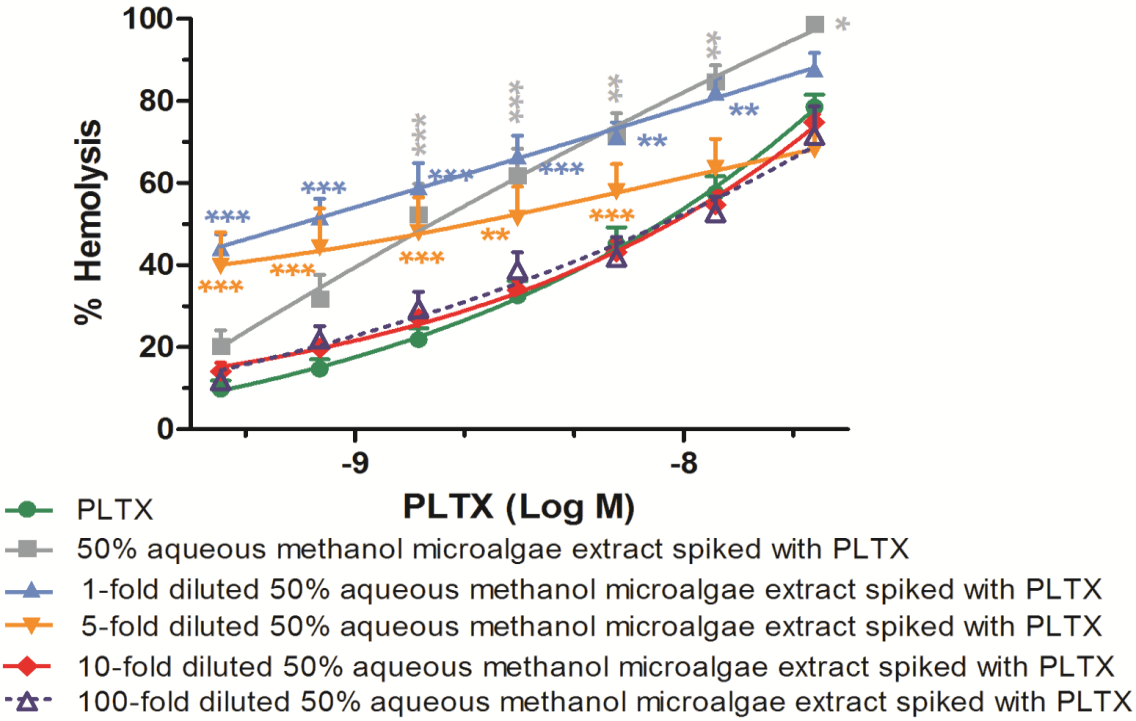

Figure 16: *Evaluation of microalgae matrix effect. Comparison between PLTX calibration curve without matrix and undiluted, 1-fold, 5-fold, 10-fold and 100-fold diluted 50 % aqueous methanol microalgae extract spiked with PLTX. Each point represents the mean ± SE of 3 different experiments. *p < 0.05; **p < 0.01; ***p < 0.001 as compared to PLTX (two-way ANOVA and Bonferroni post test).*

Due to its high sensitivity, the hemolytic assay can quantify PLTXs in microalgae at concentrations lower than those usually detected in natural samples in the Mediterranean Sea, ranging from 0.4 pg/cell to 75 pg/cell (Accoroni et al., 2011; Aligizaki et al., 2008; Bellocci et al., 2008; Brissard et al., 2014; Ciminiello et al., 2008, 2012b; Honsell et al., 2011).

Although the hemolytic assay is not able to distinguish PLTX from its analogues, this method has been widely used to detect PLTXs both in natural and cultured *Ostreopsis* ssp. samples, with a confirmatory analysis by inhibition of PLTX-induced hemolysis using OUA (Aligizaki et al., 2008;

Nascimento et al., 2012; Penna et al., 2005; Pezzolesi et al., 2012; Rhodes et al., 2000; Riobó et al., 2006; Taniyama et al., 2003). However, a full characterization of an *Ostreopsis* extract matrix effect in the hemolytic assay has never been done. This is the first report in which the interference by microalgae extract on PLTX quantitation by the hemolytic assay was fully investigated.

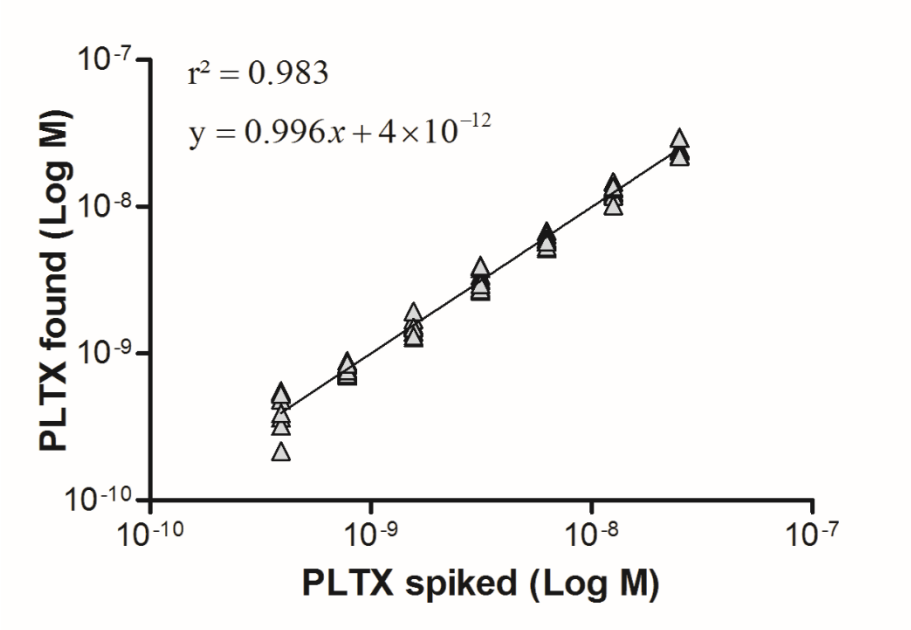

Figure 17: *Microalgae matrix effect. Linear regression analysis within the working range of the hemolytic assay ($3.9x10^{-10}$ M - $2.5x10^{-8}$ M) performed on 50% aqueous methanol microalgae extracts diluted 1:10. Linear regression analysis was performed by plotting the theoretical PLTX concentrations against toxin concentrations measured by the hemolytic assay*

Table 3: *Bias values (%) for PLTX detected in 50% aqueous methanol microalgae extracts spiked with the toxin after 1:10 dilution in comparison to the theoretical PLTX concentrations (n=10).*

PLTX concentration (M)	*Bias* (%)
$3.91x10^{-10}$	14.4
$7.81x10^{-10}$	0.3
$1.56x10^{-9}$	-2.2
$3.13x10^{-9}$	2.8
$6.25x10^{-9}$	-3.7
$1.25x10^{-8}$	0.4
$2.50x10^{-8}$	-0.4
Mean	1.6

PLTX recovery from microalgae was evaluated spiking the relevant samples with known concentrations of PLTX (0.094 pg/cell, 0.019 pg/cell, 0.004 pg/cell; $1x10^{-8}$ M, $2x10^{-9}$ M, $4x10^{-10}$ M) before the extraction. The percentage of toxin recovery and the coefficient of variability have been calculated and reported in Table 4. The toxin recovery from microalgae was around 100% (range: 80.9% - 106.4%; coefficient of variability: 7% - 16%), demonstrating both the extraction efficiency and the hemolytic assay accuracy to quantify PLTXs in microalgae. The toxin recovery from algae was comparable (95.6 – 105.5%) to that recorded by Boscolo et al. (2013) using the same extraction procedure and analyzing the extracts by an indirect sandwich ELISA.

Table 4: *Recovery of PLTX from microalgae determined by the hemolytic assay.*

PLTX concentration (M)	Recovery (%)	Coefficient of variability (%)	n° replica
$4.0x10^{-10}$	105.1	16	3
$2.0x10^{-9}$	106.4	10	3
$1.0x10^{-8}$	80.9	7	3

4.1.3.6 Improvements of the hemolytic assay

Since the sensitivity of erythrocytes to PLTX hemolysis varies between species, depending on intracellular K^+ concentration (Habermann et al., 1981), hemolysis using human red blood cells was compared to that of sheep and pig erythrocytes. Using pig erythrocytes, PLTX hemolytic potency (EC_{50} = 4.2 x10^{-10} M, 95 % CI = 2.7x10^{-10} - 6.7x10^{-10} M) was increased by more than 14 times higher than that recorded in human red blood cells (EC_{50} = 6.2x10^{-9} M, 95% CI = 5.3 - 7.2x10^{-9} M). Moreover, PLTX hemolytic potency on sheep erythrocytes (EC_{50} = 1.4x10^{-9} M, 95 % CI = 7.5x10^{-10} - 2.7x10^{-9} M) was more than 4 times higher than that recorded in human erythrocytes (Figure 18). However, problems related to the availability of pig and sheep erythrocytes and their difficult preservation limit their use.

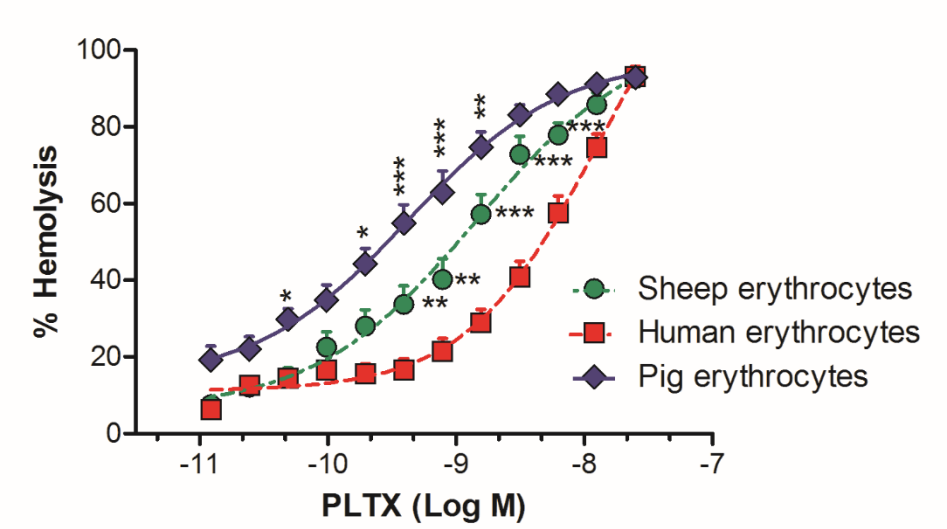

Figure 18: *PLTX-induced hemolysis in human, sheep or pig erythrocytes. Each point represents the mean ± SE of 3 different experiments. Statistical differences: *p <0.05; **p < 0.01; ***p < 0.001 as compared to human erythrocytes (two-way ANOVA and Bonferroni post test).*

4.2 Cell-based ELISA

4.2.1 Development of the cell-based ELISA

Starting from recently published data by our research group, concerning the characterization of PLTX binding to intact HaCaT skin keratinocytes using a monoclonal anti-PLTX antibody (Pelin et al., 2013a), a cell-based immunoenzymatic assay (cell-based ELISA) for PLTX quantitation in mussels was developed and characterized according to the international principles reported in Eurochem Guide (Magnusson and Ornemark, 2014). The assay is based on PLTX binding to its target, the Na^+/K^+-ATPase on HaCaT keratinocytes, and its quantitation using a monoclonal mouse anti-PLTX antibody (primary antibody) targeted by a horseradish peroxidase (HRP)-conjugated secondary anti-mouse immunoglobulin G (IgG; secondary antibody). The cell-based ELISA was developed considering the following parameters: i) different fixative solutions and incubation temperature of HaCaT cells with the primary and secondary antibodies; ii) interchange of the fixation phase and the treatment of cells with PLTX; iii) different blocking agents; iv) primary antibody dilutions.

As shown in Figure 19, exposure of HaCaT cells with increased concentrations of PLTX ($4.1x10^{-11}$ M – $1.0x10^{-8}$ M) for 10 minutes, followed by incubation with the primary (1 h) and secondary (1 h) antibodies at increasing temperatures up to 50° C, leads to an increased detected signal (optical density, O.D.), which subsequently decreased at higher temperatures. This result was recorded using different cell fixing agents (4% paraformaldehyde, PFA; 4% PFA and 1 % glutaraldehyde, Glut; neutral-buffered formalin, NBF).

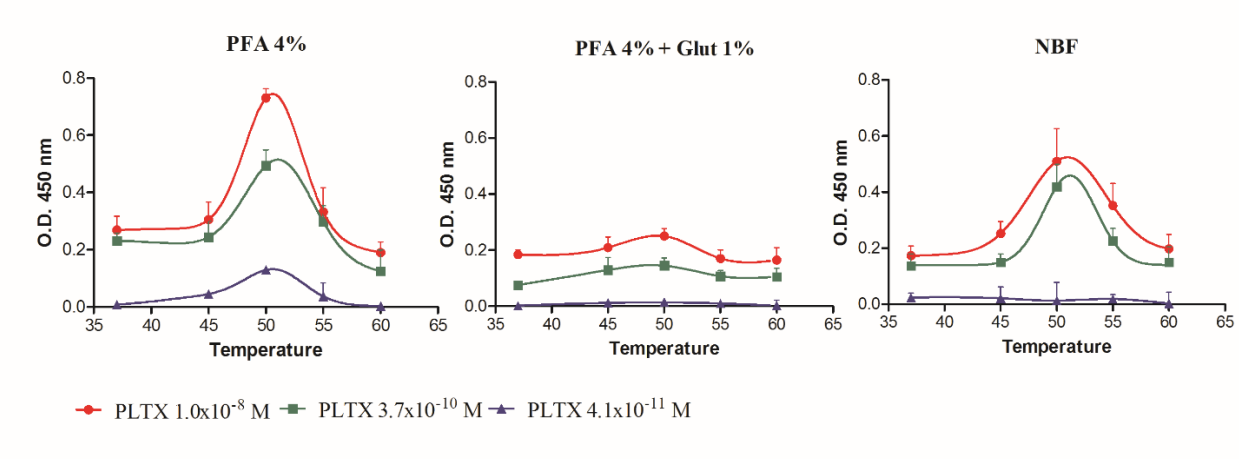

Figure 19: *Influence of the temperature during cells incubation with the antibodies on the assay signal, using three fixative solutions (4% paraformaldehyde, PFA 4%; 4% paraformaldehyde and 1% glutaraldehyde, PFA 4% + Glut 1%; neutral-buffered formalin, NBF). Each point represents the mean ± SE of 3 experiments.*

However, at 50° C, the highest signal was recorded using 4 % PFA, following by NBF (significant differences starting from $1.1x10^{-9}$ M PLTX, $p<0.05$) and 4 % PFA + 1 % glutaraldehyde (significant differences starting from $1.2x10^{-10}$ M PLTX, $p<0.01$) (Figure 20). Summarizing, an increased signal was obtained using 4% PFA as fixative solution and incubating the primary and secondary antibodies at 50 °C.

The decreased signal recorded increasing the antibodies incubation temperature is probably due to a thermal denaturation of the antibodies, that occur starting from 55 °C (Hartmann et al., 2004). Regarding the fixation phase, it allows to preserve cellular architecture to help them to withstand subsequent processing. Formaldehyde is one of the most used fixatives due to its handling, high degree of accuracy and adaptability. Aldehydes act by cross-linking proteins reacting with primary amines to form Schiff bases and with amides to form hydroxymethyl derivatives. Moreover, formaldehyde diffuses easily into the cells, permitting an optimal fixation (Thavarajah et al., 2012).

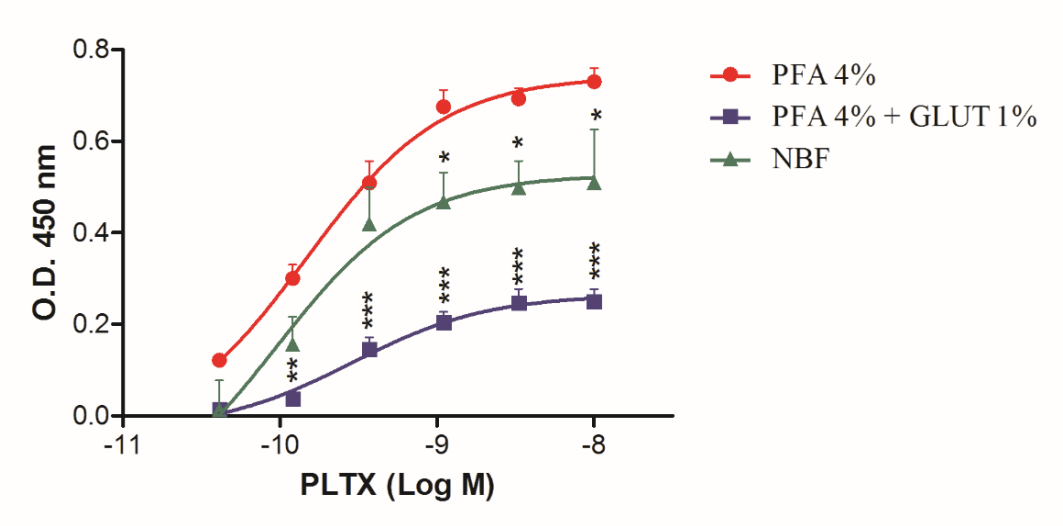

Figure 20: *Influence of the fixative solutions on the assay signal with antibodies incubation at 50 °C. Each point represents the mean ± SE of 3 experiments. Statistical differences: *p <0.05; **p < 0.01; ***p < 0.001 as compared to PFA 4% (two-way ANOVA and Bonferroni post test).*

The interchange between the fixation phase and the treatment of keratinocytes with PLTX was then evaluated to obtain fixed cells, which would allow to carry out the cell-based ELISA also in non-sterile conditions, making the assay suitable to use within monitoring program. With this aim, cells were firstly fixed with 4% PFA for 30 minutes and then exposed to increased concentration of PLTX ($4.1x10^{-11}$ M – $1.0x10^{-8}$ M). Figure 21 shows the concentration-dependent curve for PLTX recorded in these conditions in comparison to that obtained under standard conditions. As shown, the interchange between the fixation phase and the treatment of cells with PLTX and the significant decrease of the O.D. values obtained moving up the fixation phase before the exposure with the toxin was not efficient, probably due to the inability of PLTX to bind to the Na^+/K^+ ATPase of fixed cells. Hence, the subsequent experiments were carried out exposing the keratinocytes with PLTX before cells fixation with 4% PFA.

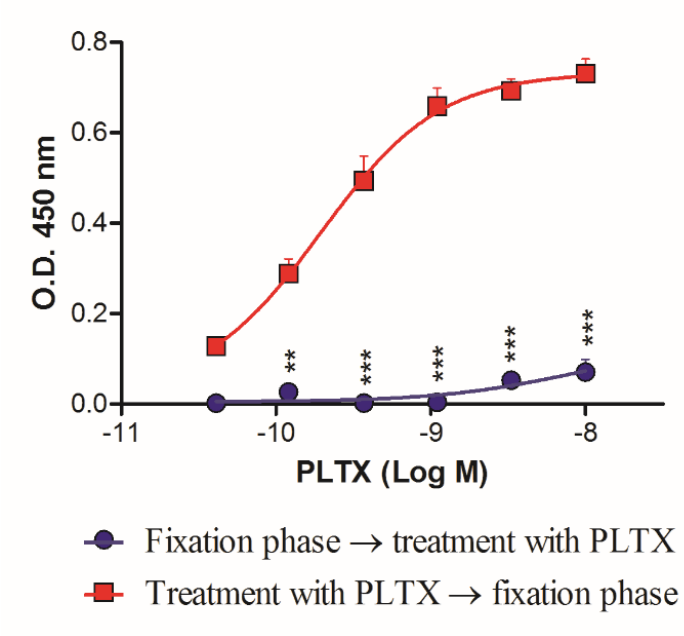

Figure 21: *Temporal change between the fixation phase (4% PFA) and cells treatment with PLTX ($4.1x10^{-11}$ M – $1.0x10^{-8}$ M). Each point represents the mean ± SE of 3 experiments. Statistical differences: **p < 0.01; ***p < 0.001 as compared to normal conditions (Treatment with PLTX → fixation phase) (two-way ANOVA and Bonferroni post test).*

Once established the best antibodies incubation temperature (50 °C) and the best fixative solution (4% PFA), which allowed to a significant increase of the cell-based ELISA signal, the influence of different blocking agents on the assay signal was also evaluated. Figure 22 represents a PLTX calibration curve ($4.1x10^{-11}$ M – $1.0x10^{-8}$ M) obtained using three blocking agents. The highest signal was recorded using a TBS solution (50 mM Trizma base, 0.15 M NaCl) containing 2 % bovine serum albumin (BSA), 0.2 % Tween 20 and 10 % horse serum as blocking agent. A significant decreased signal (starting from 1.2 x 10^{-10} M PLTX) was observed using a TBS solution containing 0.2 % Tween 20 and 1 % or 2 % dried milk powder.

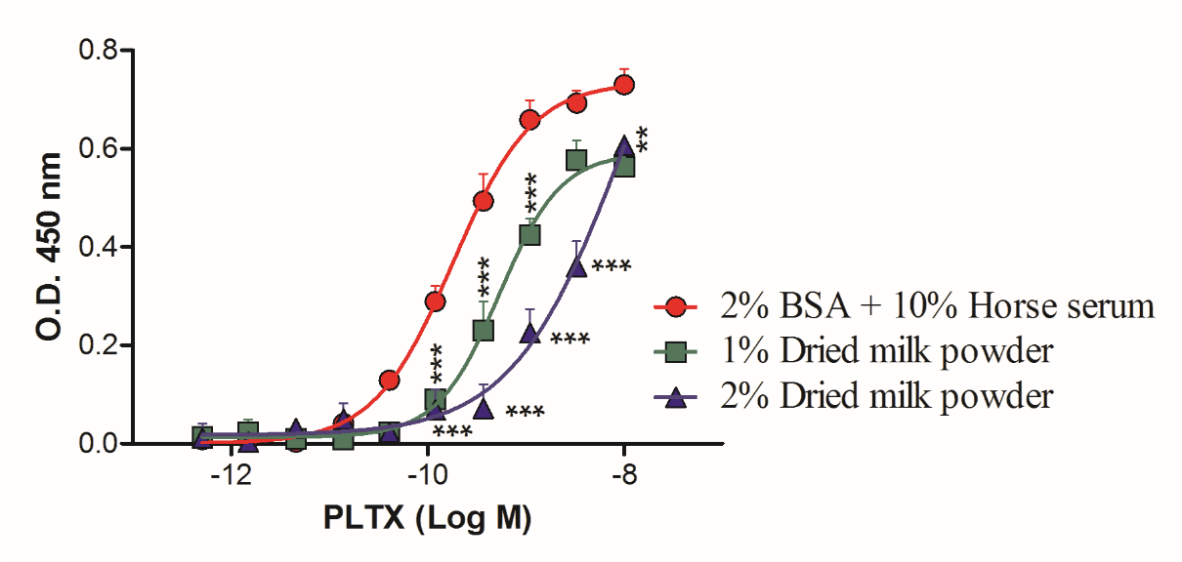

Figure 22: *Influence of three blocking agents on the assay signal. Each point represents the mean ± SE of 3 experiments. Statistical differences: **p < 0.01; ***p < 0.001 as compared to 2% BSA + 10% horse serum (two-way ANOVA and Bonferroni post test).*

Subsequently, to further increase the signal/background ratio, the influence of the primary antibody dilution on the assay signal was evaluated. As shown in Figure 23, no significant differences were observed between three primary antibody (mAb) dilutions tested (1:750, 1:1500 and 1:3000). Thus, the cell-based ELISA was carried out using the highest dilution (1:3000; 0.5 µg/mL) of the primary antibody.

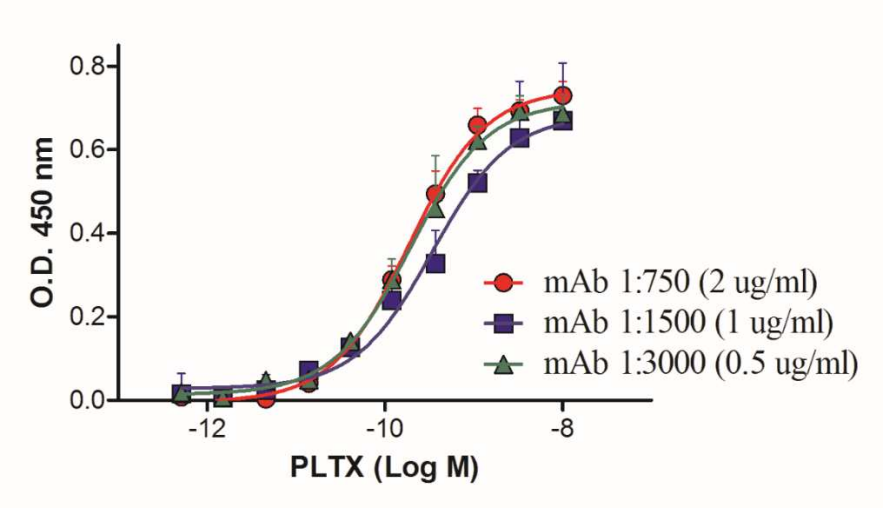

Figure 23: *Influence of the primary antibody dilution on the assay signal. Each point represents the mean ± SE of 3 experiments.*

Hence, the protocol of the developed cell-based ELISA consisted in: (1) the use of HaCaT cells exposed for 10 min to increased concentration of PLTX ($5.1x10^{-13}$-$1.0x10^{-8}$ M); (2) cells fixing for 30 min with 4% PFA; (3) cells blocking for 30 min in TBS buffer containing 2% BSA, 0.2% Tween 20 and 10% horse serum; (4) cells incubation with 0.5 µg/mL mouse anti-PLTX mAb (primary antibody) for 1 h at 50 °C under gentle agitation; (5) three-times washing with phosphate buffered saline (PBS) containing 0.1 % Tween 20 (PBS/Tw) followed by three washes with PBS; (6) incubation of the cells to 1:6000 HRP-conjugated antimouse IgG (secondary antibody) for 1 h at 50 °C under gentle agitation; (7) three-times washing with PBS/Tw and three washes with PBS; (8) cells incubation with tetramethylbenzidine (TMB) and hydrogen peroxide substrate (60 µL/well) for 20 min; (9) stopping of the colorimetric reaction by the addition of 1 M H_2SO_4 (30 µL/well); (10) measure of the optical density at 450 nm.

4.2.2 Characterization of the cell-based ELISA

4.2.2.1 Calibration curve for palytoxin

The cell-based ELISA was subsequently characterized evaluating the LOD and LOQ for PLTX, as well as the assay accuracy, repeatability and specificity. The calibration curve for PLTX reported in Figure 24A was obtained: the working range for PLTX detection was $1.4x10^{-11}$ M - $1.1x10^{-9}$ M, while the LOD and LOQ were $1.2x10^{-11}$ M (32.2 pg/mL) and $2.8x10^{-11}$ M (75.0 pg/mL), respectively. The working range was analyzed by linear regression, plotting the theoretical PLTX concentrations submitted to the assay against the measured toxin concentrations, calculating a good correlation coefficient ($r^2 = 0.9894$; n = 10) (Figure 24B). A mean Bias value (%) of 2.5% (range: -5.1% - 9.8%) was obtained (Table 5).

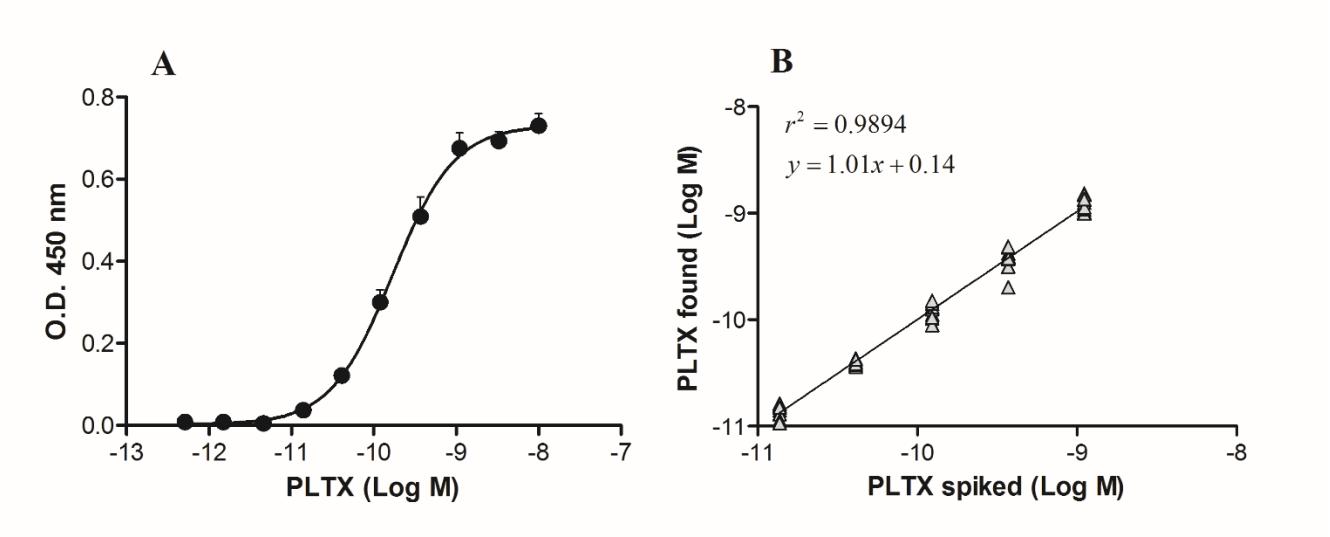

Figure 24: ***A***: *Calibration curve of the cell-based ELISA for PLTX. Each point represents the mean ± SE of ten different experiments.* ***B****: Linear regression analysis performed within the working range of the cell-based ELISA assay ($1.4x10^{-11}$ M – $1.1x10^{-9}$ M) by plotting the theoretical PLTX concentrations against the toxin concentrations measured by the cell-based ELISA assay (n = 10).*

The intra-assay repeatability was estimated over 6 replicates carried out in the same day and the inter-assay repeatability over 10 replicates carried out in a six months' period. A good correlation coefficient was calculated, with a value of $r^2 = 0.9770$ for intra-assay and of $r^2 = 0.9985$ for inter-assay (Figure 25). These data agreed with the intra-day and inter-day repeatability coefficients (relative standard deviation of repeatability) equal to 12 % and to 15 %, respectively (Table 5).

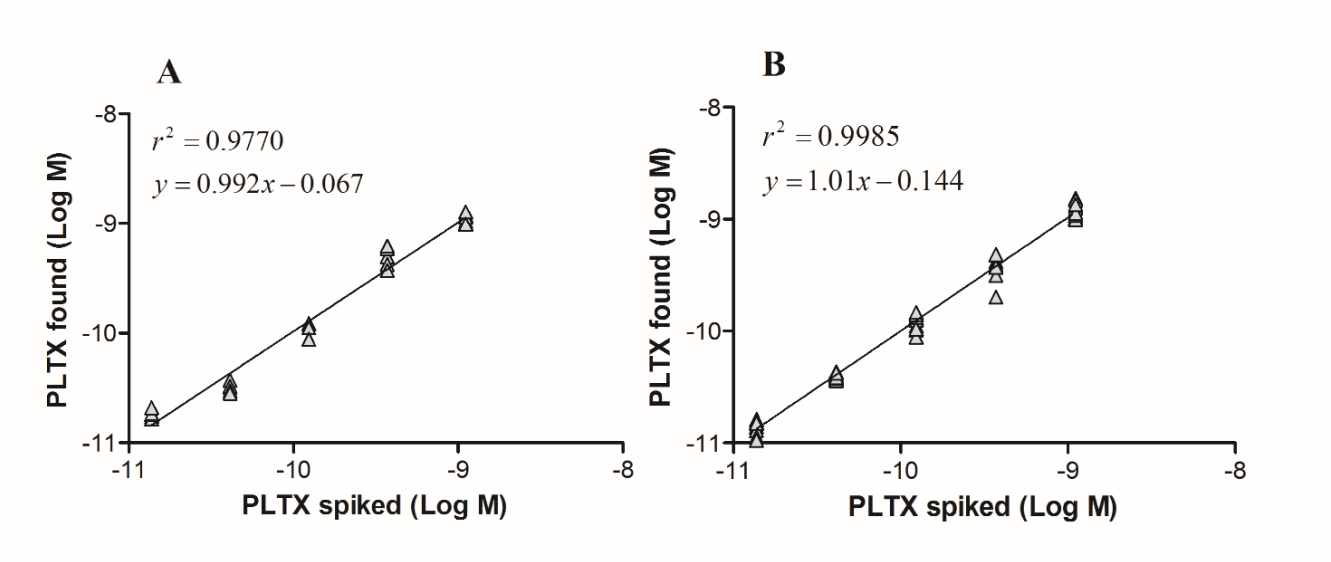

Figure 25: *Repeatability of the cell-based ELISA. Linear regression analysis performed within the working range of the assay ($1.4x10^{-11}$ M - $1.1x10^{-9}$ M) by plotting the theoretical PLTX concentrations against toxin concentrations measured by the cell-based ELISA assay.* ***A:*** *Intra-day repeatability (n = 6).* ***B****: Inter-day repeatability (six months' period, n = 10)*

Table 5: *Bias values (%) for PLTX analysis by the cell-based ELISA, intra-day (n=6, 1 day) and inter-day (n=10, 6 months) repeatability (relative standard deviation of repeatability, RSDr %) and mean of PLTX concentrations measured by the assay.*

PLTX concentration (M)	*Bias* (%)	Intra-day repeatability		Inter-day repeatability	
		Mean (M)	RSDr %	Mean (M)	RSDr %
$1.37x10^{-11}$	6.9	$1.83x10^{-11}$	8	$1.42x10^{-11}$	14
$4.12x10^{-11}$	-5.1	$3.22x10^{-11}$	10	$3.94x10^{-11}$	6
$1.24x10^{-10}$	-1.6	$1.15x10^{-10}$	12	$1.21x10^{-10}$	15
$3.70x10^{-10}$	2.6	$5.01x10^{-10}$	21	$3.80x10^{-10}$	21
$1.11x10^{-09}$	9.8	$1.11x10^{-09}$	10	$1.22x10^{-09}$	16
Mean	2.5		12		15

The sensitivity of the cell-based ELISA is higher than that of other immunoassays developed for PLTX detection (Bignami et al., 1992; Frolova et al., 2000). In addition, it is almost 35 time more sensitive than the indirect sandwich ELISA (LOD = 1.1 ng/mL), recently optimized and characterized by Boscolo et al. (2013). Thus, a significant improvement in term of sensitivity for PLTX detection, as well as in term time-consuming, was achieved. On the other hand, the sensitivity of the cell-based ELISA is lower than that of an immunoassay (0.5 pg/mL) developed by Garet et al. (2010) employing a single-chain antibodies isolated by phage display technology. Anyway, this assay is impaired by a high variability in the obtained results.

The sensitivity of the developed cell-based ELISA, expressed as instrumental LOD value (LOD = $1.2x10^{-11}$ M, 32.2 pg/mL) is more than one order of magnitude higher than that of the optimized hemolytic assay (LOD = $1.4x10^{-10}$ M), as well as more than 100-folds higher than that of a recently developed fluorescence polarization technique (LOD = 5.36 ng/mL) (Alfonso et al., 2012) and more

than 400 times higher than that of LC-HRMS (Ciminiello et al., 2015), which is considered the standard reference method to detect PLTX in different matrices.

4.2.2.2 Cross-reactivity with ovatoxin-a

The ability of the cell-based ELISA to quantify OVTX-a, the major PLTX analogue produced by *Ostrepsis* cf. *ovata* in the Mediterranean Sea, was evaluated. The cell-based ELISA was performed using OVTX-a and the relevant results were compared to those obtained using the same concentrations of PLTX. As shown in Figure 26, the O.D. values obtained using OVTX-a were significantly lower than those obtained using PLTX. The lower assay signal detected using OVTX-a with respect to that measured using PLTX was also confirmed by the relevant EC_{50} values (OVTX-a $EC_{50} = 9.1x10^{-10}$ M, 95% CI: $5.4x10^{-10} – 1.5x10^{-9}$ M, about one order of magnitude higher than that of PLTX $EC_{50} = 6.2x10^{-11}$ M, 95% CI: $3.6x10^{-11} – 1.1x10^{-10}$ M) and the OVTX-a Kd value ($1.2 \pm 0.4\times10^{-9}$ M), about 2 orders of magnitude higher ($p < 0.001$) than that of PLTX ($Kd = 2.7 \pm 0.6\times10^{-11}$ M).

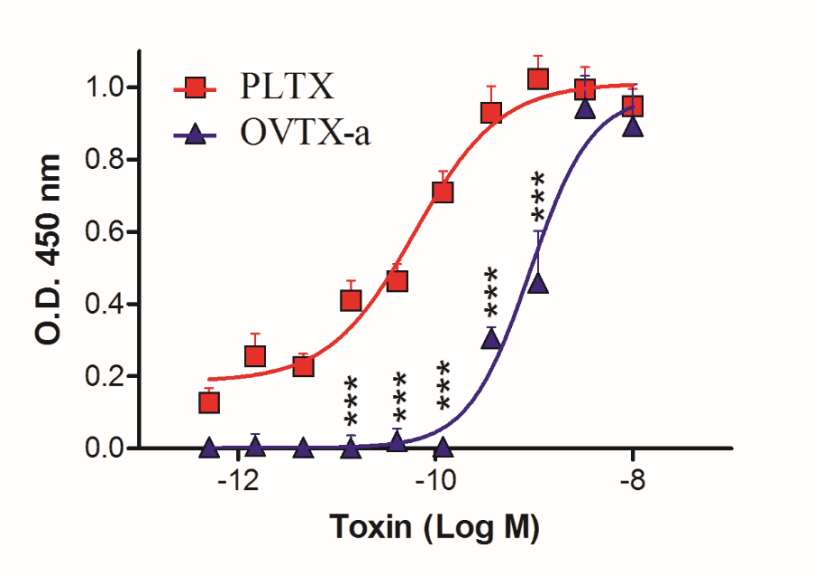

Figure 26: *Comparison between OVTX-a and PLTX detection by the cell-based ELISA. Each point represents the mean ± SE of 3 different experiments. Statistical differences: ***p < 0.001 as compared to PLTX (two-way ANOVA and Bonferroni post test).*

Since the mouse monoclonal anti-PLTX antibody 73D3 used as detection antibody in the cell based ELISA may also bind OVTX-a (Honsell et al., 2011) similarly to PLTX (Pelin et al., 2016b), the lower signal obtained using OVTX-a with respect to PLTX was probably due to a different binding of the two toxins to HaCaT cells. The reduced binding affinity of OVTX-a to HaCaT cells was in agreement with the *in-vitro* cytotoxicity of OVTX-a, demonstrated to be lower than that of the reference compound PLTX (Pelin et al., 2016b). Moreover, these results confirmed also the reduced hemolytic activity of OVTX-a with respect to PLTX, as previously demonstrated (section 4.1.3.2).

4.2.2.3 Inhibition of PLTX binding by ouabain

Ouabain (OUA) is a cardiac glycoside well known as inhibitor of PLTX effects *in vitro* (Pelin et al., 2013a; Vale-González et al., 2007). With the aim to confirm the specific detection of PLTX, the cell-based ELISA was performed exposing the cells to 1 mM OUA for 10 min, before their exposure to increasing concentrations of PLTX ($1.4x10^{-11}$ – $1.1x10^{-9}$ M). As can be seen in Figure 27, a significant reduction of the assay signal at each of the analyzed PLTX concentrations was recorded in presence of 1 mM OUA.

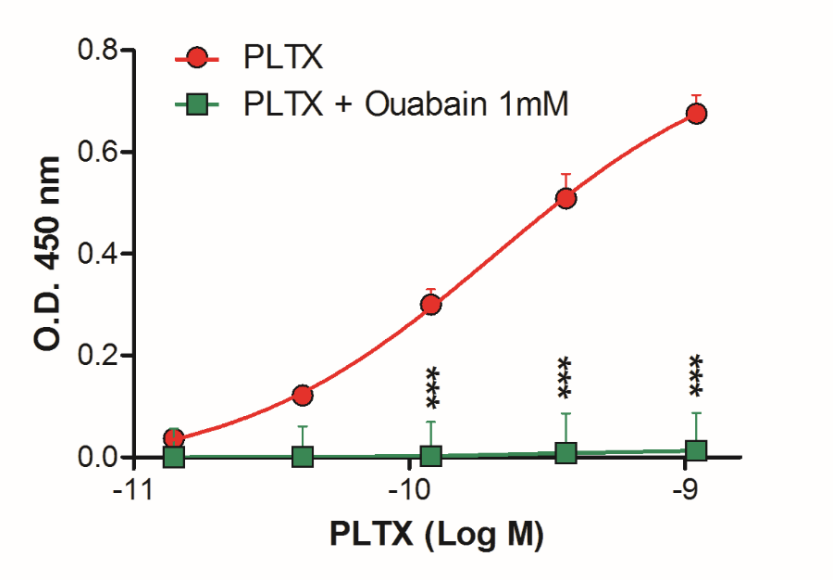

Figure 27: *Effect of cells pre-exposure to ouabain on PLTX detection by the cell-based ELISA. Each point represents the mean ± SE of 3 different experiments. Statistical differences: ***p < 0.001 as compared to PLTX (two-way ANOVA and Bonferroni post test).*

4.2.2.4 Mussels matrix effect and toxin recovery

The applicability of the cell-based ELISA to quantify PLTX in mussels was evaluated assessing the impact of matrix effect on the assay sensitivity. Hence, 1 g mussel (*Mytilus galloprovincialis*) meat free of PLTX was extracted three times with 3 mL of 80% aqueous methanol by Ultra-Turrax, obtaining an extract at 0.1 g mussels meat equivalents/mL, as described in section 3.4. Dilutions (1:1, 1:5, 1:10, 1:50) of the PLTX-free mussel extract were spiked with known PLTX concentrations to prepare different matrix matched-samples at PLTX concentrations ranging from $1.4x10^{-11}$-$1.1x10^{-9}$ M. Each sample was then analyzed by the cell-based ELISA and the optical density values were compared to those obtained with the same PLTX concentrations without matrix. The minimum extract dilution that did not interfere with the assay was 1:10 (Figure 28). At this dilution, the solvent alone did not interfere with the assay (data not shown). The linear regression analysis between the results obtained analyzing the 10-folds diluted mussels extract spiked with PLTX and those obtained analyzing the same PLTX concentrations without matrix (Figure 29) revealed a correlation coefficient ($r^2 = 0.9734$) and a mean bias value (Mean Bias= -1.4%; Table 6) indices of a satisfactory precision for PLTX detection in mussels. In addition, the LOQ for PLTX in mussels was $3.5x10^{-11}$ M, equal to 9.3 µg/kg meat, a value below the safety limit suggested by EFSA in shellfish (30 µg PLTXs/Kg of shellfish meat) (EFSA, 2009).

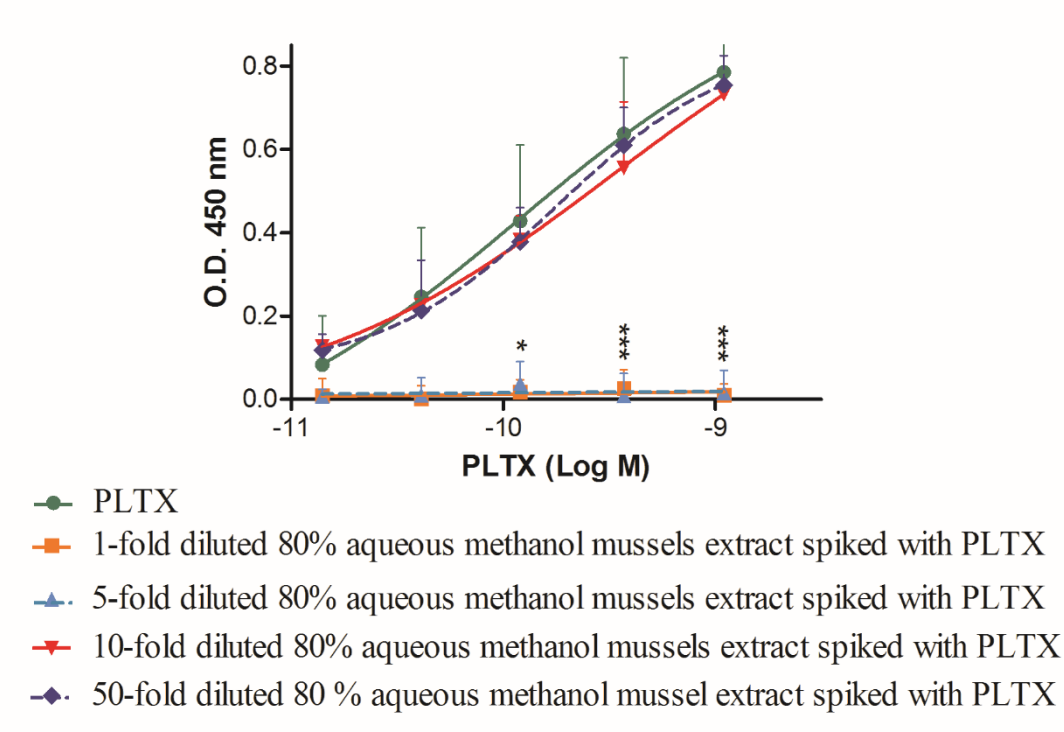

Figure 28: *Evaluation of mussels matrix effect (Mytilus galloprovincialis) on the cell-based ELISA. Comparison between PLTX calibration curve without matrix and 1-fold, 5-fold, 10-fold and 50-fold diluted 80 % aqueous methanol mussels extract spiked with PLTX. Each point represents the mean ± SE of 3 different experiments. *p < 0.05; ***p < 0.001 as compared to PLTX (two-way ANOVA and Bonferroni post test).*

The obtained results show that mussel extract interference in the cell-based ELISA was very low. At 10-fold dilution of mussel extract, that avoided the matrix effect, the sensitivity of the cell-based ELISA (LOQ = 9.3 µg PLTX/kg mussel meat) was lower than that of the hemolytic assay optimized in this study (LOQ = 640 µg PLTX eq/kg mussel meat) and that of a recently developed flow cytometry-based immunoassay (LOQ from 374 to 4430 µg/kg), which required a 30-fold dilution of the extract to eliminate the matrix effect (Fraga et al., 2016). In addition, the LOQ of the cell-based ELISA for PLTX in mussels was close to that of other detection methods, such as the sandwich ELISA (LOQ = 11 µg/kg meat) (Boscolo et al., 2013) and LC-HRMS (LOQ = 15 µg/kg meat)

(Ciminiello et al., 2015). However, it must be considered that the cell-based ELISA is a simple method, less expensive and not requiring qualified personnel with respect to LC- HRMS. Thus, it is suitable for preliminary PLTXs screening in mussels during monitoring programs.

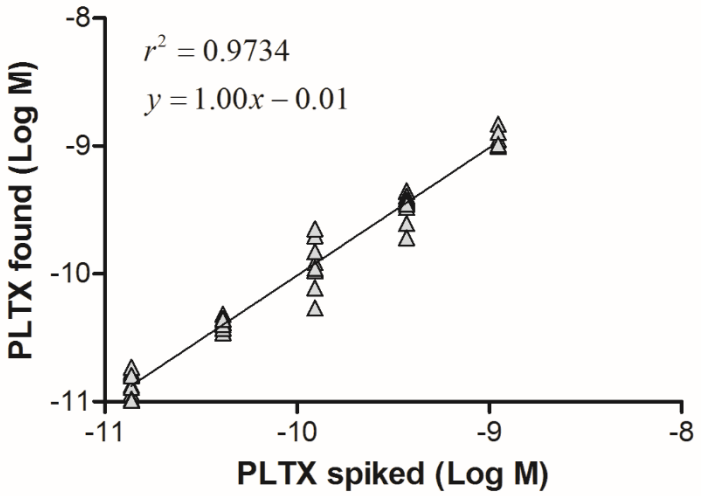

Figure 29: *Mussels matrix effect at the cell-based ELISA. Linear regression analysis within the working range of the cell-based ELISA ($1.4x10^{-11}$ M - $1.1x10^{-9}$ M) performed on 80% aqueous methanol mussels extracts diluted 1:10. Linear regression analysis was performed by plotting the theoretical PLTX concentrations against toxin concentrations measured by the cell-based ELISA assay.*

Recovery experiments were also carried out to determine the efficiency of PLTX extraction from mussels and its quantitation by the assay. Aliquots of PLTX-free mussel meat homogenate were spiked with PLTX ($1.4x10^{-11}$ M – $1.1x10^{-9}$ M) and extracted as described above to obtain extracts containing 0.1 g meat equivalents/mL. Extracts were diluted 1:10 and analyzed by the cell-based ELISA. Recoveries of PLTX from mussel matrix ranged between 93.7 % and 110.2 % (coefficient of variability: 13% - 17%), indicating a very good extraction efficiency and cell-based ELISA accuracy (Table 7). These results are in agreement with those of previous studies using LC- HRMS and a sandwich ELISA, demonstrating than the extraction method is the most suitable one for PLTX

recovery from mussels (*Mytilus galloprovincialis*) (90–100% toxin recovery) (Ciminiello et al., 2011; Boscolo et al., 2013).

Table 6: *Bias values (%) for PLTX detected in 80% aqueous methanol mussels extracts spiked with the toxin after 1:10 dilution in comparison to the theoretical PLTX concentrations (n=10).*

PLTX concentration (M)	*Bias* (%)
$1.37x10^{-11}$	-0.3
$4.12x10^{-11}$	-0.6
$1.23x10^{-10}$	1.5
$3.70x10^{-10}$	-4.8
$1.11x10^{-9}$	-3.0
Mean	-1.4

Table 7: *Recovery of PLTX from mussels analyzed by the cell-based ELISA.*

PLTX concentration (M)	Recovery (%)	Coefficient of variability (%)	n° replica
$1.37x10^{-11}$	99.6	15	5
$4.12x10^{-11}$	101.0	13	5
$1.23x10^{-10}$	93.7	17	5
$3.70x10^{-10}$	110.2	14	5
$1.11x10^{-9}$	101.9	13	5

4.2.2.5 Microalgae matrix effect and toxin recovery

To assess the suitability of the cell-based ELISA to quantify PLTXs in microalgae, also before their accumulation in seafood, the interference of microalgae matrix on PLTX-quantitation and PLTX recovery from microalgae were evaluated. Different dilutions (undiluted, 1:1, 1:5, 1:10 and 1:100) of 50% aqueous methanol *Coolia monotis* extract (obtained as described in section 3.5) were spiked with known concentrations of PLTX (from $1.4x10^{-11}$ M to $1.1x10^{-9}$ M) and analyzed by the cell-based ELISA. The relevant curves were then compared to that obtained by the same PLTX concentrations without matrices, as reported in Figure 30.

The minimum extract dilution that did not interfere with the cell-based ELISA was 1:10, whereas the undiluted, 1-fold diluted and 5-fold diluted extracts gave a significant interference on PLTX quantitation. The linear regression analysis, performed by plotting theoretic PLTX concentrations in the spiked extract after 10-fold dilution against PLTX concentrations measured by the cell-based ELISA, showed a satisfactory correlation coefficient ($r^2 = 0.9515$) (Figure 31). The accuracy of the cell-based ELISA to quantify PLTX in microalgae has been assessed calculating the bias (%) values: the average percentage of the obtained values was 2.58 % (from -6.68 % to 8.12 %), indicating a good accuracy of the method (Table 8).

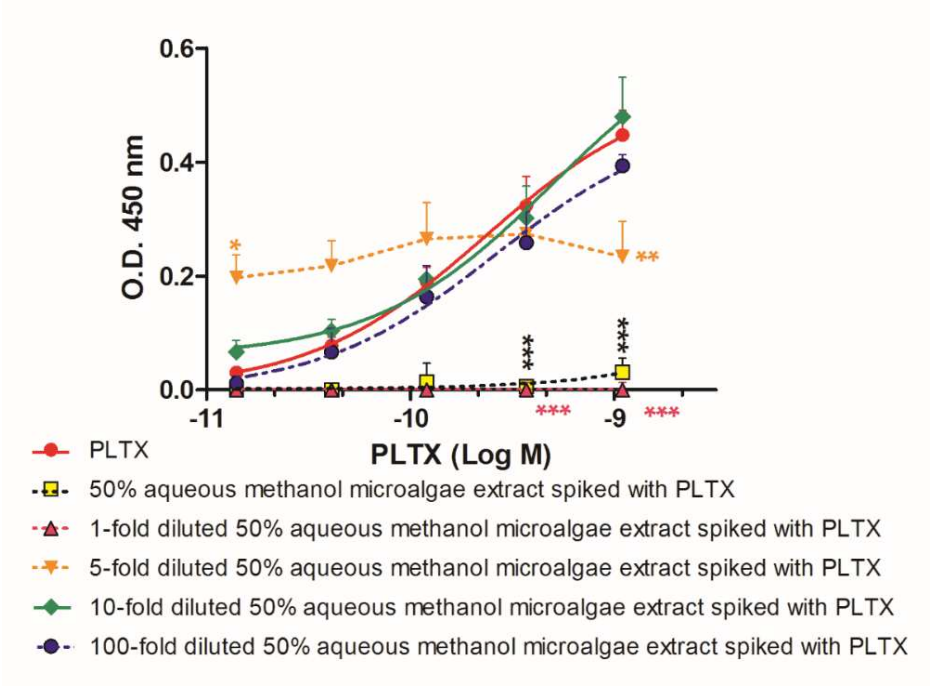

Figure 30: *Evaluation of microalgae matrix effect. Comparison between PLTX calibration curve without matrix and curves obtained analyzing undiluted, 1-fold, 5-fold, 10-fold and 100-fold diluted 50 % aqueous methanol microalgae extract spiked with PLTX. Each point represents the mean ± SE of 3 different experiments. *p < 0.05; ***p < 0.001 as compared to PLTX (two-way ANOVA and Bonferroni post test).*

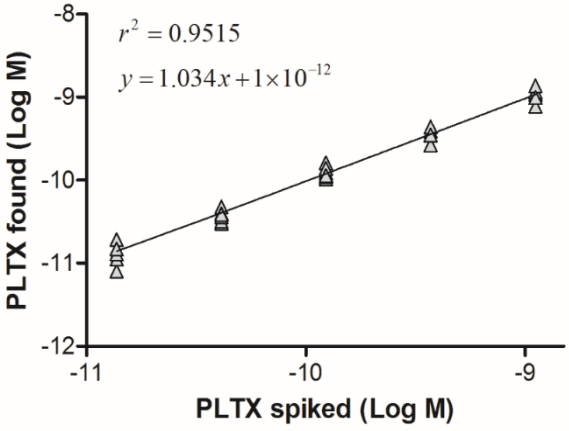

Figure 31: *Microalgae matrix effect. Linear regression analysis within the working range of the cell-based ELISA ($1.4x10^{-11}$ M - $1.1x10^{-9}$ M) performed on 50% aqueous methanol microalgae extracts diluted 1:10. Linear regression analysis was performed by plotting the theoretical PLTX concentrations against toxin concentrations measured by the cell-based ELISA assay.*

Table 8: *Bias values (%) for PLTX detected in 50% aqueous methanol microalgae extracts spiked with the toxin after 1:10 dilution in comparison to the theoretical PLTX concentrations (n=10).*

PLTX concentration (M)	*Bias* (%)
$1.37x10^{-11}$	8.12
$4.12x10^{-11}$	-6.68
1.23x10-10	1.68
3.70x10-10	5.78
1.11x10-9	3.99
Mean	2.58

The LOQ for PLTX in microalgae was 0.21 ng/mL, corresponding to 0.007 pg/cell, considering the extraction procedure and the minimum extract dilution that did not interfere with the assay. As already discussed for the hemolytic assay, also the cell-based ELISA can quantify PLTXs in microalgae at concentrations lower than those usually found in natural samples in the Mediterranean Sea, ranging from 0.4 pg/cell to 75 pg/cell (Accoroni et al., 2011; Aligizaki et al., 2008; Bellocci et al., 2008; Brissard et al., 2014; Ciminiello et al., 2008, 2012b; Honsell et al., 2011).

The cell-based ELISA resulted to be more sensitive than the hemolytic assay optimized in this study also in the quantitation of PLTX in microalgae, as shown by the LOQ values of 0.007 pg/cell and 0.04 pg/cell, respectively. Moreover, the sensitivity of the cell-based ELISA was much higher than that of the immunoassay developed by Boscolo and coworkers (LOQ = 9.6 ng/mL) (Boscolo et al., 2013).

Recovery experiments were then performed to evaluate the efficiency of the extraction procedure and the accuracy and precision of the method. PLTX recovery from microalgae was assessed spiking microalgae samples with known concentrations of PLTX (9 fg/cell, 2 fg/cell, 0.4 fg/cell; equal to $1x10^{-9}$ M, $2x10^{-10}$ M, $4x10^{-11}$ M) before their extraction. Table 9 shows the recovery percentage and the coefficient of variability for each concentration of PLTX. The average of toxin recovery (%) from microalgae was 98.3% (range: 86.4% - 114.5%; coefficient of variability: 8% - 11%), index of the efficiency of the extraction procedure and of good accuracy of the cell-based ELISA for PLTX quantitation in microalgae.

Table 9: *Recovery of PLTX from microalgae analyzed by the cell-based ELISA.*

PLTX concentration (M)	Recovery (%)	Coefficient of variability (%)	n° replica
$4.00x10^{-11}$	86.4	9	3
$2.00x10^{-10}$	94.1	8	3
$1.00x10^{-9}$	114.5	11	3

4.3 Suitability of the hemolytic assay and cell-based ELISA to quantify PLTXs in field samples of *Ostreopsis* cf. *ovata*

The ability of the hemolytic assay and that of the cell-based ELISA to quantify PLTXs in natural microalgae samples was assessed. Fourteen field samples of *Ostreopsis* cf. *ovata* cells were collected every week or every two weeks between August and September 2015/2016 along the Adriatic (Trieste, Italy; Split, Croatia) and Ligurian and Tuscany (La Spezia and Massa Carrara, Italy) coasts, where *O.* cf. *ovata* had been previously reported to bloom (Bellocci et al., 2008; Ciminiello et al., 2008; Honsell et al., 2011, 2013). Samples were collected depending on the occurrence of *Ostreopsis*, as described in section 3.6. For each collected sample, taxonomic identification, cells counting, SEM analysis and PLTXs quantitation were performed.

All the samples were collected following the guidelines for the management of the *Ostreopsis* cf. *ovata* blooms (Rapporti ISTISAN 14/19). The sample collection areas were selected in relation to geomorphological features (bottom type and depth) and physical characteristics (water temperature, hydrodynamics and wind). Typically, protected and shallow areas, such as creeks, half-closed bays and breakwaters protected sites are the most common risk area due to the poor hydrodynamics and low wave motion. For each sample, a form to collect data on field *Ostreopsis* cf. *ovata* was draw up indicating the climatic weather conditions and the characteristics of the bloom. All the forms are reported in Appendices A.

Among all the collected samples, *Ostreopsis* cf. *ovata* cells were found only in three samples collected in Trieste (T0C1 and T1C1) and Split (T0Sp1) between August and September 2015. In all other samples collected along the Ligurian and Tuscany coasts in 2015 and in the Gulf of Trieste in 2016, no *Ostreopsis* cells were found. In August and September 2015, *Ostreopsis* dinoflagellates appeared along the coast of Canovella de' Zoppoli (Gulf of Trieste, Italy), where this dinoflagellate blooms

had been reported in previous years (Honsell et al., 2011; Monti et al., 2007) and along the coast of Kastela bay (Split, Croatia). In both collection sites, visible materials were present in the water column and surface, forming brown foams and microalgae flakes. Moreover, bottom pebbles were covered by brownish and greenish mucilage of *Ostreopsis* cf. *ovat*a (Figure 32).

Figure 32: *Bottom pebbles of Canovella de' Zoppoli (T0C1 and T1C1) covered by brownish and greenish mucilage containing Ostreopsis cells. Visible material in the water surface can be also observed.*

Taxonomic identification

The taxonomic identification of *Ostreopsis* cf. *ovata* is usually based on the profile of the thecal plates and on the cell morphology, although the latter can be sometimes contradictory (Parsons et al., 2012). Sometimes, molecular methods based on PCR and quantitative real-time PCR (qPCR) technologies are recommended to improve the identification of different *Ostreopsis* species (Casabianca et al., 2013).

The taxonomic identification was performed on fixed (1% formaldehyde) and unfixed samples by the light and epifluorescence microscopy. *Ostreopsis* cells were typically drop-shaped with an

anteroposterior diameter ranging from 23.6 to 48.5 µm and dorsoventral diameter of 51.1-67.8 µm and from 28 to 45 µm and of 46-70 µm, for the samples collected in Trieste and in Split, respectively (Figure 33). The dorsoventral/anteroposterior (DV/AP) diameter ratio is considered a taxonomical character useful to discriminate *O. ovata* ad *O. siamensis*, both present in the Mediterranean Sea (Penna et al., 2005; 2010). Indeed, it has been demonstrated that dorsoventral/anteroposterior diameter ratio should be < 2 for *O. ovata* and > 4 for *O. siamensis* (Penna et al., 2005; Selina and Orlova, 2010). T0C1 and T1C1 samples are characterized by a dorsoventral/anteroposterior mean diameter ratio of 1.50 ± 0.08, while T0Sp1 of 1.61 ± 0.12, differing from previous studies in which DV/AP values of 2.31 ± 0.37 and 2.4 ± 0.4 were found in field samples of *O. ovata* collected in the North Adriatic Sea (Accoroni et al., 2012a; Monti et al., 2007). The dimension of *O. ovata* cells can vary depending on the cell growth phase, justifying the presence of different size in different conditions (Guerrini et al., 2010).

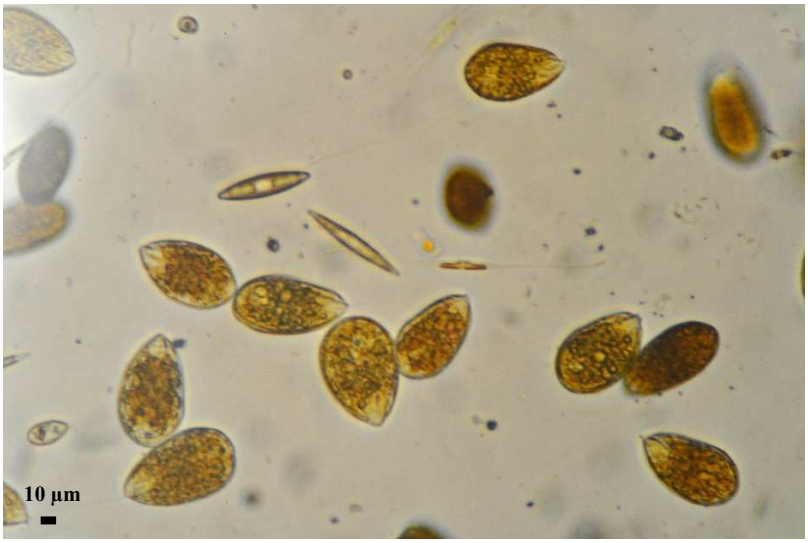

Figure 33: *Cells fixed in 1% formaldehyde, phase contrast light microscopy. Scale bar 10 µm.*

Samples were subsequently analyzed at epifluorescence microscope and stained with Calcofluor White M2R to show the thecal plates and stained with Hoechst to show the DNA. The thecal plate pattern of *O. ovata*, observable in Figure 34, is comparable to that previously described (Fukuyo, 1981; Penna et al., 2005). The nucleus, made visible by Hoechst staining, has a rounded shape and occupies the dorsal part of the cell (Figure 35).

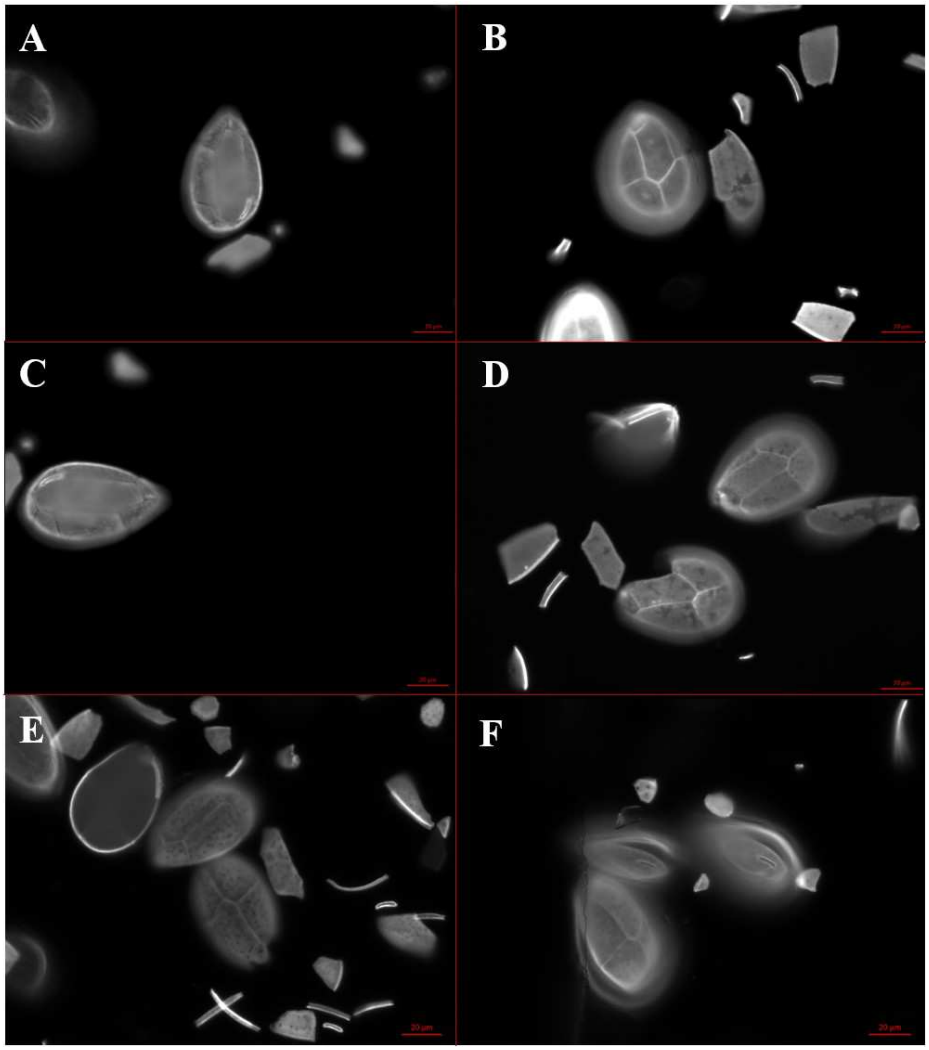

Figure 34: *Epifluorescence microscopy image of algal cells after staining with Calcofluor White to evidentiate cellulose thecal plates.* ***A****: Epitheca of an Ostreopsis cf. ovata cell (T0C1);* ***B****: Hypotheca of an Ostreopsis cf. ovata cell (T0C1);* ***C****: Epitheca of an Ostreopsis cf. ovata cell (T1C1);* ***D****: Hypotheca of an Ostreopsis cf. ovata cell (T1C1);* ***E****: Two hypothecae of Ostreopsis cf. ovata cells (T0Sp1);* ***F****: Two epithecae and a hypotheca of Ostreopsis cf. ovata cells (T0Sp1).*

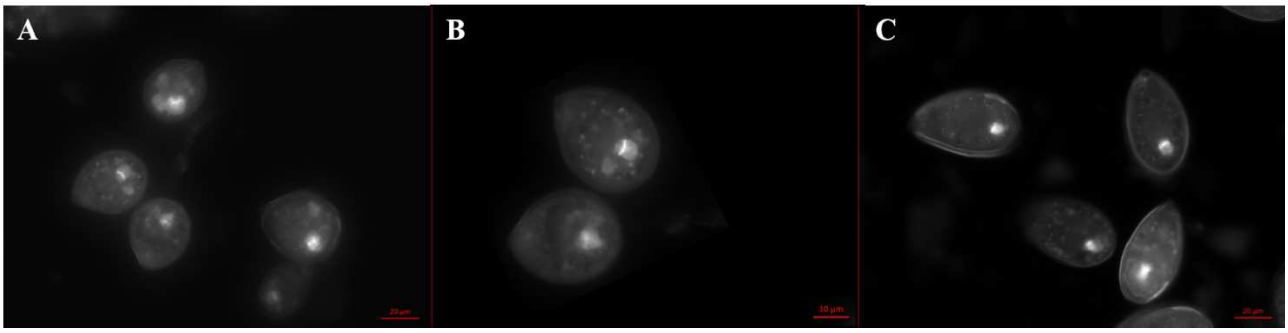

Figure 35: *Epifluorescence microscopy of algal cells after staining with Hoechst 33342 to evidentiate nuclei.* ***A****: Ostreopsis cf. ovata cells from a culture isolated from sample T0C1;* ***B****: Ostreopsis cf. ovata cells from the sample T1C1;* ***C****: Ostreopsis cf. ovata cells from the sample T0Sp1.*

Cells counting

Cells were counted following the Utermohl method on fixed (1% formaldehyde) seawater samples (Utermohl, 1958). Microscopy analysis of collected samples revealed that the most prevalent species was *Ostreopsis* cf. *ovata*. Specifically, 428 *O.* cf. *ovata* cells/mL were found in sample T0C1, while the concentration in the sample T1C1 was 757 cells/mL. The highest concentration of *Ostreopsis* cf. *ovata* cells (28,356 cell/mL) was detected in the sample from Split (T0Sp1). In each collected sample, other dinoflagellates were observed, in particular *Coolia monotis,* and diatoms such as *Nitzschia longissima*, *Navicula* spp. and *Cylindrotheca closterium.* The complete characterization of each collected sample with all the counted species is reported in Table 10.

Ostreopsis cf. *ovata* often bloomed along the rocky coast of the Adriatic Sea, as has been previously reported. However, the cell counts performed in the samples collected in 2015 were different from those reported in previous studies (Accoroni et al., 2011, 2012b; Honsell et al., 2011; Monti et al., 2007; Totti et al., 2010). From the literature is well known that several factors, such as the water temperature, the hydrodynamism, the water salinity and the abundance of nutrients, can influence the proliferation of *Ostreopsis* cf. *ovata*. Different studies showed that high temperatures promote the

growth of the harmful *Ostreopsis* cf. *ovata* dinoflagellates, supporting the global warming as one of the causes of *O.* cf. *ovata* blooms also in temperate areas. However, in the Mediterranean Sea, *Ostreopsis* blooms occur at different temperatures, depending on the area. Indeed, *Ostreopsis* was shown to proliferate from July in the North Mediterranean Sea with a water temperature around 26 °C and in late summer in the North Adriatic Sea with lower temperature (20-22 °C) (Mangialajo et al., 2011; Pistocchi et al., 2011). Also the low hydrodynamics conditions can affect *Ostreopsis* cf. *ovata* blooms occurrence. Indeed, it has been demonstrated that the highest concentration of *O.* cf. *ovata* cells was found in protected sites compared to exposed ones. Regarding the nutrient, *Ostreopsis* blooms occurs pretty everywhere, also in oligotrophic areas, however a relation between *O.* cf. *ovata* growth and sea eutrophication cannot be excluded (Glibert et al., 2010).

Given the environmental conditions as one of the main determining factors for *O.* cf. *ovata* growth, the cells concentrations in seawater often varies even within the same bloom and a careful analysis of the weather and geographical conditions before microalgae collection is essential to obtain a sample rich of cells.

Table 10: *Concentration of microalgae and cyanobacteria (cells/mL) in the natural field samples.*

Microalgae/cyanobacteria	***T0C1 (cells/mL)***	***T1C1 (cells/mL)***	***T0Sp1 (cells/mL)***
Ostreopsis* cf. *ovata	**428**	**758**	**28,356**
Coolia monotis	40	270	1,435
Amphidinium sp.		15	
Gymnodiniales		5	
Oxytoxum sp.		1	
Pennate diatoms	298	409	28,010
Nitzschia longissima	121	29	53
Amphora (small)	78	51	
Navicula spp.	38	124	
Cylindrotheca closterium	14	110	425
Centric diatoms	7	59	53
Amphora (big)	3	46	
Pleurosigma	2	5	
Licmophora	2	1	904
Chaetoceros	4		
Striatella unipunctata		49	
Melosira		7	
Big pennate diatoms		3	
Leptocylindrus minimus		3	
Nitzschia		2	
Cyanobacteris (*Oscillatoriales*)	4		

Analysis by Scanning Electron Microscopy (SEM)

Figure 36 shows *Coolia monotis* cells (Figure 36A and B) and *Ostreopsis* cf. *ovata* cells (Figure 36 C-H) from collected samples observed by SEM. *Ostreopsis* cf. *ovata* cells had an oval outline, more rounded dorsally with a protrusion in the ventral area. The thecal plates of *O.* cf. *ovata* showed a smooth surface characterized by pores surrounded by elevated areolae. The great majority of the cells showed trichocysts departing from the thecal pores. Trichocysts were mainly oriented in the same direction and converged at the ventral end of the cell where they become parallel and constitute a filamentous network that can be easily observed. These characteristics are in agreement with previous description and SEM analysis of *O.* cf. *ovata* (Escalera et al., 2014).

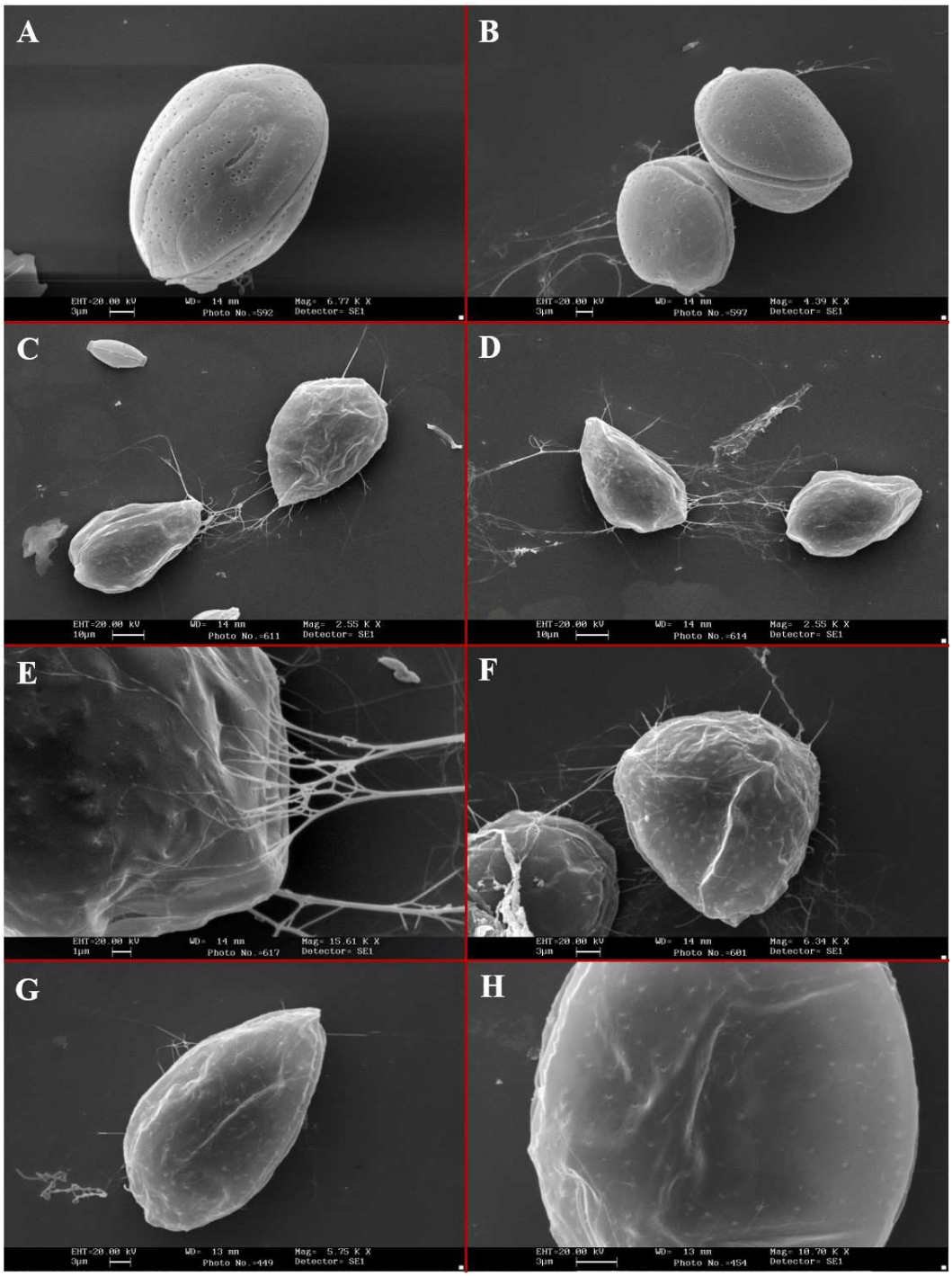

Figure 36: *SEM micrographs.* ***A, B****:* *Coolia monotis cells from natural populations of the sample T0C1;* ***C, D****:* *Ostreopsis cf. ovata cells from natural populations of the sample T0C1;* ***E, F****:* *Ostreopsis cf. ovata cells from natural populations of the sample T1C1;* ***G, H****:* *Ostreopsis cf. ovata cells from natural populations of the sample T0Sp1.*

Toxins quantitation

The samples T0C1, T1C1 and T0Sp1 collected in Trieste or Split, containing *O*. cf. *ovata* cells, were analyzed by the hemolytic assay and the cell-based ELISA in order to quantify the total amount of PLTXs (average values from different experiments, each one carried out in duplicate). The results were then compared to those obtained by LC-HR MS/MS. The calibration curve for each analysis was obtained using standard PLTX. Table 11 reports the total amount of PLTXs (pg PLTXs equivalents/cell) measured by the hemolytic assay and by the cell-based ELISA, and the total number of *Ostreopsis* cf. *ovata* cells/L in each collected sample. The two methods quantified total PLTXs within the range of 0.9-4.6 pg PLTXs equivalents/cell. PLTXs concentrations measured by the hemolytic assay were comparable to those measured by the cell-based ELISA, except for T1C1 sample where the hemolytic assay quantified 4.6 pg PLTXs equivalents/cell, whereas the cell-based ELISA detected 2.4 pg PLTXs equivalents/cell.

Table 11: *PLTXs concentrations (pg PLTXs equivalents/cell) in samples T0C1, T1C1 and T0Sp1. Results are expressed as the mean ± SE of 10 different experiments performed in duplicate.*

Sample ID	N° of algal cells (cells/L)	Hemolytic assay (pg PLTXs eq/cell)	Cell-based ELISA (pg PLTXs eq/cell)
T0C1	4.3×10^5	3.6 ± 0.8	3.4 ± 1.2
T1C1	7.6×10^5	4.6 ± 1.0	2.4 ± 0.5
T0Sp1	28.4×10^6	1.1 ± 0.2	0.9 ± 0.2

The concentrations of toxins measured by the cell-based ELISA and the hemolytic assay were then compared to those quantified by LC-HR MS/MS, in collaboration with the research group of Prof. Dell'Aversano, from the University of Napoli "Federico II". Due to the lack of standard OVTXs, the calibration curve for each analysis was obtained using only standard PLTX. Total PLTXs detected in T0C1 and T1C1 samples was 16 and 29 pg PLTX equivalents/cell, respectively, whereas T0Sp1 sample contained 6 pg PLTX equivalents/cell. LC-HR MS/MS analysis revealed that, OVTX-a was the most prevalent toxin in each sample, representing more than 50% of PLTX analogues. In addition, all the samples contained also OVTX-b, -c, a mixture of OVTX-d and -e as well as a low amount of PLTX (Table 12).

Table 12: *Total PLTXs concentration in natural field O. cf. ovata cells (pg/cell) measured by LC-HRMS/MS, hemolytic assay and the cell-based ELISA.*

Sample ID	LC-HRMS/MS (pg toxin/cell)						Hemolytic assay (pg PLTXs eq/cell)	Cell-based ELISA (pg PLTXs eq/cell)
	PLTX	OVTX-a	OVTX-b	OVTX-c	OVTX-d+e	Total		
T0C1	0.2	9.5	3.3	0.6	2.4	16	3.6	3.4
T1C1	0.2	16.7	6.2	0.9	4.8	29	4.6	2.4
T0Sp1	0.1	3.6	1.3	0.2	1.1	6	1.1	0.9

The amount of total PLTXs in *Ostreopsis* cells from the field microalgae samples was lower than that detected in samples collected in 2009 at Canovella de' Zoppoli (58 and 72 pg/cell) (Honsell et al., 2011) and near Ancona (Accoroni et al., 2011). In 2009, only OVTXs were found in microalgae samples from Canovella de' Zoppoli (Honsell et al., 2011) whereas PLTX was detected in all the field samples collected during this study, even if at very low concentrations. Nevertheless, the total PLTXs concentration in *Ostreopsis* cells from the field samples collected during this study was higher than

that measured in field samples previously collected in Liguria, where OVTX-a was the dominant toxin and PLTX the less concentrated one (Bellocci et al., 2008; Ciminiello et al., 2008). Moreover, PLTXs concentrations detected in *Ostreopsis* cells by this study are close to those previously quantified in field microalgae collected along the French Mediterranean coast, where OVTX-a represented about 50% of the total toxins (Brissard et al., 2014).

A comparison of our results to literature data related to PLTXs concentrations in cultured *O.* cf. *ovata* cells (Ciminiello et al., 2010; Guerrini et al., 2010; Pezzolesi et al., 2012; Pistocchi et al., 2011) cannot be done due to different factors, such as culture conditions, genetic differences between strains and/or possible biotransformation processes of the toxins in bloom conditions (Honsell et al., 2011).

As reported in Tables 11 and 12, the cells density was not directly related to the cells PLTXs content. Sample ToSp1, for example, displayed the highest number of *O.* cf. *ovata* cells (28.4×10^6 cells/L), but the lowest concentration of toxins, confirming a previous study in which the influence of several factors on proliferation and toxin production was demonstrated. Specifically, cell toxin content can be influenced by different factors, such as population growth phase, environmental, physical and chemical parameters, interaction with bacteria and mechanical stress (Pistocchi et al., 2011).

Finally, PLTXs content measured in field *Ostreopsis* cells detected by the hemolytic assay and the cell-based ELISA was compared to that measured by LC-HR MS/MS. As shown in Table 12, the two methods developed in this study appear to underestimate PLTXs by more than 80 % as compared to LC-HR MS/MS. Although a higher number of samples needs to be analyzed to confirm these preliminary results, it is possible to speculate that this difference is probably due to the high concentration of OVTXs in the sample, which can be detected by the hemolytic assay and the cell-based ELISA, but in a lesser extent than PLTX, as shown in section 4.1.3.2 and 4.2.2.2.

For these reasons, the hemolytic assay and the cell-based ELISA could be suitable to quantify PLTXs in field microalgae samples if coupled with a chemical confirmatory analysis of OVTXs in case of positive results. Moreover, despite these two methods seem to be not suitable to quantify PLTXs without a confirmatory analysis in natural sample of the Mediterranean Sea, where OVTXs are the most abundant toxins (Ciminiello et al., 2012a), they could be used in different areas where PLTX concentrations are higher than that of its analogues.

4.4 Further studies on sensitivity of different cell lines to PLTX

With the aim to improve the sensitivity of the cell-based ELISA as well as to develop other cell-based PLTX detection methods, different cell lines were exposed to PLTX to identify the most sensitive cell model to PLTX. Hence, the sensitivity of different cell lines to PLTX was evaluated by means of cytotoxicity (MTT assay) and PLTX binding. To this aim, a panel of cell models was selected: HaCaT (human immortalized keratinocytes), PANC-1 (human pancreatic carcinoma cell line), IHH (immortalized human hepatocytes), HepG2 (human liver cancer cell line), MDA-MB-231 and MCF-7 (human breast cancer cell line), LoVo (human colon adenocarcinoma cell line), Caco-2 (human epithelial colorectal adenocarcinoma cells) and HCT-116 (human colon cancer cells).

4.4.1 Cytotoxicity of PLTX

Cytotoxicity of PLTX toward different cell lines was evaluated on cells seeded in 96 wells plates for 72 h. Cells were exposed to increased concentrations of PLTX ($1x10^{-16}$ – $1x10^{-7}$ M) for 4 h and viability was evaluated by MTT assay. Figure 37A shows the % of cell viability compared to negative controls (untreated cells). The concentration-effect curves for PLTX obtained on different cell lines under the same experimental conditions were compared. From these curves, the relevant EC_{50} values were calculated and are reported in Table 13. The distribution of the EC_{50} values was analyzed in the box plot of Figure 37B (median $EC_{50} = 5.7x10^{-10}$ M; interquartile range = $1.5x10^{-10}$ M - $1.9x10^{-9}$ M), in which a significant variability of these values can be noted, suggesting significant differences in sensitivities towards PLTX displayed by the different cell models.

Indeed, on the basis of these EC_{50} values, the most sensitive cells were Caco-2 cells ($EC_{50} = 3.1x10^{-11}$ M; 95% C.I. = $5.9x10^{-12}$ - $3.4x10^{-11}$) followed by HCT-116 cells ($EC_{50} = 1.2x10^{-10}$ M; 95% C.I. = $3.4x10^{-11}$ - $2.8x10^{-10}$). The less sensitive cell lines were MCF-7 ($EC_{50} = 8.2x10^{-09}$ M; 95% C.I. = $2.2x10^{-9}$ - $9.2x10^{-9}$) and IHH ($EC_{50} = 2.9x10^{-9}$ M, 95% C.I.: $1.6x10^{-9}$ - $3.5x10^{-9}$) (Figure 37).

These results agree with those obtained by previous studies on different cell models: the cytotoxic effects of PLTX was also evaluated on Neuro-2a cells were PLTX reduced the cell viability with an EC_{50} of $1.5x10^{-10}$ M after 4 h exposure (Ledreux et al., 2009). Moreover, a similar EC_{50} value was measured on neuroblastoma cell line NG108-15 after 24h exposure with PLTX, even if the longer exposure time to PLTX must be taken into account (Cañete and Diogène, 2008). However, the Caco2 cell line used in this study appears to be more sensitive to PLTX also with respect to the two neuroblastoma cell lines used in previous studies. Moreover, these results confirm previous studies showing that Caco2 cell line is more sensitive to PLTX than HaCaT cells when the EC_{50} values are compared (Pelin et al., 2011, 2012).

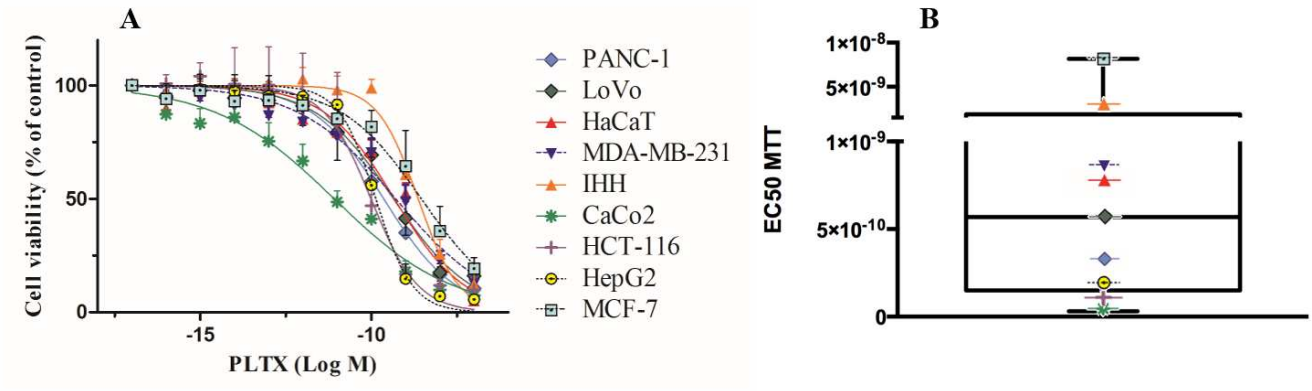

Figure 37: ***A:*** *Cytotoxicity of PLTX evaluated by MTT assay. Concentration-effect curves of PLTX obtained using different cell lines under the same experimental conditions. Results are reported as % of control (untreated cells). Each point is the mean ± SE of 3 independent experiments.* ***B:*** *Box plot showing the distribution of* EC_{50} *values obtained by MTT assays.*

Table 13: *Cytotoxicity of PLTX evaluated by MTT assay.* EC_{50} *toward different cell lines exposed to PLTX (*$1x10^{-16}$ *–* $1x10^{-7}$ *M) for 4 h.*

Cell line	MTT assay ($EC_{50,}$ M)	95% C.I.
PANC-1	$3.0x10^{-10}$	$1.5x10^{-10}$ - $3.5x10^{-10}$
HaCaT	$7.0x10^{-10}$	$2.9x10^{-10}$ - $8.7x10^{-10}$
IHH	$2.9x10^{-09}$	$1.6x10^{-9}$ - $3.5x10^{-9}$
LoVo	$5.7x10^{-10}$	$1.9x10^{-10}$ - $1.1x10^{-9}$
HCT-116	$1.2x10^{-10}$	$3.4x10^{-11}$ - $2.8x10^{-10}$
Caco-2	$3.1x10^{-11}$	$5.9x10^{-12}$ - $3.4x10^{-11}$
HepG2	$1.8x10^{-10}$	$8.5x10^{-11}$ - $2.2x10^{-10}$
MCF-7	$8.2x10^{-09}$	$2.2x10^{-9}$ - $9.2x10^{-9}$
MDA-MB-231	$8.7x10^{-10}$	$2.5x10^{-10}$ - $1.1x10^{-9}$

4.4.2 Binding experiments

The sensitivity of different cell lines to PLTX was also evaluated by means of toxin binding measured after cells exposure to increasing concentrations of PLTX ($5.1x10^{-13}$ – $1.0x10^{-8}$ M) for 10 minutes. Nonspecific binding was measured in presence of 1mM OUA (20 µL/well), which was added 10 minutes before the toxin. The toxin binding was then evaluated as described in section 3.9. The obtained results for each cell model were normalized on the protein content.

Figure 38 shows the saturation curves of the specific binding of PLTX obtained subtracting the relevant nonspecific binding from the total one. From these curves, Kd and Bmax values were calculated and reported in Table 14; their distribution was analyzed in the box plot of Figure 39 (median Kd = $8.1x10^{-10}$ M; interquartile range = $2.2x10^{-10}$ M - $2.4x10^{-9}$ M; median Bmax = 0.015; interquartile range = 0.0095 – 0.02738).

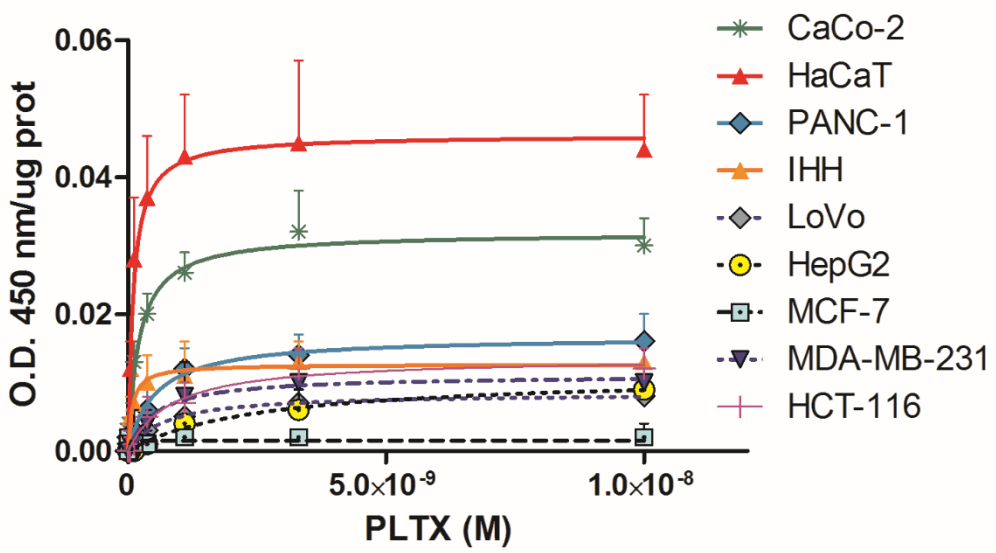

Figure 38: *Saturation curves of the specific binding of PLTX. Results are expressed as the mean ± SE of three experiments performed in triplicate.*

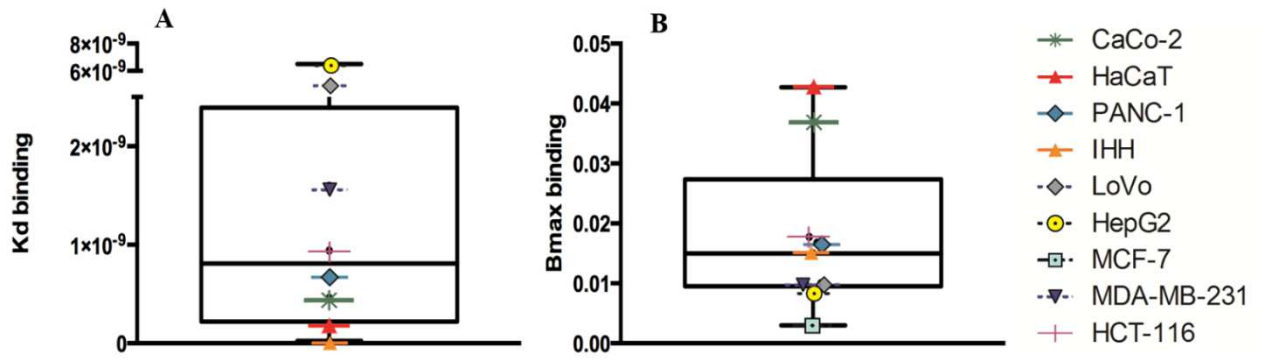

Figure 39: *Box plot showing the distribution of Kd values. **A**: and Bmax values; **B**: obtained by the binding assay for PLTX.*

Similarly to cytotoxicity, also variable PLTX binding (Kd and Bmax values) was recorded. In particular, HaCaT and Caco-2 cells can be assumed as the most sensitive cell lines for PLTX binding, as confirmed by the Bmax (0.043 and 0.037, respectively) and Kd values ($1.4x10^{-10}$ and $4.6x10^{-10}$ M, respectively). On the contrary, the less sensitive cell models for PLTX binding were HepG2 (Bmax = 0.009; Kd = $6.5x10^{-9}$ M) and MCF-7 cells (Bmax = 0.003; Kd = not detectable) (Figure 39, Table 14).

Intriguingly, Kd values significantly correlate with Bmax values (r = -0.8117, p value = 0.0095; non-parametric Spearman correlation). The negative correlation coefficient suggests that increased Bmax values imply an increase of binding affinity (decreased Kd values). Given that Bmax is an index of the number of receptor sites, it could be reasonable to hypothesize that binding affinity could be related to the expression levels of the Na^+/K^+ ATPase. Hence, the expression of Na^+/K^+ ATPase in each cell models considered in this study was investigated.

Table 14: *Sensitivity of different cell lines to PLTX evaluated by toxin binding (Bmax and Kd).*

Cell line	Kd (M)	Bmax
PANC-1	$6.8x10^{-10}$	0.017
HaCaT	$1.4x10^{-10}$	0.043
IHH	$2.3x10^{-11}$	0.015
LoVo	$2.7x10^{-9}$	0.01
HCT-116	$9.4x10^{-10}$	0.018
Caco-2	$4.6x10^{-10}$	0.037
HepG2	$6.5x10^{-9}$	0.009
MCF-7	n.d.	0.003
MDA-MB-231	$1.6x10^{-9}$	0.01

4.4.3 Expression of the Na^+/K^+ ATPase

The expression of the Na^+/K^+ ATPase in each cell model was investigated by flow cytofluorimetry analysis. Fixed cells were incubated with anti-Na^+/K^+ ATPase antibody followed by incubation with Alexa Fluor® 488-conjugated secondary anti-mouse antibody. In Figure 40, flow cytofluorimetry histograms are represented, while the relevant geometric mean (median fluorescence intensity, MFI) are reported in Table 15. HepG2 cells, followed by Caco-2 cells, displayed the highest geometric mean values, indices of a high expression of the Na^+/K^+ ATPase (Geo Mean = 88 ± 12 and 82 ± 7, respectively). These values were almost three times higher than those of LoVo, IHH and PANC-1 cell lines (geometric mean of 31 ± 7, 32 ± 4, 33 ± 6, respectively), which were the cell models in which the Na^+/K^+ ATPase was less expressed.

Table 15: *Geometric mean values (median fluorescence intensity, MFI) obtained by flow cytofluorimetry analysis. Results are expressed as the mean of three experiments ± standard deviation (SD).*

Cell line	Geometric mean ± SD
PANC-1	33 ± 6
HaCaT	38 ± 10
IHH	32 ± 4
LoVo	31 ± 7
HCT-116	56 ± 3
Caco-2	82 ± 7
HepG2	88 ± 12
MCF-7	62 ± 15
MDA-MB-231	69 ± 12

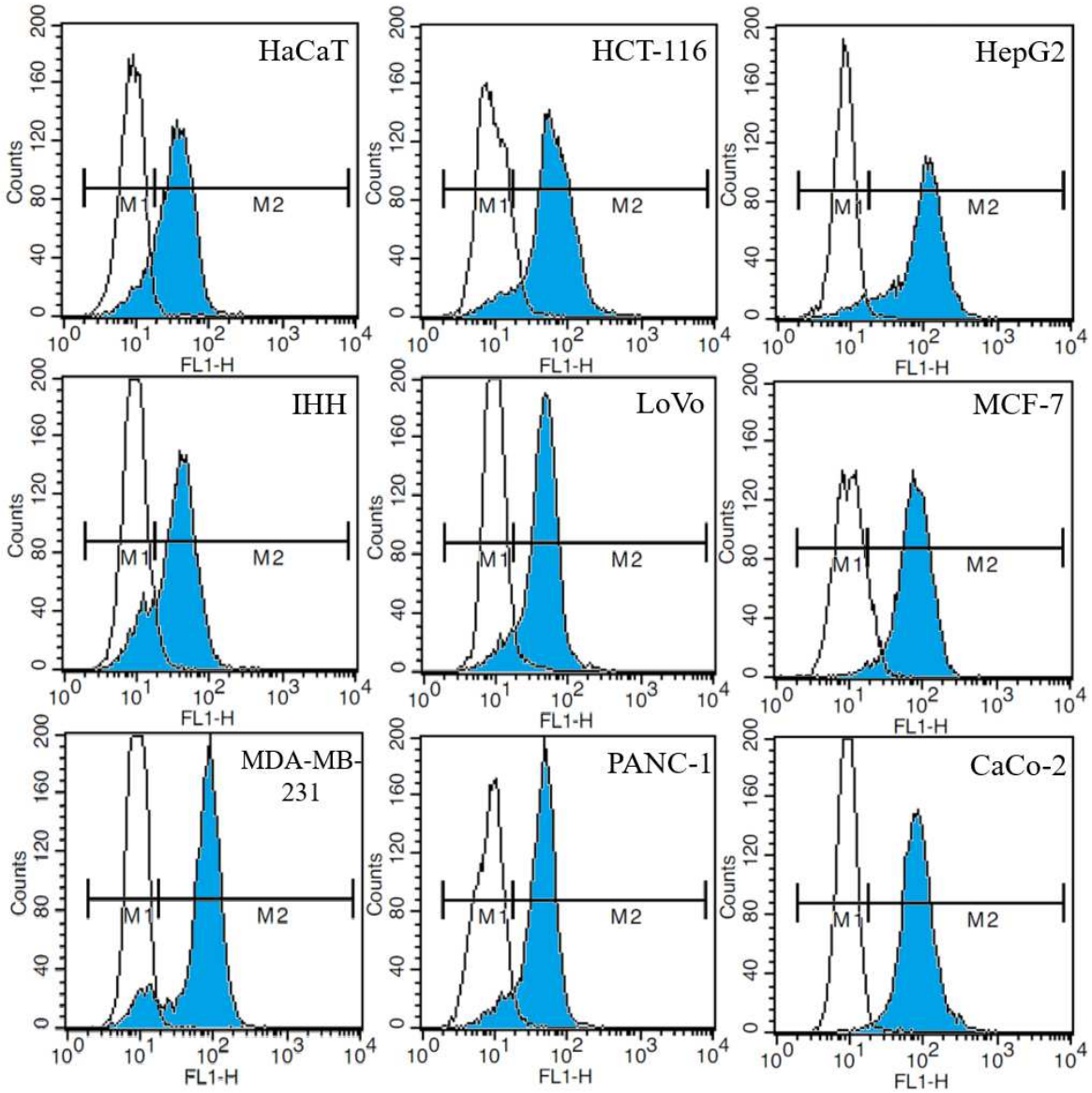

Figure 40: *Flow cytofluorimetry histograms of the selected cells models treated with anti-Na^+/K^+ ATPase alpha antibody. Markers were used to look for positive cells (blue pick). The numbers represent the geometric mean calculated on 20000 events. Results are the mean of three independent experiments.*

Correlation analyses revealed that the expression of the Na^+/K^+ ATPase was neither related with Bmax values (r = -0.1674, p value = 0.6529; non parametric Spearman correlation) nor with the Kd values (r = 0.3095, p value = 0.4618; non parametric Spearman correlation), suggesting that PLTX binding is not related with the level of Na^+/K^+ ATPase expression. Similarly, no correlation was also found between the expression of the Na^+/K^+ ATPase and the EC_{50} values measured by the MTT assay (r = -0.3333, p value = 0.3853; non parametric Spearman correlation), suggesting that also the cytotoxic effect is not dependent on the level of Na^+/K^+ ATPase expression.

Intriguingly, the structure of Na^+/K^+ ATPase contains three different subunits: the catalytic α subunit, which is represented by four isoforms; the β subunit, represented by three isoforms and a γ subunit (Geering, 2008). The subunit composition of the Na^+/K^+ ATPase and in particular the isoforms of α subunit has been demonstrated to confer a different sensitivity to the cardiac glycoside OUA (Scarrone et al., 2007). Hence, even though the different cytotoxic potencies exerted by PLTX on the selected cell models could be dependent on different intracellular pathways, cell sensitivity in terms of PLTX binding could be affected by the presence of different Na^+/K^+ ATPase isoforms. Experiments are already in progress to identify the expression of 4 α and 3 β subunits in the selected cell lines by real time PCR analysis.

5. Conclusions

PLTX is considered one of the most toxic marine compounds. Due to its marked toxicity and given the growing cases of adverse effects ascribed to inhalational exposure to aerosolized seawater during *Ostreopsis* blooms and PLTXs detection in *Ostreopsis*, marine aerosols and in some marine edible organisms, the development of simple, and specific methods for PLTX detection, easy to use both in mussels and in microalgae during monitoring programs is recommended. In this study, two methods for PLTX detection were developed and an intra-laboratory characterization was performed in the attempt to overcome the lacks and the limitations of the available methods.

The hemolytic assay and the cell-based ELISA developed in this study were characterized by a good sensitivity, accuracy, specificity and repeatability. However, the hemolytic assay does not allow any PLTX quantitation in mussels at concentration below the maximum limit suggested by EFSA (30 µg PLTXs equivalents/kg mussels meat) (EFSA, 2009), due to the high matrix effect. Thus, the hemolytic assay for PLTX quantitation in seafood could be used only after a careful evaluation of the specific matrix effect. On the contrary, the cell-based ELISA had a good sensitivity for PLTX quantitation in mussels due to the minimal mussels matrix effect, which makes this method suitable for preliminary PLTXs screening in mussels during monitoring program.

Investigating the ability of the hemolytic assay and the cell-based ELISA to quantify PLTXs in microalgae, both methods were shown to be able to quantify PLTXs in algal cells at concentrations lower than those usually found in natural samples of the Mediterranean Sea. However, comparing PLTX concentrations detected in three field *Ostreopsis* samples by the hemolytic assay and the cell-based ELISA with those measured by the LC-HR MS/MS, the two methods developed in this study seem to underestimate PLTXs by more than the 80%, probably due to a low detection of OVTXs in comparison to PLTX. However, a higher number of samples must be analyzed to confirm these preliminary results.

With the aim to define the most sensitive cell model to PLTX as a further improvement of the cell-based ELISA, the sensitivity of different cell models to PLTX was evaluated by means of cytotoxicity and binding assay. Caco-2 and HaCaT cell lines turned out to be the most sensitive cell models to PLTX-induced cytotoxicity (MTT assay) and PLTX binding, respectively. The high sensitivity did not correlate with the expression of the Na^+/K^+ ATPase, suggesting that other factors, such as the expression of specific Na^+/K^+ ATPase isoforms, may play an important role in PLTX sensitivity. Further studies are already in progress to identify the most sensitive Na^+/K^+ ATPase isoform for PLTX binding.

6. References

Accoroni, S., Romagnoli, T., Colombo, F., Pennesi, C., Di Camillo, C.G., Marini, M., Battocchi, C., Ciminiello, P., Dell'Aversano, C., Dello Iacovo, E., et al. (2011). *Ostreopsis* cf. ovata bloom in the northern Adriatic Sea during summer 2009: ecology, molecular characterization and toxin profile. Mar. Pollut. Bull. *62*, 2512–2519.

Accoroni, S., Romagnoli, T., Pichierri, S., Colombo, F., and Totti, C. (2012a). Morphometric analysis of *Ostreopsis* cf. *ovata* cells in relation to environmental conditions and bloom phases. Harmful Algae *19*, 15–22.

Accoroni, S., Colombo, F., Pichierri, S., Romagnoli, T., Marini, M., Battocchi, C., Penna, A., and Totti, C. (2012b). Ecology of *Ostreopsis* cf. *ovata* Blooms in the Northwestern Adriatic Sea. Cryptogam. Algol. *33*, 191–198.

Ahnert-Hilger, G., Chhatwal, G.S., Hessler, H.J., and Habermann, E. (1982). Changes in erythrocyte permeability due to palytoxin as compared to amphotericin B. Biochim. Biophys. Acta *688*, 486–494.

Alcala, A.C., Alcala, L.C., Garth, J.S., Yasumura, D., and Yasumoto, T. (1988). Human fatality due to ingestion of the crab *Demania reynaudii* that contained a palytoxin-like toxin. Toxicon Off. J. Int. Soc. Toxinology *26*, 105–107.

Alfonso, A., Fernández-Araujo, A., Alfonso, C., Caramés, B., Tobio, A., Louzao, M.C., Vieytes, M.R., and Botana, L.M. (2012). Palytoxin detection and quantification using the fluorescence polarization technique. Anal. Biochem. *424*, 64–70.

Aligizaki, K., Katikou, P., Nikolaidis, G., and Panou, A. (2008). First episode of shellfish contamination by palytoxin-like compounds from *Ostreopsis* species (Aegean Sea, Greece). Toxicon Off. J. Int. Soc. Toxinology *51*, 418–427.

Aligizaki, K., Katikou, P., Milandri, A., and Diogène, J. (2011). Occurrence of palytoxin-group toxins in seafood and future strategies to complement the present state of the art. Toxicon Off. J. Int. Soc. Toxinology *57*, 390–399.

Ares, I.R. (2005). Actin cytoskeleton of rabbit intestinal cells is a target for potent marine phycotoxins. J. Exp. Biol. *208*, 4345–4354.

Artigas, P., and Gadsby, D.C. (2004). Large diameter of palytoxin-induced Na/K pump channels and modulation of palytoxin interaction by Na/K pump ligands. J. Gen. Physiol. *123*, 357–376.

Barroso García, P., Rueda de la Puerta, P., Parrón Carreño, T., Marín Martínez, P., and Guillén Enríquez, J. (2008). Brote con síntomas respiratorios en la provincia de Almería por una posible exposición a microalgas tóxicas. Gac Sanit 578–584.

Bellocci, M., Ronzitti, G., Milandri, A., Melchiorre, N., Grillo, C., Poletti, R., Yasumoto, T., and Rossini, G.P. (2008). A cytolytic assay for the measurement of palytoxin based on a cultured monolayer cell line. Anal. Biochem. *374*, 48–55.

Bignami, G.S. (1993). A rapid and sensitive hemolysis neutralization assay for palytoxin. Toxicon Off. J. Int. Soc. Toxinology *31*, 817–820.

Bignami, G.S., Raybould, T.J., Sachinvala, N.D., Grothaus, P.G., Simpson, S.B., Lazo, C.B., Byrnes, J.B., Moore, R.E., and Vann, D.C. (1992). Monoclonal antibody-based enzyme-linked immunoassays for the measurement of palytoxin in biological samples. Toxicon Off. J. Int. Soc. Toxinology *30*, 687–700.

Biré, R., Trotereau, S., Lemée, R., Delpont, C., Chabot, B., Aumond, Y., and Krys, S. (2013). Occurrence of palytoxins in marine organisms from different trophic levels of the French Mediterranean coast harvested in 2009. Harmful Algae *28*, 10–22.

Boscolo, S., Pelin, M., De Bortoli, M., Fontanive, G., Barreras, A., Berti, F., Sosa, S., Chaloin, O., Bianco, A., Yasumoto, T., et al. (2013). Sandwich ELISA assay for the quantitation of palytoxin and its analogs in natural samples. Environ. Sci. Technol. *47*, 2034–2042.

Brissard, C., Herrenknecht, C., Séchet, V., Hervé, F., Pisapia, F., Harcouet, J., Lémée, R., Chomérat, N., Hess, P., and Amzil, Z. (2014). Complex toxin profile of French Mediterranean *Ostreopsis* cf. *ovata* strains, seafood accumulation and ovatoxins prepurification. Mar. Drugs *12*, 2851–2876.

Brissard, C., Hervé, F., Sibat, M., Séchet, V., Hess, P., Amzil, Z., and Herrenknecht, C. (2015). Characterization of ovatoxin-h, a new ovatoxin analog, and evaluation of chromatographic columns for ovatoxin analysis and purification. J. Chromatogr. A *1388*, 87–101.

Brovedani, V., Sosa, S., Poli, M., Forino, M., Varello, K., Tubaro, A., and Pelin, M. (2016). A revisited hemolytic assay for palytoxin detection: Limitations for its quantitation in mussels. Toxicon Off. J. Int. Soc. Toxinology *119*, 225–233.

Cañete, E., and Diogène, J. (2008). Comparative study of the use of neuroblastoma cells (Neuro-2a) and neuroblastomaxglioma hybrid cells (NG108-15) for the toxic effect quantification of marine toxins. Toxicon Off. J. Int. Soc. Toxinology *52*, 541–550.

Carnicer, O., Guallar, C., Andree, K.B., Diogène, J., and Fernández-Tejedor, M. (2015). *Ostreopsis* cf. ovata dynamics in the NW Mediterranean Sea in relation to biotic and abiotic factors. Environ. Res. *143*, *Part B*, 89–99.

Casabianca, S., Casabianca, A., Riobó, P., Franco, J.M., Vila, M., and Penna, A. (2013). Quantification of the toxic dinoflagellate *Ostreopsis* spp. by qPCR assay in marine aerosol. Environ. Sci. Technol. *47*, 3788–3795.

Ciminiello, P., Dell'Aversano, C., Fattorusso, E., Forino, M., Magno, G.S., Tartaglione, L., Grillo, C., and Melchiorre, N. (2006). The Genoa 2005 outbreak. Determination of putative palytoxin in Mediterranean *Ostreopsis ovata* by a new liquid chromatography tandem mass spectrometry method. Anal. Chem. *78*, 6153–6159.

Ciminiello, P., Dell'Aversano, C., Fattorusso, E., Forino, M., Tartaglione, L., Grillo, C., and Melchiorre, N. (2008). Putative palytoxin and its new analogue, ovatoxin-a, in *Ostreopsis ovata* collected along the Ligurian coasts during the 2006 toxic outbreak. J. Am. Soc. Mass Spectrom. *19*, 111–120.

Ciminiello, P., Dell'Aversano, C., Dello Iacovo, E., Fattorusso, E., Forino, M., Grauso, L., Tartaglione, L., Florio, C., Lorenzon, P., De Bortoli, M., et al. (2009). Stereostructure and Biological Activity of 42-Hydroxy-palytoxin: A New Palytoxin Analogue from Hawaiian *Palythoa* Subspecies. Chem. Res. Toxicol. *22*, 1851–1859.

Ciminiello, P., Dell'Aversano, C., Dello Iacovo, E., Fattorusso, E., Forino, M., Grauso, L., Tartaglione, L., Guerrini, F., and Pistocchi, R. (2010). Complex palytoxin-like profile of *Ostreopsis ovata.* Identification of four new ovatoxins by high-resolution liquid chromatography/mass spectrometry. Rapid Commun. Mass Spectrom. RCM *24*, 2735–2744.

Ciminiello, P., Dell'Aversano, C., Dello Iacovo, E., Fattorusso, E., Forino, M., and Tartaglione, L. (2011a). LC-MS of palytoxin and its analogues: State of the art and future perspectives. Toxicon Off. J. Int. Soc. Toxinology *57*, 376–389.

Ciminiello, P., Dell'Aversano, C., Dello Iacovo, E., Fattorusso, E., Forino, M., Tartaglione, L., Rossi, R., Soprano, V., Capozzo, D., and Serpe, L. (2011b). Palytoxin in seafood by liquid chromatography tandem mass spectrometry: investigation of extraction efficiency and matrix effect. Anal. Bioanal. Chem. *401*, 1043–1050.

Ciminiello, P., Dell'Aversano, C., Dello Iacovo, E., Fattorusso, E., Forino, M., Grauso, L., Tartaglione, L., Guerrini, F., Pezzolesi, L., Pistocchi, R., et al. (2012a). Isolation and structure elucidation of ovatoxin-a, the major toxin produced by *Ostreopsis ovata*. J. Am. Chem. Soc. *134*, 1869–1875.

Ciminiello, P., Dell'Aversano, C., Dello Iacovo, E., Fattorusso, E., Forino, M., Grauso, L., and Tartaglione, L. (2012b). High resolution LC-MS(n) fragmentation pattern of palytoxin as template to gain new insights into ovatoxin-a structure. The key role of calcium in MS behavior of palytoxins. J. Am. Soc. Mass Spectrom. *23*, 952–963.

Ciminiello, P., Dell'Aversano, C., Dello Iacovo, E., Forino, M., Tartaglione, L., Pelin, M., Sosa, S., Tubaro, A., Chaloin, O., Poli, M., et al. (2014a). Stereoisomers of 42-hydroxy palytoxin from Hawaiian *Palythoa toxica* and *P. tuberculosa*: stereostructure elucidation, detection, and biological activities. J. Nat. Prod. *77*, 351–357.

Ciminiello, P., Dell'Aversano, C., Iacovo, E.D., Fattorusso, E., Forino, M., Tartaglione, L., Benedettini, G., Onorari, M., Serena, F., Battocchi, C., et al. (2014b). First Finding of *Ostreopsis* cf. *ovata* Toxins in Marine Aerosols. Environ. Sci. Technol. *48*, 3532–3540.

Ciminiello, P., Dell'Aversano, C., Dello Iacovo, E., Forino, M., and Tartaglione, L. (2015). Liquid chromatography-high-resolution mass spectrometry for palytoxins in mussels. Anal. Bioanal. Chem. *407*, 1463–1473.

Coca, R., Soler, F., and Fernández-Belda, F. (2008). Characterization of the palytoxin effect on Ca^{2+}-ATPase from sarcoplasmic reticulum (SERCA). Arch. Biochem. Biophys. *478*, 36–42.

Colles, S.M., and Chisolm, G.M. (2000). Lysophosphatidylcholine-induced cellular injury in cultured fibroblasts involves oxidative events. J. Lipid Res. *41*, 1188–1198.

Deeds, J.R., Handy, S.M., White, K.D., and Reimer, J.D. (2011). Palytoxin found in *Palythoa* sp. zoanthids (Anthozoa, Hexacorallia) sold in the home aquarium trade. PloS One *6*, e18235.

Del Favero, G., Sosa, S., Pelin, M., D'Orlando, E., Florio, C., Lorenzon, P., Poli, M., and Tubaro, A. (2012). Sanitary problems related to the presence of *Ostreopsis* spp. in the Mediterranean Sea: a multidisciplinary scientific approach. Ann. Ist. Super. Sanita *48*, 407–414.

Del Favero, G., Beltramo, D., Sciancalepore, M., Lorenzon, P., Coslovich, T., Poli, M., Testai, E., Sosa, S., and Tubaro, A. (2013). Toxicity of palytoxin after repeated oral exposure in mice and in vitro effects on cardiomyocytes. Toxicon Off. J. Int. Soc. Toxinology *75*, 3–15.

D. M. 30 marzo 2010, n° 119, "Definizione dei criteri per determinare il divieto di balneazione, nonchè modalita' e specifiche tecniche per l'attuazione del decreto legislativo 30 maggio 2008, n. 116,

di recepimento della direttiva 2006/7/CE, relativa alla gestione della qualità delle acque di balneazione."

Durando, P., Ansaldi, F., Oreste, P., Moscatelli, P., Marensi, L., Grillo, C., Gasparini, R., Icardi, G., and Collaborative Group for the Ligurian Syndromic Algal Surveillance (2007). *Ostreopsis ovata* and human health: epidemiological and clinical features of respiratory syndrome outbreaks from a two-year syndromic surveillance, 2005-06, in north-west Italy. Euro Surveill. Bull. Eur. Sur Mal. Transm. Eur. Commun. Dis. Bull. *12*, E070607.1.

EFSA Panel on Contaminants in the Food Chain (CONTAM) (2009). Scientific Opinion on marine biotoxins in shellfish - Palytoxin group: Marine Biotoxins in Shellfish - Palytoxin group. EFSA J. *7*, 1393.

Escalera, L., Benvenuto, G., Scalco, E., Zingone, A., and Montresor, M. (2014). Ultrastructural features of the benthic dinoflagellate *Ostreopsis* cf. *ovata* (Dinophyceae). Protist *165*, 260–274.

Espiña, B., Cagide, E., Louzao, M.C., Fernandez, M.M., Vieytes, M.R., Katikou, P., Villar, A., Jaen, D., Maman, L., and Botana, L.M. (2009). Specific and dynamic detection of palytoxins by in vitro microplate assay with human neuroblastoma cells. Biosci. Rep. *29*, 13–23.

Facchini, L., Losito, I., Cianci, C., Cataldi, T.R.I., and Palmisano, F. (2016). Structural characterization and profiling of lyso-phospholipids in fresh and in thermally stressed mussels by hydrophilic interaction liquid chromatography-electrospray ionization-Fourier transform mass spectrometry. Electrophoresis *37*, 1823–1838.

Fraga, M., Vilariño, N., Louzao, M.C., Fernández, D.A., Poli, M., and Botana, L.M. (2016). Detection of palytoxin-like compounds by a flow cytometry-based immunoassay supported by functional and analytical methods. Anal. Chim. Acta *903*, 1–12.

Frolova, G.M., Kuznetsova, T.A., Mikhaĭlov, V.V., and Eliakov, G.B. (2000). Immunoenzyme method for detecting microbial producers of palytoxin. Bioorg. Khim. *26*, 315–320.

Gallitelli, M., Ungaro, N., Addante, L.M., Procacci, V., Silveri, N.G., Silver, N.G., and Sabbà, C. (2005). Respiratory illness as a reaction to tropical algal blooms occurring in a temperate climate. JAMA *293*, 2599–2600.

Gao, S., Zheng, X., Hu, B., Sun, M., Wu, J., Jiao, B., and Wang, L. (2017). Enzyme-linked, aptamer-based, competitive biolayer interferometry biosensor for palytoxin. Biosens. Bioelectron. *89*, 952–958.

García-Altares, M., Tartaglione, L., Dell'Aversano, C., Carnicer, O., de la Iglesia, P., Forino, M., Diogène, J., and Ciminiello, P. (2015). The novel ovatoxin-g and isobaric palytoxin (so far referred to as putative palytoxin) from *Ostreopsis* cf. *ovata* (NW Mediterranean Sea): structural insights by LC-high resolution MS(n.). Anal. Bioanal. Chem. *407*, 1191–1204.

Garet, E., Cabado, A.G., Vieites, J.M., and González-Fernández, A. (2010). Rapid isolation of single-chain antibodies by phage display technology directed against one of the most potent marine toxins: Palytoxin. Toxicon Off. J. Int. Soc. Toxinology *55*, 1519–1526.

Geering, K. (2008). Functional roles of Na,K-ATPase subunits: Curr. Opin. Nephrol. Hypertens. *17*, 526–532.

Ginsburg, I., Ward, P.A., and Varani, J. (1989). Lysophosphatides enhance superoxide responses of stimulated human neutrophils. Inflammation *13*, 163–174.

Gleibs, S., and Mebs, D. (1999). Distribution and sequestration of palytoxin in coral reef animals. Toxicon Off. J. Int. Soc. Toxinology *37*, 1521–1527.

Gleibs, S., Mebs, D., and Werding, B. (1995). Studies on the origin and distribution of palytoxin in a Caribbean coral reef. Toxicon Off. J. Int. Soc. Toxinology *33*, 1531–1537.

Glibert, P.M., Allen, J.I., Bouwman, A.F., Brown, C.W., Flynn, K.J., Lewitus, A.J., and Madden, C.J. (2010). Modeling of HABs and eutrophication: Status, advances, challenges. J. Mar. Syst. *83*, 262–275.

Guennoun-Lehmann, S., Fonseca, J.E., Horisberger, J.-D., and Rakowski, R.F. (2007). Palytoxin Acts on Na^+, K^+-ATPase but not Nongastric H^+, K^+-ATPase. J. Membr. Biol. *216*, 107–116.

Guerrini, F., Pezzolesi, L., Feller, A., Riccardi, M., Ciminiello, P., Dell'Aversano, C., Tartaglione, L., Dello Iacovo, E., Fattorusso, E., Forino, M., et al. (2010). Comparative growth and toxin profile of cultured *Ostreopsis ovata* from the Tyrrhenian and Adriatic Seas. Toxicon Off. J. Int. Soc. Toxinology *55*, 211–220.

Habermann, E. (1983). Action and binding of palytoxin, as studied with brain membranes. Naunyn. Schmiedebergs Arch. Pharmacol. *323*, 269–275.

Habermann, E. (1989). Palytoxin acts through Na^+,K^+-ATPase. Toxicon Off. J. Int. Soc. Toxinology *27*, 1171–1187.

Habermann, E., and Chhatwal, G.S. (1982). Ouabain inhibits the increase due to palytoxin of cation permeability of erythrocytes. Naunyn. Schmiedebergs Arch. Pharmacol. *319*, 101–107.

Habermann, E., Ahnert-Hilger, G., Chhatwal, G.S., and Beress, L. (1981). Delayed haemolytic action of palytoxin. General characteristics. Biochim. Biophys. Acta *649*, 481–486.

Harmel, N., and Apell, H.-J. (2006). Palytoxin-induced effects on partial reactions of the Na,K-ATPase. J. Gen. Physiol. *128*, 103–118.

Hartmann, W.K., Saptharishi, N., Yang, X.Y., Mitra, G., and Soman, G. (2004). Characterization and analysis of thermal denaturation of antibodies by size exclusion high-performance liquid chromatography with quadruple detection. Anal. Biochem. *325*, 227–239.

Hilgemann, D.W. (2003). From a pump to a pore: how palytoxin opens the gates. Proc. Natl. Acad. Sci. U. S. A. *100*, 386–388.

Honsell, G., De Bortoli, M., Boscolo, S., Dell'Aversano, C., Battocchi, C., Fontanive, G., Penna, A., Berti, F., Sosa, S., Yasumoto, T., et al. (2011). Harmful dinoflagellate *Ostreopsis* cf. *ovata* Fukuyo: detection of ovatoxins in field samples and cell immunolocalization using antipalytoxin antibodies. Environ. Sci. Technol. *45*, 7051–7059.

Honsell, G., Bonifacio, A., De Bortoli, M., Penna, A., Battocchi, C., Ciminiello, P., Dell'aversano, C., Fattorusso, E., Sosa, S., Yasumoto, T., et al. (2013). New insights on cytological and metabolic features of *Ostreopsis* cf. *ovata* Fukuyo (Dinophyceae): a multidisciplinary approach. PloS One *8*, e57291.

Ishida, Y., Takagi, K., Takahashi, M., Satake, N., and Shibata, S. (1983). Palytoxin isolated from marine coelenterates. The inhibitory action on (Na,K)-ATPase. J. Biol. Chem. *258*, 7900–7902.

Ito, E., and Yasumoto, T. (2009). Toxicological studies on palytoxin and ostreocin-D administered to mice by three different routes. Toxicon Off. J. Int. Soc. Toxinology *54*, 244–251.

Kermarec, F., Dor, F., Armengaud, A., Charlet, F., Kantin, R., Sauzade, D., and De Haro, L. (2008). Les risques sanitaires liés à la présence d'*Ostreopsis ovata* dans les eaux de baignade ou d'activités nautiques. Environ. Risques Santé *7*, 357–363.

Kim, D., Sato, Y., Miyazaki, Y., Oda, T., Muramatsu, T., Matsuyama, Y., and Honjo, T. (2002). Comparison of hemolytic activities among strains of Heterocapsa circularisquama isolated in various localities in Japan. Biosci. Biotechnol. Biochem. *66*, 453–457.

Kockskämper, J., Ahmmed, G.U., Zima, A.V., Sheehan, K.A., Glitsch, H.G., and Blatter, L.A. (2004). Palytoxin disrupts cardiac excitation-contraction coupling through interactions with P-type ion pumps. Am. J. Physiol. Cell Physiol. *287*, C527-538.

Kodama, A.M., Hokama, Y., Yasumoto, T., Fukui, M., Manea, S.J., and Sutherland, N. (1989). Clinical and laboratory findings implicating palytoxin as cause of ciguatera poisoning due to *Decapterus macrosoma* (mackerel). Toxicon Off. J. Int. Soc. Toxinology *27*, 1051–1053.

Kregenow, F.M. (1971). The response of duck erythrocytes to hypertonic media. Further evidence for a volume-controlling mechanism. J. Gen. Physiol. *58*, 396–412.

Ledreux, A., Krys, S., and Bernard, C. (2009). Suitability of the Neuro-2a cell line for the detection of palytoxin and analogues (neurotoxic phycotoxins). Toxicon Off. J. Int. Soc. Toxinology *53*, 300–308.

Lenoir, S., Ten-Hage, L., Turquet, J., Quod, J.-P., Bernard, C., and Hennion, M.-C. (2004). First evidence of palytoxin analogues from an *Ostreopsis mascarenensis* (Dinophyceae) benthic bloom in South-Western Indian Ocean. J. Phycol. *40*, 1042–1051.

Levine, L., Fujiki, H., Gjika, H.B., and Van Vunakis, H. (1987). Production of antibodies to palytoxin: neutralization of several biological properties of palytoxin. Toxicon Off. J. Int. Soc. Toxinology *25*, 1273–1282.

Levine, L., Fujiki, H., Gjika, H.B., and Van Vunakis, H. (1988). A radioimmunoassay for palytoxin. Toxicon *26*, 1115–1121.

Lowe, M.L., Gin, J.B., and Demetriou, J.A. (1973). Stability of erythrocytic enzymes for screening tests. Clin. Chem. *19*, 529–530.

Magnusson, B., and Ornemark, U. (2014). Eurachem Guide: The Fitness for Purpose of Analytical Methods – A Laboratory Guide to Method Validation and Related Topics.

Mahnir, V.M., Kozlovskaya, E.P., and Kalinovsky, A.I. (1992). Sea anemone Radianthus macrodactylus--a new source of palytoxin. Toxicon Off. J. Int. Soc. Toxinology *30*, 1449–1456.

Malagoli D. (2007). A full-length protocol to test hemolytic activity of palytoxin on human erythrocytes. Invertebr. Surviv. J. *4*, 92–94.

Manger, R.L., Leja, L.S., Lee, S.Y., Hungerford, J.M., and Wekell, M.M. (1993). Tetrazolium-based cell bioassay for neurotoxins active on voltage-sensitive sodium channels: semiautomated assay for saxitoxins, brevetoxins, and ciguatoxins. Anal. Biochem. *214*, 190–194.

Mangialajo, L., Ganzin, N., Accoroni, S., Asnaghi, V., Blanfuné, A., Cabrini, M., Cattaneo-Vietti, R., Chavanon, F., Chiantore, M., Cohu, S., et al. (2011). Trends in *Ostreopsis* proliferation along the Northern Mediterranean coasts. Toxicon Off. J. Int. Soc. Toxinology *57*, 408–420.

Mereish, K.A., Morris, S., Cullers, G.M., Taylor, T.J., and Bunner, D.L. (1991). Analysis of Palytoxin by Liquid Chromatography and Capillary Electrophoresis. J. Liq. Chromatogr. *14*, 1025–1031.

Monti, M., Minocci, M., Beran, A., and Ivesa, L. (2007). First record of *Ostreopsis* cfr. *ovata* on macroalgae in the Northern Adriatic Sea. Mar. Pollut. Bull. *54*, 598–601.

Moore, G.L. (1991). Long-term storage and preservation of red blood cells. Biotechnol. Read. Mass *19*, 31–46.

Moore, R.E., and Scheuer, P.J. (1971). Palytoxin: a new marine toxin from a coelenterate. Science *172*, 495–498.

Munday, R. (2011). Palytoxin toxicology: Animal studies. Toxicon *57*, 470–477.

Nascimento, S.M., Corrêa, E.V., Menezes, M., Varela, D., Paredes, J., and Morris, S. (2012). Growth and toxin profile of *Ostreopsis* cf. *ovata* (Dinophyta) from Rio de Janeiro, Brazil. Harmful Algae *13*, 1–9.

Nicolas, J., Bovee, T.F.H., Kamelia, L., Rietjens, I.M.C.M., and Hendriksen, P.J.M. (2015). Exploration of new functional endpoints in neuro-2a cells for the detection of the marine biotoxins saxitoxin, palytoxin and tetrodotoxin. Toxicol. Vitro Int. J. Publ. Assoc. BIBRA *30*, 341–347.

Oku, N., Sata, N.U., Matsunaga, S., Uchida, H. 'omi, and Fusetani, N. (2004). Identification of palytoxin as a principle which causes morphological changes in rat 3Y1 cells in the zoanthid *Palythoa* aff. *margaritae*. Toxicon Off. J. Int. Soc. Toxinology *43*, 21–25.

Onuma, Y., Satake, M., Ukena, T., Roux, J., Chanteau, S., Rasolofonirina, N., Ratsimaloto, M., Naoki, H., and Yasumoto, T. (1999). Identification of putative palytoxin as the cause of clupeotoxism. Toxicon Off. J. Int. Soc. Toxinology *37*, 55–65.

Pagliara, P., and Caroppo, C. (2012). Toxicity assessment of Amphidinium carterae, Coolia cfr. monotis and *Ostreopsis* cfr. *ovata* (Dinophyta) isolated from the northern Ionian Sea (Mediterranean Sea). Toxicon Off. J. Int. Soc. Toxinology *60*, 1203–1214.

Parrish, C.C., Bodennec, G., and Gentien, P. (1998). Haemolytic glycoglycerolipids from Gymnodinium species. Phytochemistry *47*, 783–787.

Parsons, M.L., Aligizaki, K., Bottein, M.-Y.D., Fraga, S., Morton, S.L., Penna, A., and Rhodes, L. (2012). Gambierdiscus and *Ostreopsis:* Reassessment of the state of knowledge of their taxonomy, geography, ecophysiology, and toxicology. Harmful Algae *14*, 107–129.

Pelin, M., Zanette, C., De Bortoli, M., Sosa, S., Loggia, R.D., Tubaro, A., and Florio, C. (2011). Effects of the marine toxin palytoxin on human skin keratinocytes: role of ionic imbalance. Toxicology *282*, 30–38.

Pelin, M., Sosa, S., Della Loggia, R., Poli, M., Tubaro, A., Decorti, G., and Florio, C. (2012). The cytotoxic effect of palytoxin on Caco-2 cells hinders their use for in vitro absorption studies. Food Chem. Toxicol. Int. J. Publ. Br. Ind. Biol. Res. Assoc. *50*, 206–211.

Pelin, M., Boscolo, S., Poli, M., Sosa, S., Tubaro, A., and Florio, C. (2013a). Characterization of palytoxin binding to HaCaT cells using a monoclonal anti-palytoxin antibody. Mar. Drugs *11*, 584–598.

Pelin, M., Ponti, C., Sosa, S., Gibellini, D., Florio, C., and Tubaro, A. (2013b). Oxidative stress induced by palytoxin in human keratinocytes is mediated by a H^+-dependent mitochondrial pathway. Toxicol. Appl. Pharmacol. *266*, 1–8.

Pelin, M., Brovedani, V., Sosa, S., and Tubaro, A. (2016a). Palytoxin-Containing Aquarium Soft Corals as an Emerging Sanitary Problem. Mar. Drugs *14*.

Pelin, M., Forino, M., Brovedani, V., Tartaglione, L., Dell'Aversano, C., Pistocchi, R., Poli, M., Sosa, S., Florio, C., Ciminiello, P., et al. (2016b). Ovatoxin-a, A Palytoxin Analogue Isolated from *Ostreopsis* cf. *ovata* Fukuyo: Cytotoxic Activity and ELISA Detection. Environ. Sci. Technol. *50*, 1544–1551.

Penna, A., Vila, M., Fraga, S., Giacobbe, M.G., Andreoni, F., Riobó, P., and Vernesi, C. (2005). Characterization of *Ostreopsis* and *Coolia* (Dinophyceae) isolates in the Western Mediterranean Sea based on morphology, toxicity and internal transcribed spacer 5.8S rDNA sequences. J. Phycol. *41*, 212–225.

Pezzolesi, L., Guerrini, F., Ciminiello, P., Dell'Aversano, C., Dello Iacovo, E., Fattorusso, E., Forino, M., Tartaglione, L., and Pistocchi, R. (2012). Influence of temperature and salinity on *Ostreopsis* cf. *ovata* growth and evaluation of toxin content through HR LC-MS and biological assays. Water Res. *46*, 82–92.

Pistocchi, R., Pezzolesi, L., Guerrini, F., Vanucci, S., Dell'aversano, C., and Fattorusso, E. (2011). A review on the effects of environmental conditions on growth and toxin production of *Ostreopsis ovata*. Toxicon Off. J. Int. Soc. Toxinology *57*, 421–428.

Pleissner, D., and Eriksen, N.T. (2012). Effects of phosphorous, nitrogen, and carbon limitation on biomass composition in batch and continuous flow cultures of the heterotrophic dinoflagellate Crypthecodinium cohnii. Biotechnol. Bioeng. *109*, 2005–2016.

Qiu, L.Y., Swarts, H.G.P., Tonk, E.C.M., Willems, P.H.G.M., Koenderink, J.B., and De Pont, J.J.H.H.M. (2006). Conversion of the low affinity ouabain-binding site of non-gastric H,K-ATPase into a high affinity binding site by substitution of only five amino acids. J. Biol. Chem. *281*, 13533–13539.

Ramos, V., and Vasconcelos, V. (2010). Palytoxin and analogs: biological and ecological effects. Mar. Drugs *8*, 2021–2037.

Rhodes, L., Adamson, J., Suzuki, T., Briggs, L., and Garthwaite, I. (2000). Toxic marine epiphytic dinoflagellates, *Ostreopsis siamensis* and *Coolia monotis* (Dinophyceae), in New Zealand. N. Z. J. Mar. Freshw. Res. *34*, 371–383.

Rhodes, L., Towers, N., Briggs, L., Munday, R., and Adamson, J. (2002). Uptake of palytoxin-like compounds by shellfish fed *Ostreopsis siamensis* (Dinophyceae). N. Z. J. Mar. Freshw. Res. *36*, 631–636.

Riobó, P., and Franco, J.M. (2011). Palytoxins: biological and chemical determination. Toxicon Off. J. Int. Soc. Toxinology *57*, 368–375.

Riobó, P., Paz, B., and Franco, J.M. (2006). Analysis of palytoxin-like in *Ostreopsis* cultures by liquid chromatography with precolumn derivatization and fluorescence detection. Anal. Chim. Acta *566*, 217–223.

Riobó, P., Paz, B., Franco, J.M., Vázquez, J.A., Murado, M.A., and Cacho, E. (2008a). Mouse bioassay for palytoxin. Specific symptoms and dose-response against dose-death time relationships. Food Chem. Toxicol. Int. J. Publ. Br. Ind. Biol. Res. Assoc. *46*, 2639–2647.

Riobó, P., Paz, B., Franco, J.M., Vázquez, J.A., and Murado, M.A. (2008b). Proposal for a simple and sensitive haemolytic assay for palytoxin: Toxicological dynamics, kinetics, ouabain inhibition and thermal stability. Harmful Algae *7*, 415–429.

Rodrigues, A.M., Almeida, A.-C.G., Infantosi, A.F.C., Teixeira, H.Z., and Duarte, M.A. (2008). Model and simulation of Na+/K+ pump phosphorylation in the presence of palytoxin. Comput. Biol. Chem. *32*, 5–16.

Rossini, G.P. (2005). Functional assays in marine biotoxin detection. Toxicology *207*, 451–462.

Rossini, G.P., and Bigiani, A. (2011). Palytoxin action on the Na(+),K(+)-ATPase and the disruption of ion equilibria in biological systems. Toxicon Off. J. Int. Soc. Toxinology *57*, 429–439.

Scarrone, S., Balestrino, M., Frassoni, F., Pozzi, S., Gandolfo, C., Podestà, M., and Cupello, A. (2007). Sex differences in human lymphocyte Na,K-ATPase as studied by labeled ouabain binding. Int. J. Neurosci. *117*, 275–285.

Schilling, W.P., Snyder, D., Sinkins, W.G., and Estacion, M. (2006). Palytoxin-induced cell death cascade in bovine aortic endothelial cells. Am. J. Physiol. Cell Physiol. *291*, C657-667.

Seemann, P., Gernert, C., Schmitt, S., Mebs, D., and Hentschel, U. (2009). Detection of hemolytic bacteria from *Palythoa caribaeorum* (Cnidaria, Zoantharia) using a novel palytoxin-screening assay. Antonie Van Leeuwenhoek *96*, 405–411.

Selwood, A.I., van Ginkel, R., Harwood, D.T., McNabb, P.S., Rhodes, L.R., and Holland, P.T. (2012). A sensitive assay for palytoxins, ovatoxins and ostreocins using LC-MS/MS analysis of cleavage fragments from micro-scale oxidation. Toxicon Off. J. Int. Soc. Toxinology *60*, 810–820.

Sheridan, R.E., Deshpande, S.S., and Adler, M. (2005). Cytotoxic actions of palytoxin on aortic smooth muscle cells in culture. J. Appl. Toxicol. *25*, 365–373.

Suzuki, T., Watanabe, R., Matsushima, R., Ishihara, K., Uchida, H., Kikutsugi, S., Harada, T., Nagai, H., Adachi, M., Yasumoto, T., et al. (2013). LC-MS/MS analysis of palytoxin analogues in blue humphead parrotfish Scarus ovifrons causing human poisoning in Japan. Food Addit. Contam. Part Chem. Anal. Control Expo. Risk Assess. *30*, 1358–1364.

Taniyama, S., Mahmud, Y., Tanu, M.B., Takatani, T., Arakawa, O., and Noguchi, T. (2001). Delayed haemolytic activity by the freshwater puffer Tetraodon sp. toxin. Toxicon Off. J. Int. Soc. Toxinology *39*, 725–727.

Taniyama, S., Mahmud, Y., Terada, M., Takatani, T., Arakawa, O., and Noguchi, T. (2002). Occurrence of a food poisoning incident by palytoxin from a serranid Epinephelus sp. in Japan. J. Nat. Toxins *11*, 277–282.

Taniyama, S., Arakawa, O., Terada, M., Nishio, S., Takatani, T., Mahmud, Y., and Noguchi, T. (2003). *Ostreopsis* sp., a possible origin of palytoxin (PTX) in parrotfish Scarus ovifrons. Toxicon Off. J. Int. Soc. Toxinology *42*, 29–33.

Tartaglione, L., Mazzeo, A., Dell'Aversano, C., Forino, M., Giussani, V., Capellacci, S., Penna, A., Asnaghi, V., Faimali, M., Chiantore, M., et al. (2016a). Chemical, molecular, and eco-toxicological investigation of *Ostreopsis* sp. from Cyprus Island: structural insights into four new ovatoxins by LC-HRMS/MS. Anal. Bioanal. Chem. *408*, 915–932.

Tartaglione, L., Dell'Aversano, C., Mazzeo, A., Forino, M., Wieringa, A., and Ciminiello, P. (2016b). Determination of Palytoxins in Soft Coral and Seawater from a Home Aquarium. Comparison between *Palythoa*- and *Ostreopsis*-Related Inhalatory Poisonings. Environ. Sci. Technol. *50*, 1023–1030.

Thavarajah, R., Mudimbaimannar, V.K., Elizabeth, J., Rao, U.K., and Ranganathan, K. (2012). Chemical and physical basics of routine formaldehyde fixation. J. Oral Maxillofac. Pathol. JOMFP *16*, 400–405.

Tichadou, L., Glaizal, M., Armengaud, A., Grossel, H., Lemée, R., Kantin, R., Lasalle, J.-L., Drouet, G., Rambaud, L., Malfait, P., et al. (2010). Health impact of unicellular algae of the *Ostreopsis* genus blooms in the Mediterranean Sea: experience of the French Mediterranean coast surveillance network from 2006 to 2009. Clin. Toxicol. Phila. Pa *48*, 839–844.

Tognetto, L., Bellato, S., Moro, I., and Andreoli, C. (1995). Occurrence of *Ostreopsis ovata* (Dinophyceae) in the Tyrrhenian Sea during Summer 1994. Bot. Mar. *38*.

Totti, C., Accoroni, S., Cerino, F., Cucchiari, E., and Romagnoli, T. (2010). *Ostreopsis ovata* bloom along the Conero Riviera (northern Adriatic Sea): Relationships with environmental conditions and substrata. Harmful Algae *9*, 233–239.

Tubaro, A., Del Favero, G., Beltramo, D., Ardizzone, M., Forino, M., De Bortoli, M., Pelin, M., Poli, M., Bignami, G., Ciminiello, P., et al. (2011a). Acute oral toxicity in mice of a new palytoxin analog: 42-hydroxy-palytoxin. Toxicon Off. J. Int. Soc. Toxinology *57*, 755–763.

Tubaro, A., Durando, P., Del Favero, G., Ansaldi, F., Icardi, G., Deeds, J.R., and Sosa, S. (2011b). Case definitions for human poisonings postulated to palytoxins exposure. Toxicon Off. J. Int. Soc. Toxinology *57*, 478–495.

Tubaro, A., del Favero, G., Pelin, M., Bignami, G., and Poli, M. (2014). Palytoxin and Analogues: Biological Effects and Detection. In Seafood and Freshwater Toxins, (CRC Press), pp. 741–772.

Uchida, H., Taira, Y., and Yasumoto, T. (2013). Structural elucidation of palytoxin analogs produced by the dinoflagellate *Ostreopsis ovata* IK2 strain by complementary use of positive and negative ion liquid chromatography/quadrupole time-of-flight mass spectrometry: Structural elucidation of ovatoxin-a, -d, -e IK2 by LC/QTOFMS. Rapid Commun. Mass Spectrom. *27*, 1999–2008.

Utermohl, H. (1958). Zur Vervollkommnung der quantitativen Phytoplanktonmethodik. Mitt Int Ver. Limnol *9*, 1–38.

Vale, C., Alfonso, A., Suñol, C., Vieytes, M.R., and Botana, L.M. (2006). Modulation of calcium entry and glutamate release in cultured cerebellar granule cells by palytoxin. J. Neurosci. Res. *83*, 1393–1406.

Vale-González, C., Gómez-Limia, B., Vieytes, M.R., and Botana, L.M. (2007). Effects of the marine phycotoxin palytoxin on neuronal pH in primary cultures of cerebellar granule cells. J. Neurosci. Res. *85*, 90–98.

Vila, M., Garcés, E., and Masó, M. (2001). Potentially toxic epiphytic dinoflagellate assemblages on macroalgae in the NW Mediterranean. Aquat. Microb. Ecol. *26*, 51–60.

Vila, M., Arin, L., Battocchi, C., Bravo, I., Fraga, S., Penna, A., Reñé, A., Riobó, P., Rodriguez, F., Sala, M.M., et al. (2012). Management of *Ostreopsis* Blooms in Recreational waters along the Catalan Coast (NW Mediterranean Sea): Cooperation between a Research Project and a Monitoring Program. Cryptogam. Algol. *33*, 143–152.

Volpe, G., Cozzi, L., Migliorelli, D., Croci, L., and Palleschi, G. (2014). Development of a haemolytic-enzymatic assay with mediated amperometric detection for palytoxin analysis: application to mussels. Anal. Bioanal. Chem. *406*, 2399–2410.

Wachi, K.M., and Hokama, Y. (2001). Diversity of marine biotoxins in the near-shore ocean area: presence of a palytoxin-like entity at Barber's Point Harbor, Oahu. J. Nat. Toxins *10*, 317–333.

Wattenberg, E.V. (2007). Palytoxin: exploiting a novel skin tumor promoter to explore signal transduction and carcinogenesis. Am. J. Physiol. Cell Physiol. *292*, C24-32.

Wu, C.H. (2009). Palytoxin: membrane mechanisms of action. Toxicon Off. J. Int. Soc. Toxinology *54*, 1183–1189.

Wu, M.-L., Yang, C.-C., Deng, J.-F., and Wang, K.-Y. (2014). Hyperkalemia, hyperphosphatemia, acute kidney injury, and fatal dysrhythmias after consumption of palytoxin-contaminated goldspot herring. Ann. Emerg. Med. *64*, 633–636.

Yakes, B.J., DeGrasse, S.L., Poli, M., and Deeds, J.R. (2011). Antibody characterization and immunoassays for palytoxin using an SPR biosensor. Anal. Bioanal. Chem. *400*, 2865–2869.

Yasumoto, T., Oshima, Y., and Yamaguchi, M. (1978). Occurrence of a new type of shellfish poisoning in the Tohoku district. Nippon Suisan Gakkaishi *44*, 1249–1255.

Yasumoto, T., Yasumura, D., Ohizumi, Y., Takahashi, M., Alcala, A.C., and Alcala, L.C. (1986). Palytoxin in Two Species of Xanthid Crab from the Philippines. Agric. Biol. Chem. *50*, 163–167.

Zamolo, V.A., Valenti, G., Venturelli, E., Chaloin, O., Marcaccio, M., Boscolo, S., Castagnola, V., Sosa, S., Berti, F., Fontanive, G., et al. (2012). Highly sensitive electrochemiluminescent nanobiosensor for the detection of palytoxin. ACS Nano *6*, 7989–7997.

Zehnder, L., Schulzki, T., Goede, J.S., Hayes, J., and Reinhart, W.H. (2008). Erythrocyte storage in hypertonic (SAGM) or isotonic (PAGGSM) conservation medium: influence on cell properties. Vox Sang. *95*, 280–287.

7. Appendices

Appendix A

Form to collect data on field Ostreopsis cf. ovata.

Day **18/09/2015** hour **10/00**

Bathing area	ID **T0Sp1** Geographic coordinates **43° 32' 2'' N, 16° 26' 55'' E** Region, district, country **Kastela bay, Split, Croatia**
Monitoring point	Geographic coordinates **43° 32' 2'' N, 16° 26' 55'' E** Depth **30-100 cm** Distance from the cost **3 m** Sea bottom type **Rocky**
Climatic weather conditions	
Hydrodynamism	**x** Absent □ Moderate □ Strong
Wind force	**x** Absent □ Moderate □ Strong
Wind direction	□ Landward □ Seaward □ Other
Meteorological conditions	□ Rainy □ Cloudy **x** Sunny
Weather and sea conditions from last 5 days **Sunny weather without wind** Notes (other observations)…….. …….....	
Bloom	Presence of visible material (reddish-brown foams, flakes) □ No **x** Yes Location of the material □ Sea bottom **x** Water column **x** Water surface Shoreline: extension (meter)……..... area **x** bathing area □ no bathing area
Samples	□ Water column **x** Visible material
Temperature	Water |2|4|,|0| °C Air |2|6|,|0| °C

Day **31/08/2015** hour **11/30**

Bathing area	ID **T0C1** Geographic coordinates **45° 44' 58'' N, 13° 39' 20'' E** Region, district, country **Canovella de' Zoppoli, Trieste, Italy**
Monitoring point	Geographic coordinates **45° 44' 58'' N, 13° 39' 20'' E** Depth **30-100 cm** Distance from the cost **3-4 m** Sea bottom type **Rocky**
Climatic weather conditions	
Hydrodynamism	**x** Absent □ Moderate □ Strong
Wind force	**x** Absent □ Moderate □ Strong
Wind direction	□ Landward □ Seaward □ Other
Meteorological conditions	□ Rainy □ Cloudy **x** Sunny
Weather and sea conditions from last 5 days **Sunny weather with moderate wind** Notes (other observations)…….. …….....	
Bloom	Presence of visible material (reddish-brown foams, flakes) □ No **x** Yes Location of the material **x** Sea bottom **x** Water column **x** Water surface Shoreline: extension (meter) **10 m** area **x** bathing area □ no bathing area
Samples	□ Water column **x** Visible material
Temperature	Water |2|5|,|5| °C Air |2|9|,|0| °C

Day **22/09/2015** hour **11/00**

Bathing area	ID **T1C1** Geographic coordinates **45° 44' 58'' N, 13° 39' 20'' E** Region, district, country **Canovella de' Zoppoli, Trieste, Italy**
Monitoring point	Geographic coordinates **45° 44' 58'' N, 13° 39' 20'' E** Depth **30-100 cm** Distance from the cost **3-4 m** Sea bottom type **Rocky**
Climatic weather conditions	
Hydrodynamism	**x** Absent □ Moderate □ Strong
Wind force	**x** Absent □ Moderate □ Strong
Wind direction	□ Landward □ Seaward □ Other
Meteorological conditions	□ Rainy □ Cloudy **x** Sunny
Weather and sea conditions from last 5 days **Sunny weather with moderate wind (wind direction: east)** Notes (other observations)…….. …….....	
Bloom	Presence of visible material (reddish-brown foams, flakes) □ No **x** Yes Location of the material **x** Sea bottom **x** Water column **x** Water surface Shoreline: extension (meter) **10 m** area **x** bathing area □ no bathing area
Samples	□ Water column **x** Visible material
Temperature	Water |2|0|,|1| °C Air |2|0|,|3| °C

Day **03/09/2015** hour **10/00**

Bathing area	ID **T0S1** Geographic coordinates **44° 02' 60.0" N, 9° 59' 20.0" E** Region, district, country **Fiumaretta, La Spezia, Italy**		
Monitoring point	Geographic coordinates **44° 02' 60.0" N, 9° 59' 20.0" E** Depth **30-100 cm** Distance from the cost **1-2 m** Sea bottom type **Sandy**		
Climatic weather conditions			
Hydrodynamism	**x** Absent	□ Moderate	□ Strong
Wind force	**x** Absent	□ Moderate	□ Strong
Wind direction	□ Landward	□ Seaward	□ Other
Meteorological conditions	□ Rainy	□ Cloudy	**x** Sunny
Weather and sea conditions from last 5 days **Sunny weather** Notes (other observations)…….. …….....			
Bloom	Presence of visible material (reddish-brown foams, flakes) **x** No □ Yes Location of the material □ Sea bottom □ Water column □ Water surface Shoreline: extension (meter) area **x** bathing area □ no bathing area		
Samples	**x** Water column	□ Visible material	
Temperature	Water |2|4|,|4| °C	Air |2|4|,|7| °C	

Day **03/09/2015** hour **10/30**

Bathing area	ID **T0S2** Geographic coordinates **44° 02' 44.4" N, 9° 59' 07.7" E** Region, district, country **Bocca di Magra, La Spezia, Italy**		
Monitoring point	Geographic coordinates **44° 02' 44.4" N, 9° 59' 07.7" E** Depth **30-100 cm** Distance from the cost **1-2 m** Sea bottom type **Rocky**		
Climatic weather conditions			
Hydrodynamism	**x** Absent	□ Moderate	□ Strong
Wind force	□ Absent	**x** Moderate	□ Strong
Wind direction	□ Landward	**x** Seaward	□ Other
Meteorological conditions	□ Rainy	□ Cloudy	**x** Sunny
Weather and sea conditions from last 5 days **Sunny weather** Notes (other observations)…….. …….....			
Bloom	Presence of visible material (reddish-brown foams, flakes) **x** No □ Yes Location of the material □ Sea bottom □ Water column □ Water surface Shoreline: extension (meter) area **x** bathing area □ no bathing area		
Samples	**x** Water column	□ Visible material	
Temperature	Water |2|4|,|2| °C	Air |2|3|,|9| °C	

Day **03/09/2015** hour **11/00**

Bathing area	ID **T0S3** Geographic coordinates **44° 04' 51.5" N, 9° 52' 54.1" E** Region, district, country **Santa Teresa Lerici, La Spezia, Italy**
Monitoring point	Geographic coordinates **44° 04' 51.5" N, 9° 52' 54.1" E** Depth **30-100 cm** Distance from the cost **1-2 m** Sea bottom type **Rocky**
Climatic weather conditions	
Hydrodynamism	**x** Absent □ Moderate □ Strong
Wind force	□ Absent **x** Moderate □ Strong
Wind direction	**x** Landward □ Seaward □ Other
Meteorological conditions	□ Rainy □ Cloudy **x** Sunny
Weather and sea conditions from last 5 days **Sunny weather** Notes (other observations)…….. …….....	
Bloom	Presence of visible material (reddish-brown foams, flakes) **x** No □ Yes Location of the material □ Sea bottom □ Water column □ Water surface Shoreline: extension (meter) area **x** bathing area □ no bathing area
Samples	**x** Water column □ Visible material
Temperature	Water |2|3|,|9| °C Air |2|3|,|1| °C

Day **08/09/2015** hour **10/00**

Bathing area	ID **T1S1** Geographic coordinates **44° 02' 60.0" N, 9° 59' 20.0" E** Region, district, country **Fiumaretta, La Spezia, Italy**		
Monitoring point	Geographic coordinates **44° 02' 60.0" N, 9° 59' 20.0" E** Depth **30-100 cm** Distance from the cost **1-2 m** Sea bottom type **Sandy**		
Climatic weather conditions			
Hydrodynamism	**x** Absent	□ Moderate	□ Strong
Wind force	□ Absent	**x** Moderate	□ Strong
Wind direction	□ Landward	**x** Seaward	□ Other
Meteorological conditions	□ Rainy	□ Cloudy	**x** Sunny
Weather and sea conditions from last 5 days **Sunny weather** Notes (other observations)…….. …….....			
Bloom	Presence of visible material (reddish-brown foams, flakes) **x** No □ Yes Location of the material □ Sea bottom □ Water column □ Water surface Shoreline: extension (meter) area **x** bathing area □ no bathing area		
Samples	**x** Water column	□ Visible material	
Temperature	Water |2|4|,|2| °C	Air |2|5|,|0| °C	

Day **08/09/2015** hour **10/30**

Bathing area	ID **T1S2** Geographic coordinates **44° 02' 03.6" N, 10° 02' 07.8" E** Region, district, country **Marina di Carrara, Massa-Carrara, Italy**		
Monitoring point	Geographic coordinates **44° 02' 03.6" N, 10° 02' 07.8" E** Depth **30-100 cm** Distance from the cost **1-2 m** Sea bottom type **Sandy**		
Climatic weather conditions			
Hydrodynamism	**x** Absent	□ Moderate	□ Strong
Wind force	□ Absent	**x** Moderate	□ Strong
Wind direction	□ Landward	**x** Seaward	□ Other
Meteorological conditions	□ Rainy	□ Cloudy	**x** Sunny
Weather and sea conditions from last 5 days **Sunny weather** Notes (other observations)…….. …….....			
Bloom	Presence of visible material (reddish-brown foams, flakes) **x** No □ Yes Location of the material □ Sea bottom □ Water column □ Water surface Shoreline: extension (meter) area **x** bathing area □ no bathing area		
Samples	**x** Water column	□ Visible material	
Temperature	Water |2|4|,|0| °C	Air |2|5|,|0| °C	

Day **08/09/2015** hour **11/00**

Bathing area	ID **T1S3** Geographic coordinates **44° 01' 41.9" N, 10° 03' 43.3" E** Region, district, country **Marina di Massa, Massa-Carrara, Italy**
Monitoring point	Geographic coordinates **44° 01' 41.9" N, 10° 03' 43.3" E** Depth **30-100 cm** Distance from the cost **1-2 m** Sea bottom type **Sandy**
Climatic weather conditions	
Hydrodynamism	**x** Absent □ Moderate □ Strong
Wind force	**x** Absent □ Moderate □ Strong
Wind direction	□ Landward □ Seaward □ Other
Meteorological conditions	□ Rainy □ Cloudy **x** Sunny
Weather and sea conditions from last 5 days **Sunny weather** Notes (other observations)…….. …….....	
Bloom	Presence of visible material (reddish-brown foams, flakes) **x** No □ Yes Location of the material □ Sea bottom □ Water column □ Water surface Shoreline: extension (meter) area **x** bathing area □ no bathing area
Samples	**x** Water column □ Visible material
Temperature	Water |2|5|,|0| °C Air |2|6|,|0| °C

Day **10/09/2015** hour **10/00**

Bathing area	ID **T2S1** Geographic coordinates **44° 02' 60.0" N, 9° 59' 20.0" E** Region, district, country **Fiumaretta, La Spezia, Italy**
Monitoring point	Geographic coordinates **44° 02' 60.0" N, 9° 59' 20.0" E** Depth **30-100 cm** Distance from the cost **1-2 m** Sea bottom type **Sandy**
Climatic weather conditions	
Hydrodynamism	**x** Absent □ Moderate □ Strong
Wind force	□ Absent **x** Moderate □ Strong
Wind direction	**x** Landward □ Seaward □ Other
Meteorological conditions	□ Rainy □ Cloudy **x** Sunny
Weather and sea conditions from last 5 days **Sunny weather** Notes (other observations)…….. ……...	
Bloom	Presence of visible material (reddish-brown foams, flakes) **x** No □ Yes Location of the material □ Sea bottom □ Water column □ Water surface Shoreline: extension (meter) area **x** bathing area □ no bathing area
Samples	**x** Water column □ Visible material
Temperature	Water |2|3|,|9| °C Air |2|3|,|6| °C

Day **10/09/2015** hour **10/30**

Bathing area	ID **T2S2** Geographic coordinates **44° 02' 03.6" N, 10° 02' 07.8" E** Region, district, country **Marina di Carrara, Massa-Carrara, Italy**
Monitoring point	Geographic coordinates **44° 02' 03.6" N, 10° 02' 07.8" E** Depth **30-100 cm** Distance from the cost **1-2 m** Sea bottom type **Sandy**
Climatic weather conditions	
Hydrodynamism	**x** Absent □ Moderate □ Strong
Wind force	**x** Absent □ Moderate □ Strong
Wind direction	□ Landward □ Seaward □ Other
Meteorological conditions	□ Rainy □ Cloudy **x** Sunny
Weather and sea conditions from last 5 days **Sunny weather** Notes (other observations)…….. …….....	
Bloom	Presence of visible material (reddish-brown foams, flakes) **x** No □ Yes Location of the material □ Sea bottom □ Water column □ Water surface Shoreline: extension (meter) area **x** bathing area □ no bathing area
Samples	**x** Water column □ Visible material
Temperature	Water |2|3|,|0| °C Air |2|4|,|0| °C

Day **10/09/2015** hour **11/00**

Bathing area	ID **T1S3** Geographic coordinates **44° 01' 41.9" N, 10° 03' 43.3" E** Region, district, country **Marina di Massa, Massa-Carrara, Italy**
Monitoring point	Geographic coordinates **44° 01' 41.9" N, 10° 03' 43.3" E** Depth **30-100 cm** Distance from the cost **1-2 m** Sea bottom type **Sandy**
Climatic weather conditions	
Hydrodynamism	**x** Absent □ Moderate □ Strong
Wind force	**x** Absent □ Moderate □ Strong
Wind direction	□ Landward □ Seaward □ Other
Meteorological conditions	□ Rainy □ Cloudy **x** Sunny
Weather and sea conditions from last 5 days **Sunny weather** Notes (other observations)…….. …….....	
Bloom	Presence of visible material (reddish-brown foams, flakes) **x** No □ Yes Location of the material □ Sea bottom □ Water column □ Water surface Shoreline: extension (meter) area **x** bathing area □ no bathing area
Samples	**x** Water column □ Visible material
Temperature	Water |2|3|,|0| °C Air |2|5|,|0| °C

Day **13/09/2016** hour **11/30**

Bathing area	ID **T0C2** Geographic coordinates **45° 44' 58'' N, 13° 39' 20'' E** Region, district, country **Canovella de' Zoppoli, Trieste, Italy**
Monitoring point	Geographic coordinates **45° 44' 58'' N, 13° 39' 20'' E** Depth **30-100 cm** Distance from the cost **3-4 m** Sea bottom type **Rocky**
Climatic weather conditions	
Hydrodynamism	**x** Absent □ Moderate □ Strong
Wind force	**x** Absent □ Moderate □ Strong
Wind direction	□ Landward □ Seaward □ Other
Meteorological conditions	□ Rainy □ Cloudy **x** Sunny
Weather and sea conditions from last 5 days **Cloudy and rainy weather** Notes (other observations)…….. …….....	
Bloom	Presence of visible material (reddish-brown foams, flakes) **x** No □ Yes Location of the material □ Sea bottom □ Water column □ Water surface Shoreline: extension (meter) **10 m** area **x** bathing area □ no bathing area
Samples	**x** Water column □ Visible material
Temperature	Water |2|4|,|2| °C Air |2|3|,|4| °C

Day **29/09/2016** hour **11/30**

Bathing area	ID **T1C2** Geographic coordinates **45° 44' 58'' N, 13° 39' 20'' E** Region, district, country **Canovella de' Zoppoli, Trieste, Italy**		
Monitoring point	Geographic coordinates **45° 44' 58'' N, 13° 39' 20'' E** Depth **30-100 cm** Distance from the cost **3-4 m** Sea bottom type **Rocky**		
Climatic weather conditions			
Hydrodynamism	**x** Absent	□ Moderate	□ Strong
Wind force	**x** Absent	□ Moderate	□ Strong
Wind direction	□ Landward	□ Seaward	□ Other
Meteorological conditions	□ Rainy	**x** Cloudy	□ Sunny
Weather and sea conditions from last 5 days **Sunny weather** Notes (other observations)…….. …….....			
Bloom	Presence of visible material (reddish-brown foams, flakes) **x** No □ Yes Location of the material □ Sea bottom □ Water column □ Water surface Shoreline: extension (meter) **10 m** area **x** bathing area □ no bathing area		
Samples	**x** Water column	□ Visible material	
Temperature	Water |2|2|,|2| °C	Air |2|0|,|0| °C	